A NORMAL INCIDENCE, HIGH RESOLUTION X-RAY TELESCOPE FOR SOLAR CORONAL OBSERVATIONS

Grant NAGW-397

Semiannual Progress Report No. 4

For the period 1 May 1984 through 31 October 1984

Principal Investigator:

Dr. Leon Golub

November 1984

Prepared for

National Aeronautics and Space Administration

Washington, DC 20546

Smithsonian Institution
Astrophysical Observatory
Cambridge, MA 02138

The Smithsonian Astrophysical Observatory
is a member of the
Harvard-Smithsonian Center for Astrophysics

The NASA Technical Officer for this grant is Dr. J. David Bonlin, Code EZ-7
NASA Headquarters, Washington, DC 20546

A NORMAL INCIDENCE, HIGH RESOLUTION X-RAY TELESCOPE FOR SOLAR CORONAL OBSERVATIONS

Grant NAGW-397

Semiannual Progress Report No. 4

For the period 1 May 1984 through 31 October 1984

Principal Investigator:

Dr. Leon Golub

November 1984

Prepared for

National Aeronautics and Space Administration

Washington, DC 20546

Smithsonian Institution
Astrophysical Observatory
Cambridge, MA 02138

The Smithsonian Astrophysical Observatory is a member of the Harvard-Smithsonian Center for Astrophysics

The NASA Technical Officer for this grant is Dr. J. David Bohlin, Code EZ-7
NASA Headquarters, Washington, DC 20546

NIXT PROGRESS REPORT

Table of Contents

0. Introduction

0. Introduction

This Progress Report describes the work which has been performed during the past six months under NASA Grant NAGW-397. Portions of the work are also being performed under Grant NAG5-626; tasks covered under both grants are described in this report.

Our current effort has been directed toward completion of the telescope assembly design, procurement of major components and coordination of the optical fabrication and X-ray multilayer testing with personnel at IBM. In addition to the work specifically mentioned in the body of this report, we have also:

(i) begun fabrication of the flight prefilters;

(ii) completed mirror assembly components;

(iii) completed a Project Initiation Conference (PIC) at the Wallops Flight Facility;

(iv) designed and ordered components for a small, low-cost Hα camera to provide real time imaging of Solar activity during the flight;

(v) set up a conjugate image experiment whose goal is test the image quality of the NIXT Prototy8pe mirror at the sub-arcsecond level.

1. NIXT Rocket Payload Engineering Studies

a. Calculated Weights NIXT Program

NIXT PROGRAM
CALCULATED WEIGHTS

NOTE: These are the calculated weights to date and will be updated over life of program. * is an estimated value.

PART NAME	PART WEIGHT	QTY/REQ'D	TOTAL WEIGHT
PRIMARY MIRROR	14.85 TOTAL	1	14.85
INVAR BASE PLATE	30.28	1	30.28
MOUNTING BOLTS	.13	3	.39
SPHERICAL MACOR WASHERS	.03	3 DUPLEX SETS	.18
TELESCOPE TUBE	15.52	1	15.52
CAMERA BASE RING*	4.63	1	4.63
CAMERA TUBE*	3.0	1	3.00
CAMERA MTG.*	1.0	1	1.00
TELESCOPE TUBE FLANGE	8.52		8.52
SECONDARY ASSY			
MIRROR	.34	1	
SHAFT	.15	1	
PIVOT	.34	1	
PLATE ADJ.	.1	1	
NUT CLAMP	.01	1	
SPRING	.001	1	
NUT	.02	1	
BLADES	.1	6	
MAIN RING	.81	1	
MTG'S	.08	3	
			2.61
SECONDARY ASSY WEIGHT			
SECONDARY MOUNT	.15	3	.45
FWD CABLE	1.00	1	1.00
LISS MOUNT	.29	1	.29
LISS SUN SENSOR	.46	1	.46
MASS MOUNT	.19	1	.19
MASS SUN SENSOR	.09	1	.09
UPPER HEAT SHIELD	8.84	1	8.84
LOWER HEAT SHIELD	7.83	1	7.83
WEIGHT HEAT SHIELD ISOLATORS	VARIES	9	.58
BASE HEAT SHIELD MTG.	.06	3	.18
FILTER	3.41		3.41
			104.30

b. Temperature Gradients

MEMORANDUM

TO: L.Golub, G.Nystrom

16 September 1984

FROM: D.Boyd

DAB-84-022

SUBJECT: Temperature Gradients in NIXT Mirrors

CC: L.Cohen, B.Dias (memo only)

If the NIXT filters are placed at the rear of the telescope, allowing the mirrors to be illuminated by the sun, I have calculated that the resulting temperature gradients in the mirrors will cause deformations of about one arcsecond in each mirror. Engineering notebook sheets bearing the calculations are attached. I outline below the assumptions and a few caveats on the results.

Mirror sizes were scaled from the telescope layout.
Primary reflectivity = 0 for calculating heating of the primary
=0.2 for determining input to the secondary
Secondary reflectivity = 0, concentration ratio = 15
(These assumptions result in answers that are about 20% high if the true reflectivity = 0.2. Secondary deformation is roughly proportional to primary reflectivity, but probably will not be acceptable unless this reflectivity << 0.1)
Coefficient of expansion for the Zerodur blanks = -0.1ppm/C
(this value was obtained from Lester Cohen)

Front-back delta-T in primary = 15C at the end of 300 seconds, yielding deformation of 0.8 arcsecond.
Front-back delta-T in secondary = 22C at the end of 300 seconds, yielding deformation of 0.9 arcsecond.

The temperature gradients were also assumed to be linear through the glass for calculation of deformation; this gives answers that are larger than normal but probably not by as much as a factor of two. The most favorable assumptions and accurate calculations possible would probably reduce deformations by as much as a factor of two, which would still be quite large, so additional analysis of this subject does not appear necessary.

c. Prefilter Survival Tests

TO: David Boyd
Leon Golub
George Nystrom

FROM: Peter Cheimets

DATE: June 12, 1984

SUBJECT: Results of Test of Filter Survival

In a memo dated March 5, 1984 I proposed a test to determine if the NIXT pre-filters would survive direct exposure to on solar constant in a vacuum. That test, slightly modified, was performed this morning. The filter that only had a dag coating melted almost immediately while the aluminum coated filter survived two exposures to radiation level near that of the sun for 5 seconds each.

Test Description:

The apparatus was identical to that described in the March 3rd memo. The precedure was slightly different. First the lamp's radiation output was measured using the induced temperature change in a small block brass cone. The integrated emitted radiation from the lamp was found to be 500 watts, this meant that at a separation of 6.9 inches the radiation flux would be one solar constant. The cone was placed at that distance and the lamp flux remeasured. The flux did in fact equal one sun.

The unaluminized filter was placed at 6.5 [illegible] lamp and vacuum drawn. The lamp was switched on and [illegible] with variac. The filter melted away 3 seconds after [illegible] full voltage.

The aluminized filter was then mounted in the bell jar at a separation of 9.2 inches a distance that would yield a flux of half the solar constant. The filter was exposed for about 3 seconds. One part of the filter that was not covered with aluminum did start to melt the remainder of the filter was intact. The filter was then moved to a spacing of 6.5 inch, the flaw covered and the light turned on. The filter survived two 5 second exposures with no further visible effect.

Suggestions:

I would suggest that as the filter making procedure gets more advanced and we began to turn out flight quality filter we rerun this test. Then the flight filter(s) should be tested here and at Goddard. In the Goddard test I suggest a full 5 minute exposure to radiation whose spectral content is the same as the sun.

$

TO: Distribution

FROM: P. CHEIMETS

DATE: SEPTEMBER 26, 1984

SUBJECT: Results of NIXT Filter Test

Four filters resembling those that will be flown on the NIXT rocket experiment were tested in a solar simulator. All four filters withstood 2 solar constants, those that were exposed to a radiation level equal to 4 times that of the sun were melted instantly.

The solar simulator consisting of a 550 watt bulb and a stand to support the filters was placed in a vacuum chamber. The filters were placed at various distances from the lamp. The first two filters were tested at 9.5 inches, 6.6",4.6",3.75" and 3.25" and exposed for 3 seconds. This corresponds to .5,1,2,3,4 times solar equivalent radiation flux level (Cs) respectively. The two filters each had an aluminized surface facing the lamp and a graphite coated surface facing away. One of the filters was cut by accident during handling. In spite of this the cut filter survived all the exposures until 3.75". The uncut filter melted at 3.25" (4XCS).

A third filter prepared the same way was exposed to the lamp at 3.25" (4XCs) and melted immediately.

Finally a fourth filter, this one with both sides graphited and one side aluminized, was tested. It was exposed at 6.6",5.5" (1.5XCs) and 4.6" each for 3 seconds. The filter survived all exposures.

These methods of preparation seem adequate to assure that the filters will survive direct exposure to the sun. A few filters should be made in the flight frames and tested. There appears to be a strain level dependence in the melting temperature. If these survive, and there seems little doubt that they will, the flight filters should be made, tested here to at least 1.5XCs and then tested in the NASA solar simulator for 350 seconds, the mission duration.

Distribution:

David Boyd
Bruce Dias
John Gerdes
Leon Golub
George Nystrom

2. Vibration Test Specifications and Bonding Procedures

TO: George Nystrom
Leon Golub
Lester Cohen

ORIGINAL
OF POOR QUALITY

FROM: Peter Cheimets

DATE: July 19,1984

SUBJECT: Vibration Specification for Nixt Primary Mirror

SCOPE:

This specification describes the test procedure of the NIXT primary mirror assembly in vibration loads resembling those expected during launch. The test, setup, required equipment, personnel and reported data are outlined.

TEST ARTICLE:

The mirror ring (NIXT-1000) with a flat mirror blank bonded in place will be subjected to vibration loads described in table 1. These conditions are suggested by NASA for "prototype" testing of designs intended to be launched using a Black Brant motor. The components that will be tested are the mirror ring, mirror blank, epoxy bond, and the mounting scheme.

TEST SET-UP:

The mirror/ring will be mounted, by means of an adapter, to the shake table (see figure 1). The adapter will be provided by SAO. It will be bolted to the 16 inch bolt circle on the shake table using bolts torqued to a minimum of 16 ft-lb. The mirror assembly will be mounted to the adapter with standoffs. The mirror mounting bolts will be torqued to between 14 -16 ft-lbs. A control three-axis accelerometer will be mounted to the adapter and a second three-axis accelerometer will be mounted to the edge of the mirror. The Z or thrust and one cross axis will be tested in this way (see fig 2).

REQUIRED EQUIPMENT:

This test will require:

1) Torque wrench,

2) Two 3-axis accelerometers with signal conditioning electronics and recording devices for each channel,

3) An adapter plate supplied by SAO.

TEST SEQUENCE:

1) Sine sweep Z-Z,

2) Random Z-Z,

3) Sine sweep cross axis,

4) Random cross axis,

EXAMINATION, DURING TEST:

The assembly will be thoroughly examined between tests to determine if the mounting bolts have loosened, the adhesive weaked or the mirror cracked. Any unusual changes will be noted before proceeding.

EXAMINATION, POST TEST:

Visual examination of all the components for signs of deterioration due to the vibration loads. The ring and blank will then be wrapped to protect the surfaces, boxed for transport back to IBM.

TEST REPORT:

The test report should include:

1) The output of the three-axis accelerometers from both the sine sweep and the random vibration tests;

2) Graphs of the frequency content of the random vibration tests;

3) Present engineering judgement of the success or failure of the design, any recommendations and calculations.

$

TABLE 1

	Black Brant V and Nike Black Brant V		Composite for Components	
	Design Qualification	Flight Acceptance	Design Qualification	Flight Acceptance
Balance	See Note*			
1. Static		300 oz-in**		
2. Dynamic		20,000 oz-in²**		
Vibration				
1. Sinusoidal				
Sweep Rate	2 oct/min-prototype 4 oct/min-protoflight		2 oct/min-prototype 4 oct/min-protoflight	
Thrust Axis	±5.76 in/sec | 5-24 Hz ±2.3 g | 24-110 ±5.3 g | 110-800 ±15.0 g | 800-2000		±11.07 in/sec | 5-35 Hz ±11.3 g | 35-800 ±15.0 g | 800-2000 ±30 g | 2000-3000	
Lateral Axes	Same as for thrust axis.		Same as for thrust axis.	
2. Random				
Duration	20 sec/axis-prototype 10 sec/axis-protoflight	10 sec/axis	20 sec/axis-prototype 10 sec/axis-protoflight	10 sec/axis
Thrust Axis	19.1 g-rms | Overall 0.023-.225 g²/Hz | @ 1.8 db/oct. | 20-1000 Hz 0.225 g²/Hz | 1000-2000	12.7 g-rms 0.010-.10 g²/Hz @ 1.8 db/oct. 0.10 g²/Hz	22.5 g-rms | Overall 0.256 g²/Hz | 20-1000 Hz	15.0 g-rms 0.114 g²/Hz
Lateral Axes	Same as for thrust axis.	Same as for thrust axis.	Same as for thrust axis.	Same as for thrust axis.
3. Shock/Transient			Twice-prototype Once-protoflight 60 g acceleration | 10 Hz to 30 g in | thrust axis 4 cycles | only.	

ORIGINAL PAGE IS OF POOR QUALITY

6/1/78

*Note: Balance is not required for prototype (non-flight) models. For protoflight models, use flight acceptance balance specification.

**Note: Combined static and dynamic unbalance must be plottable within the rectangle whose legs are the specified values.

REVISIONS				
ZONE	LTR	DESCRIPTION	DATE	APPROVED
	A	INITIAL RELEASE	7-18-84	

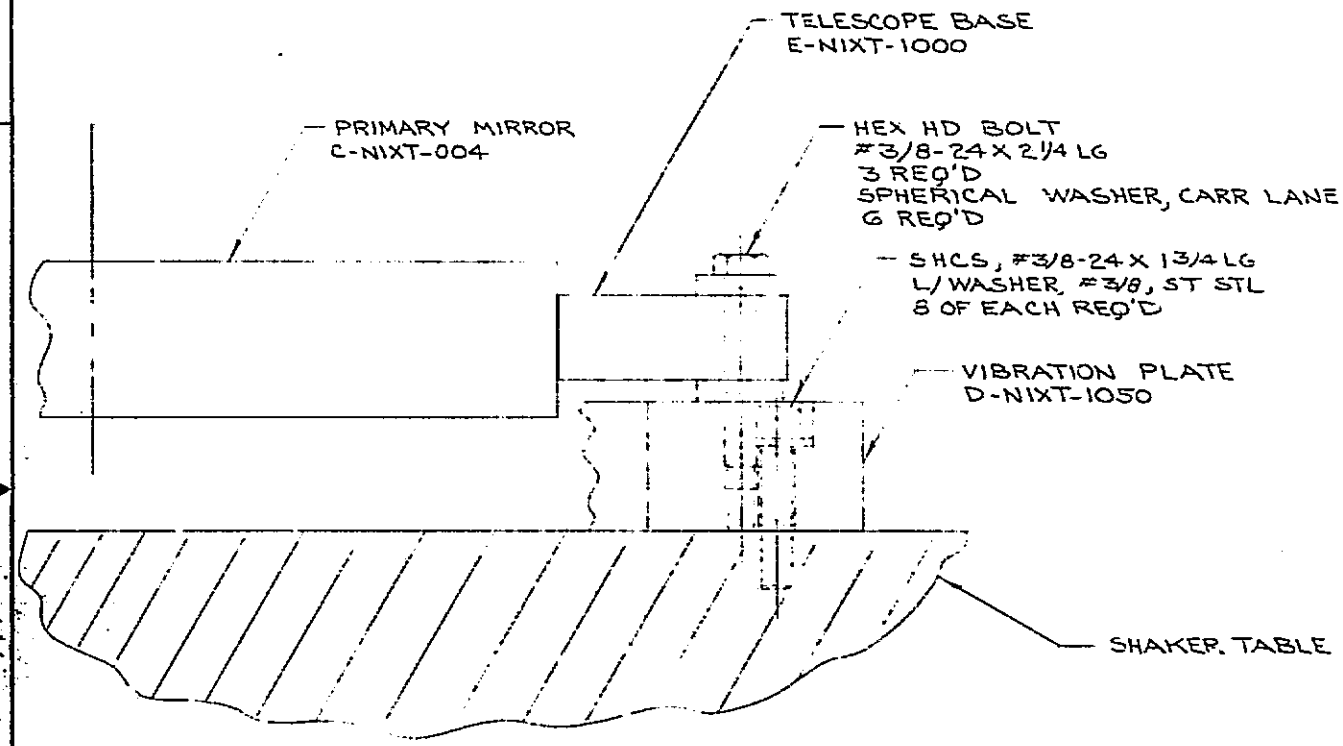

ORIGINAL PAGE IS
OF POOR QUALITY

QTY	ITEM OR FIND NO.	DWG SIZE		PART NO. OR IDENTIFYING NO.	DESCRIPTION

PARTS LIST

UNLESS OTHERWISE SPECIFIED DIMENSIONS ARE IN INCHES
TOLERANCES ON
FRACTIONS ± DECIMALS .xx ± .xxx ± ANGLES ±

MACH FIN: ✓
HT TR:
FIN:
MATL:

DR J. LOGAN CHK
DATE 18 JULY 84 DATE
DSGN APPD
DATE
ENGR APPD
DATE
PROJ APPD
DATE
OTHER APPD
DATE

NEXT ASSY	USED ON
	NIXT
APPLICATION	

SMITHSONIAN ASTROPHYSICAL OBSERVATORY CAMBRIDGE, MA.

TITLE
VIBRATION TEST ASSY
PRIMARY MIRROR, NIXT

SIZE	CODE IDENT NO.	DWG NO.	REV
C	50944	NIXT-509	A

SCALE FULL SHEET 1 OF 1

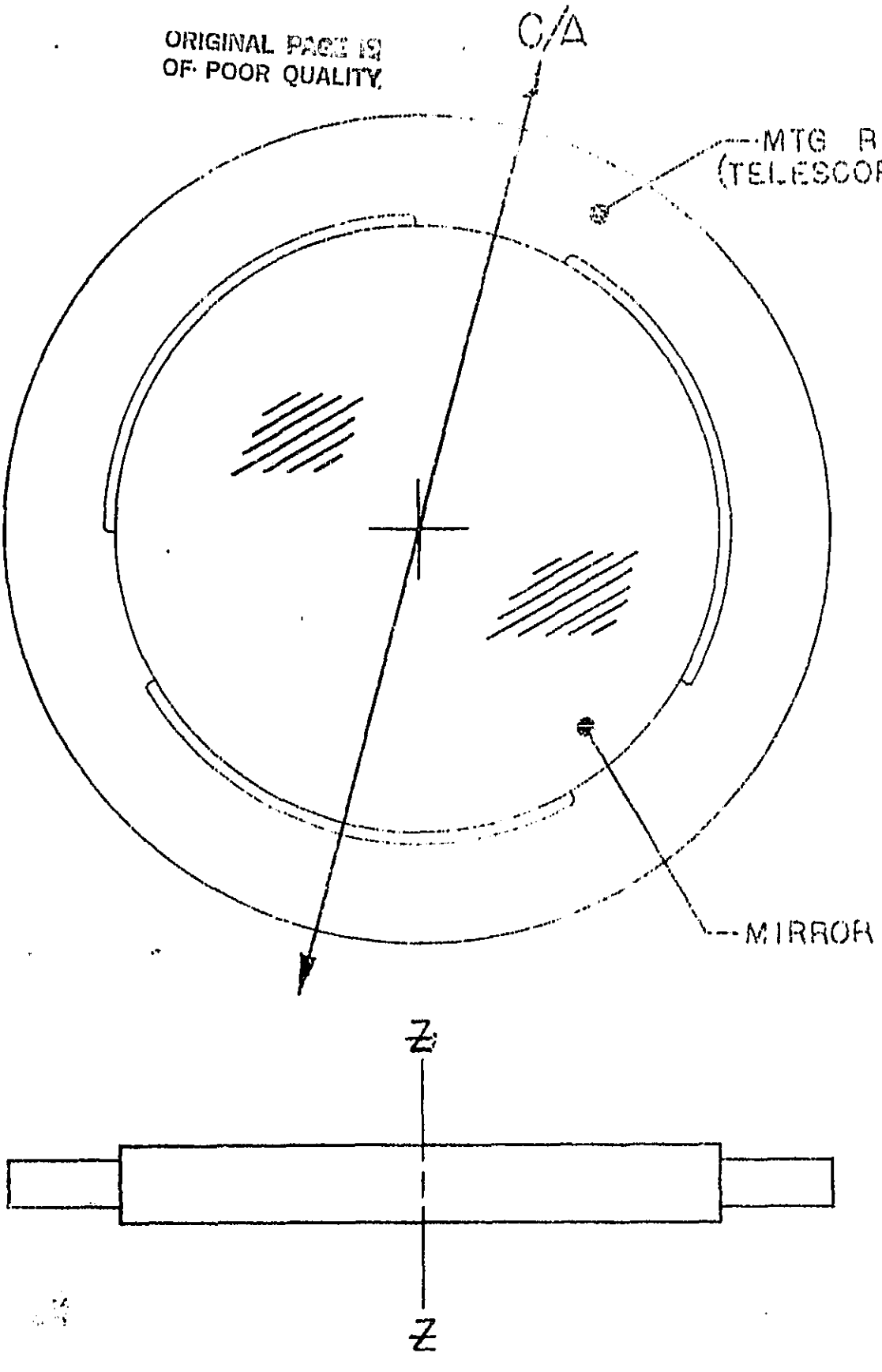

FIGURE 2

TO: Distribution

FROM: Peter Cheimets

DATE: August, 1984

SUBJECT: Report of Bonding and Test a Mirror Blank for NIXT

Scope:

This memo describes the procedures used in bonding a mirror blank into the NIXT flight base ring and the testing of this subassembly of the NIXT telescope. It also presents the results of those tests and discusses planned future actions.

Pre Bond Test:

The optical flat was polished by IBM. We measured it in their ZYGO interferometer. The plate measured out to be flat to a 1/50th of a wave RMS. The fringe lines were straight and evenly spaced for all of the central portion of the optic. The mirrors thickness was measured at 46.61 mm.

Bonding:

The blank and ring were scrubbed with acetone at the bond locations. The blank was then set on a stone surface plate with a sheet of plastic between it and the plate. Three Job block stacks each 10.60 mm high were placed at 120 degrees around the mirror to support the ring (See fig 1.). This height brought the center point of the ring, and thus the center of the bond, in line with the center point of the mirror. Care was taken so that the block did not sit on a wrinkle in the plastic or under a hole in the ring and thus tip the plane of the ring. The locations of the job blocks were then marked on the ring.

The epoxy (HYSOL 9313) was mixed in two batches, the extra for spare. It was de-gassed somewhat less than adequately as a good vacuum jar was not available at IBM. The epoxy was then let to stand for about 1.25 hours to increase its viscosity. The epoxy was injected by means of a 50 cc syringe into the three bond joints. The adhesive was observed through the flat to see that it filled, released the remaining bubbles and wetted the surface of the glass. This all seemed to go fine and there were only one or two bubbles visible in the bonds. The assembly was left on the surface table for a week before anything was moved to permit the epoxy to set up completely.

Post-Gluing Tests:

A static strength test was performed by IBM. IBM placed about 200 lbs. of lead on the ring to determine if the epoxy had at least that much strength. This had no visible effect on the bond. The mounted optic was then put into the interferometer and the quality of the flat was measured again. The surface had noticeably deteriorated. It was about a 1/20th of a wave surface. The class of the surface could be described as a dish though this could only be inferred. There was more marked distortion at the areas near the bond but there was visible change throughout the surface.

Two biaxial strain gages were placed on the unpolished side of the mirror. They were placed on a radial line beginning at the center point of one of the gluing pads. One at the edge of the flat and the other at the center. They were aligned with each other and oriented such that one axis of each gage was parallel to the tangent of the flat at the bisected gluing pad (see fig 2). The gages were tested and their output was found to be very low, this was attributed to the thickness of the flat.

The assembly, along with an adapter plate were brought to Stanford Technologies in Connecticut. Here the mirror/flat was tested per a shake spec written July 19, 1984. Basically the flat was given the vibration load suggested by NASA for all prototypes of payloads to be flown on a Black Brant missile. The test was performed on two axes, one perpendicular to the optical axis and along the radial line on which the strain gages were mounted, the other parallel to the optical axis. The assembly was to be given both a sine sweep from 5 to 2000 Hz and a 19.6 g rms random shake in each axis.

Shake Tests:

Cross Axis:

The cross-axis was tested first. The adapter was bolted directly to the slide table. The ring was initially attached to the adapter by three screws with spherical washers above and below the plates (See Fig 3.) During the procedure some problems were encountered. The sine sweep showed a strong individual resonance at 1000 Hz. The quality of this singularity was so high that the shake table was an able to drive the specified g-level in that frequency range. The mounting arrangement was changed eliminating the spherical washers and bolting the ring directly to the adapter. This shifted the resonance up scale to 1800 Hz. The quality of this resonance was still too high for the slide table to drive. The frequency range was then truncated at 1800 Hz for both the sine and random vibration. Both test were performed with no visible deterioration in the bond and no large strains measured in the gages.

Optical Axis:

The mounting was then changed to shake along the optical axis. This was done by removing the slide table, rotating the shaker 90^{o} and bolting the assembly directly to the shaker. The sine sweep in the optical axis showed a family of fairly strong resonances around 1000 Hz. These were not strong enough to hinder running the test as specified. When the random shake was run a distinct change in sound was observed in the start up segment of the test. The test proceeded with no further incident.

Post Test:

Examination of the glue joints after testing showed that two of them had partially parted taking some of the glass with them. The mirror was still soundly attached to the plate. The change in sound was attributed to this bond breakage.

The flat was brought back to IBM and once again placed on the interferometer. The quality of the surface was unchanged both in surface flatness and in shape. Review of the type of failure and the resonances measure indicate that an "oil can" mode was set up in the telescope ring causing high moment loads in epoxy. The loads tended to pull the adhesive away from the glass. The joint, thus relieved, could no longer transmit the high loads, yet could still support the shear force. In this way the assembly was able to hold together under later vibration loads.

Future:

The optical flat will be sawn out of the ring and photographed by IBM. This will give us a better view of the exact nature of the cracking in the glass. In the mean time we are reviewing possible mounting and bonding alternatives for the next pass. Lester is working up a number of models of these alternatives and we will make a list of candidate arrangements that should reduce both the likelihood of bond failure and distortion in the mirror. The methods under review each endeavor to create a bond that acts as a hinge when a moment is applied to the bond yet still supports shear loading. In this way we hope to create the bond arrangement that resulted by accident this go around.

Two approaches are:

1) Notch the ring to create a cantilever (See fig 4a) and glue to the cantilever. The cantilever will be unable to pass large stresses to the glass as a movement is applied to the joint.

2) Place a U-shaped piece of metal in the joint (See fig 4b). The metal will flex if a moment is applied yet be fairly stiff for any shear loads.

Distribution:
G. Nystrom
D. Boyd
B. Dias
L. Cohen
L. Golub
D. Goddard
J. Gerdes
File

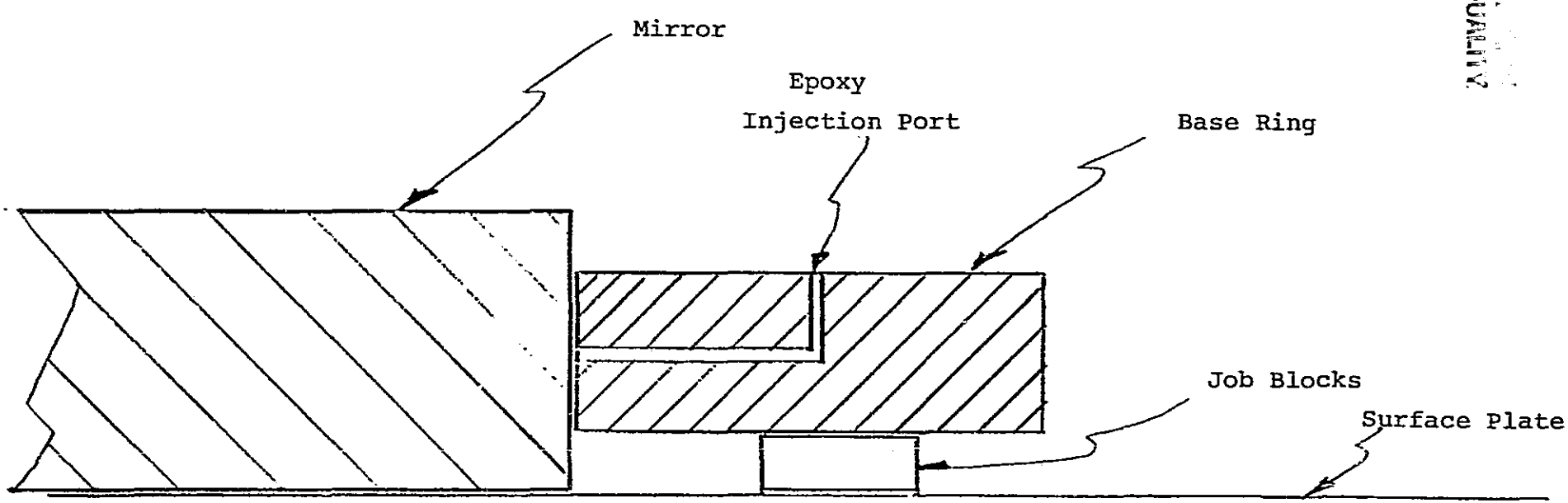

Fig 1 Bonding Assembly

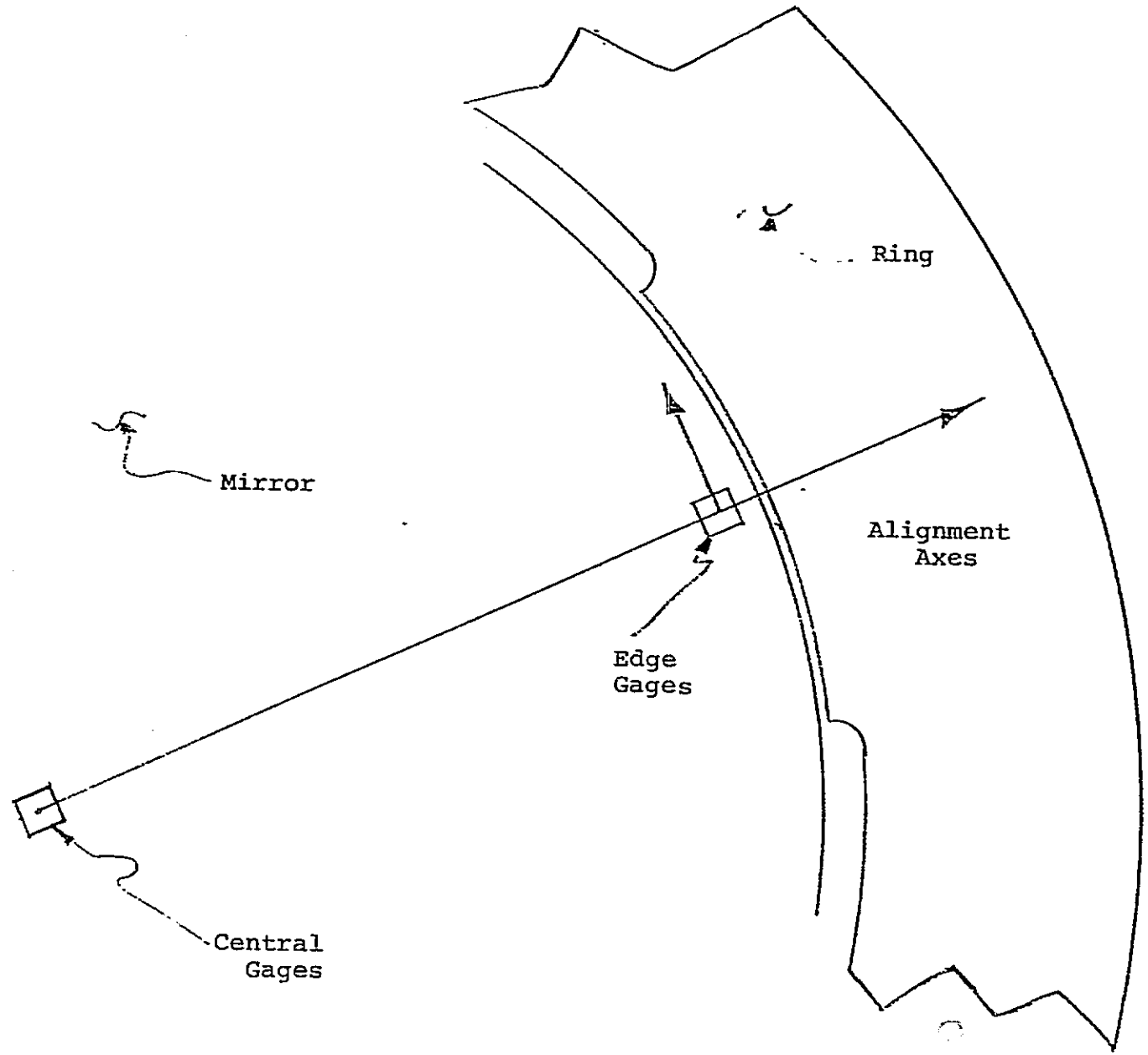

Fig 2 Strain Gage Alignment

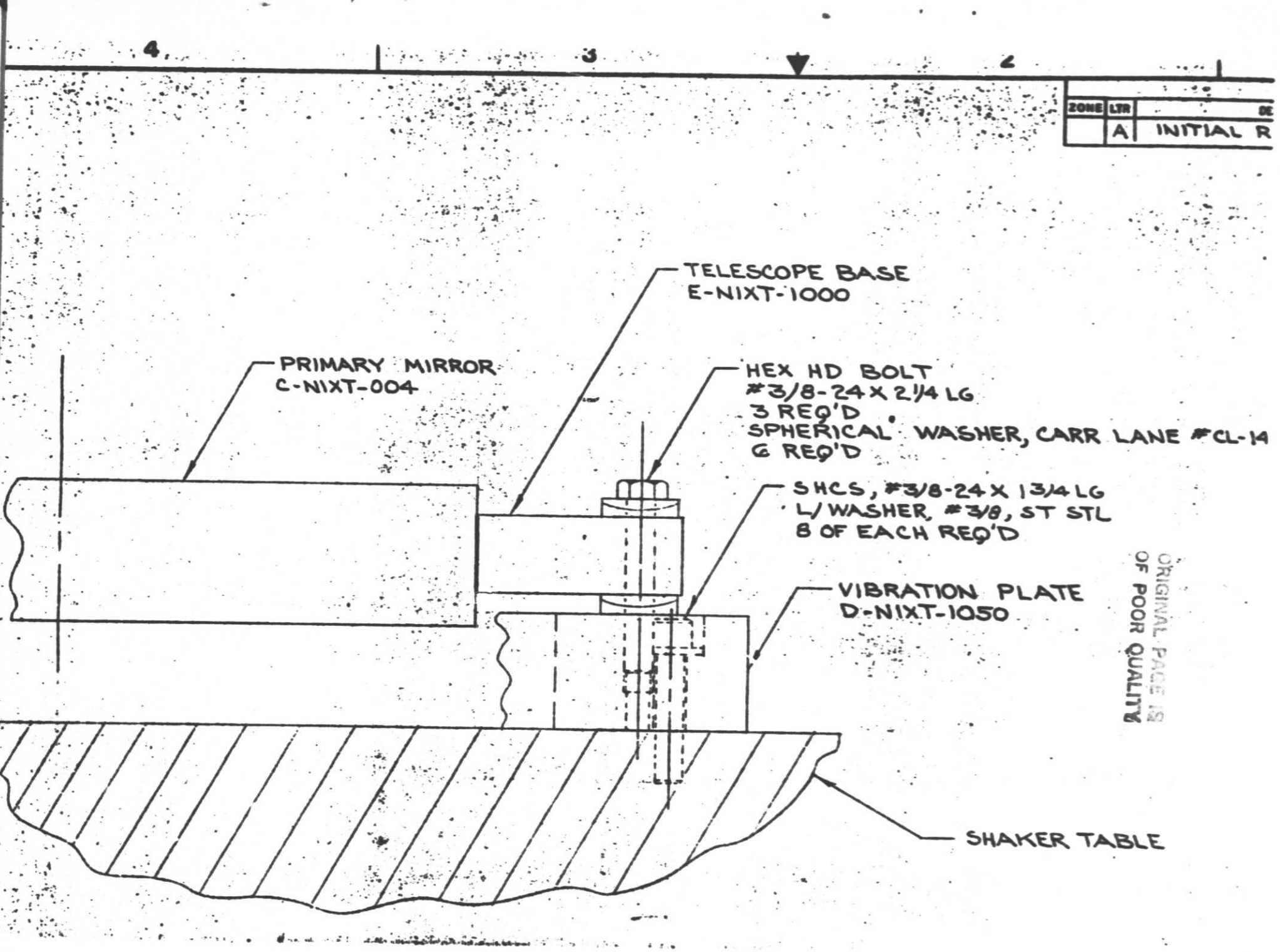

Fig 3 Shake table mounting

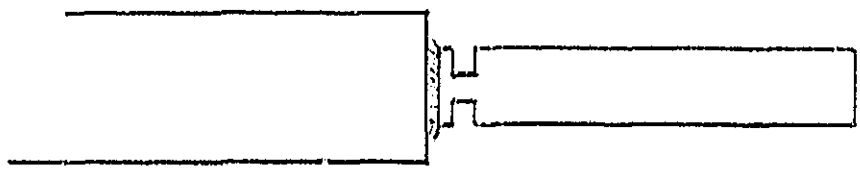

Fig. 4A Milled Ring to Reduce Stress

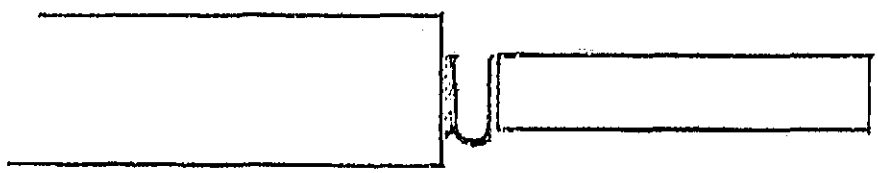

Fig. 4B U-Spring

3. Hasselblad Camera Flight Qualification Tests

TEST REPORT No. 04003

500 EL/M modified for Smithsonian Institution

Project No. 60332

Tested by Saab Space, Göteborg

Participants: Claes Mårtensson SQM, Saab Space
Stig Ekberg, Quality Dept, Hasselblad
Leif Ahlning, Spec Appl Dept, - " -

Appendix

1984-07-31

Leif Ahlning/Special Applications Department

LA/th

Projektnummer: 60352
Forstärkt 500 EL/M for sondraket

TESTSCHEMA

		Composite for Components: Design Qualification	
Vibration 1. Sinusoidal Sweep Rate	Totalvikt: 1900 g	2 oct/min-prototype	
Thrust Axis	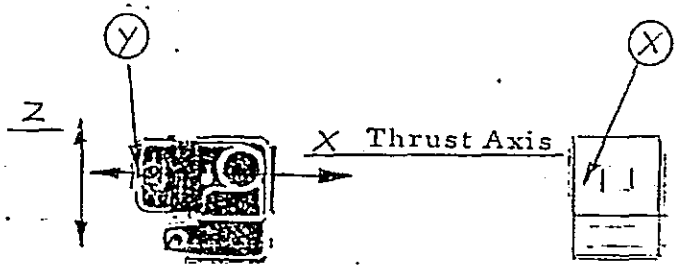	±11.07 in/sec | 5-35 Hz ±11.3 g | 35-800 ±15.0 g | 800-2000 ±30 g | 2000-3000	
Lateral Axes		Same as for thrust axis.	
2. Random Duration		20 sec/axis-prototype	
Thrust Axis	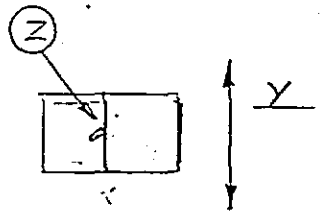	22.5 g-rms | Overall 0.256 g^2/Hz | 20-2000 Hz	
Lateral Axes		Same as for thrust axis.	
3. Shock/Transient		Twice-prototype	
		60 g decaying to 30 g in 4 cycles | 96 Hz Thrust axis only.	

The camera function shall be tested with 5-10 exposures after each test.

(x) (y) (z) indicate the placing of the accelerometer for the resonance searching.

Date: 1984-06-05

Test	Direction	Mag	Mag Weight	Comment
Sinusodial vibration	X	70	616 g	Film wind rewinder at magazine over to red. Went back after one exposure. Otherwise 5 exposures OK.
Sinusodial vibration	y	70	616	Film wind rewinder and frame counter out of order. Otherwise 5 exposures OK.
Sinusodial vibration	z	70	616	Film wind rewinder and frame counter out of order. Otherwise 5 exposures OK.
Random duration	z	70	616	Film wind rewinder and frame counter out of order. Otherwise 5 exposures OK.
Random	z	100/200	599	5 exposures OK.
After changing films in the 70-magazine the film wind rewinder and the frame counter started to work.				
Random duration	y	70	654	5 exposures OK.
- " -	y	100/200	599	5 exposures OK.
- " -	x	100/200	599	Film wind rewinder at magazine went over to red. Went back after one exposure. Otherwise 5 exposures OK.
- " -	x	70	654	- " -.

Test	Direction	Mag	Mag	Weight	Comment
Shock twice		70	654		The camera made one exposure directly after both chocks. Otherwise 5 exposures OK.
Shock twice		100/20	599		The camera made one exposure directly after both shocks. After the second shock the magazine had shook itself loose from the camera body (see sketch). Apart from that the camera body was still functioning.

Comment: The clearance between the camera body and magazine had increased gradually during the test.

The external plate of the magazine was deformed.

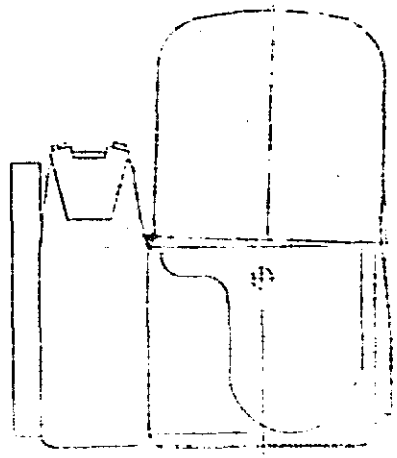

Adjustments and Reinforcements made after the first test

Adjustments: The outer plate of the magazine was rechanged.

Reinforcements:

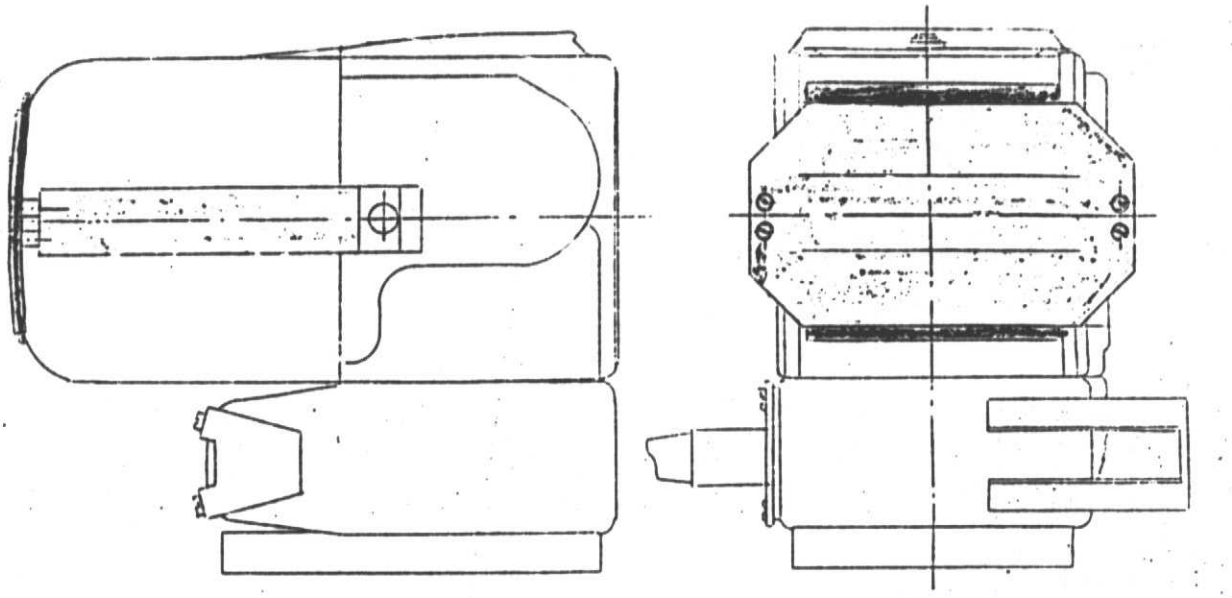

Second test

Date:	1984-06-13
Test:	Shock
Magazine:	70, weight 654 g.
First shock:	The camera made an exposure directly after the shock. Otherwise 5 exposures OK.
Second shock:	The camera was blocked. The magnet arm had turned over to the wrong side of the release lever.
	The camera was repaired directly.
Third shock:	The magazine shook itself loose from the camera body in the same way as in the first test. The outer plate at the magazine was deformed.

Reinforcements and adjustments after the second test

Adjustments: The magnet arm was lengthened in order to restrain the type of blocking as in the second test.

The outer plate at the magazine was rechanged.

Reinforcements:

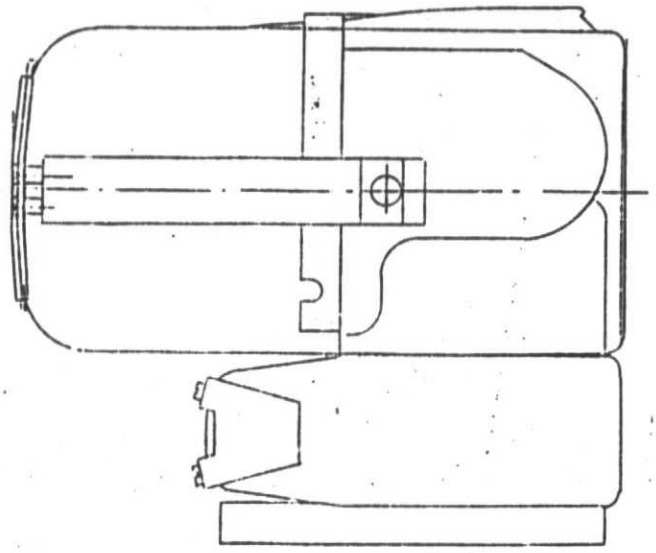

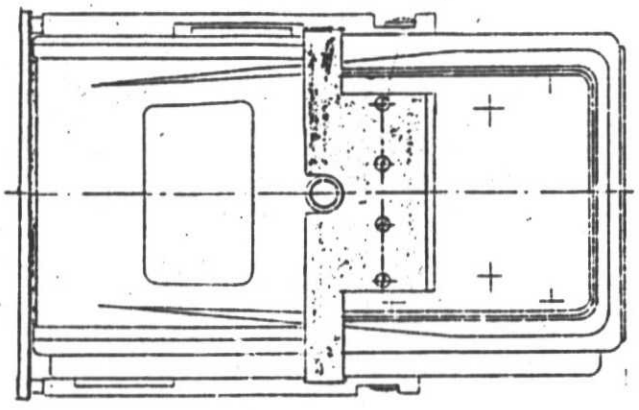

Third test

Date:	1984-06-27
Test:	Sinusodial vibration and shock
Magazine:	70, weight, 654 g.
Sinusodial vibration in y-direction:	5 exposures, all functions OK.

Note: In this direction, in the first test the film wind rewinder and frame counter went out of order.

Shock, twice:	The camera made an exposure directly after both shocks. Otherwise all functions OK.
	The spring between outer plate and magazine support was deformed.
Comments:	During the shock test one could see the magazine shaking in the direction as shown below.

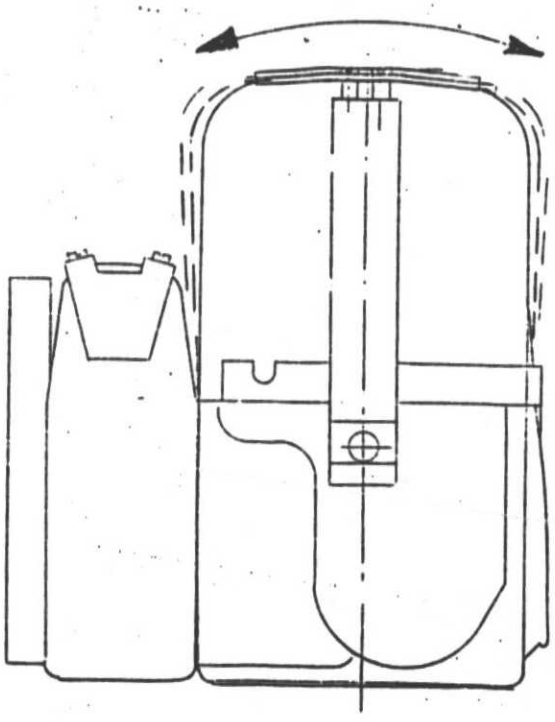

Adjustments made after third test

The springs (13821) between outer plate and magazine support were rechanged.

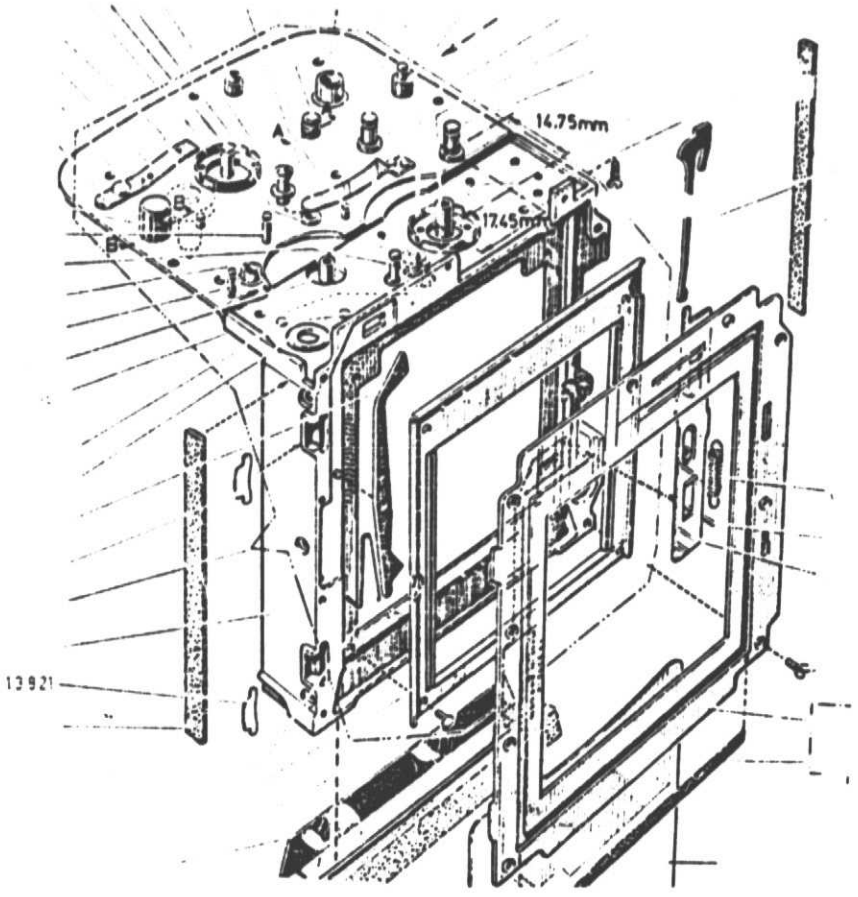

SAAB-SCANIA

ACCELERATIONSNIVÅ-DIAGRAM

Provföremål	Mätpunkt	Mätriktning	Mätpunkt	Mätriktning	Datum
500 EL/I Magazine 70	Magazine 70	X			1984-06-05
Vibrationsriktning / **Provning nr**	**Filtrerad**	**Ofiltrerad**	**Filtrerad**	**Ofiltrerad**	**Utförd**
X (THRUST) / Res. Search	yes				Claes P.
Stränghetsgrad	**Bandbredd Hz/Frekvensområde Hz**		**Bandbredd Hz/Frekvensområde Hz**		**Anmärkning**
12 m/s² 2 oct/min	12 % val				

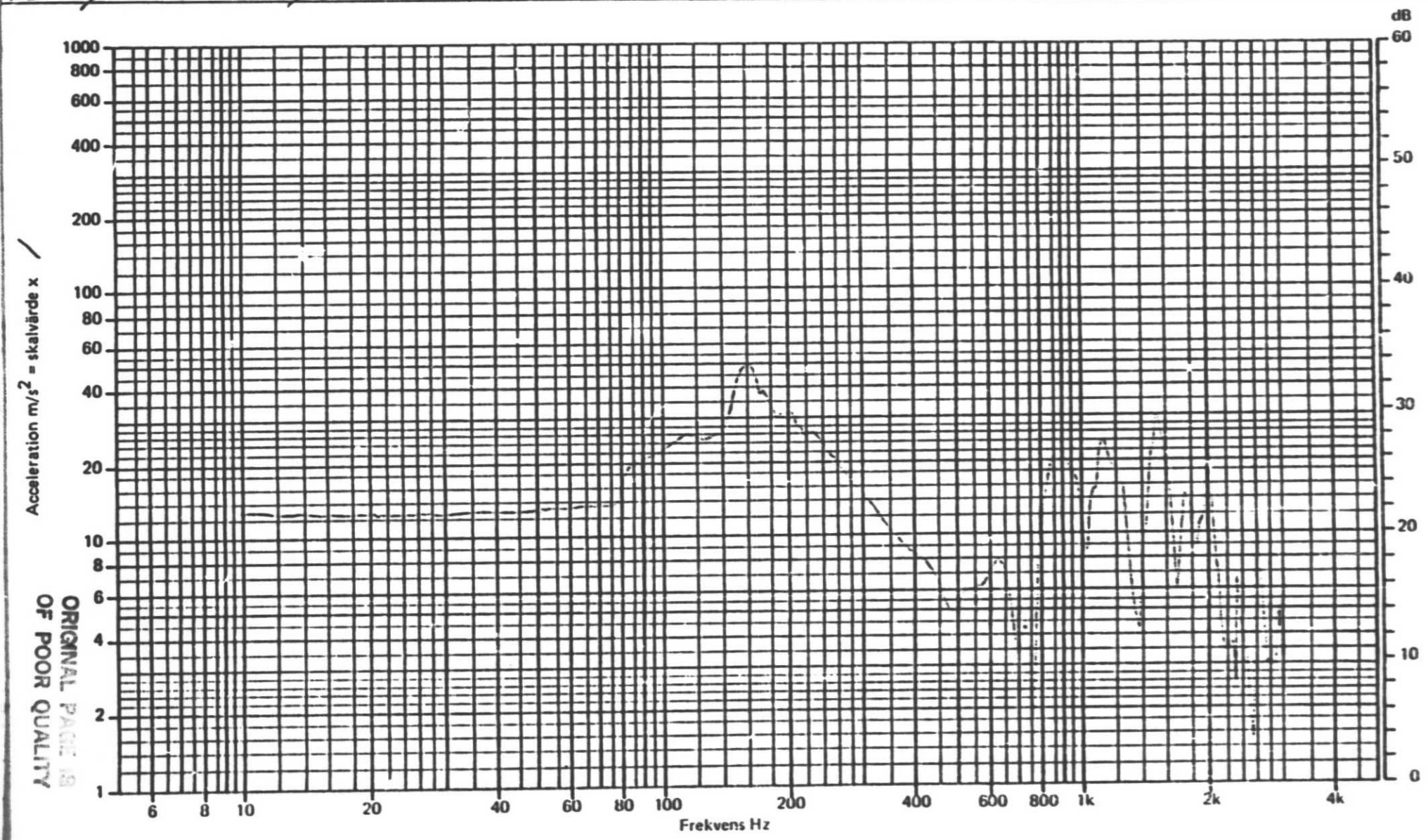

SAAB-SCANIA

ACCELERATIONSNIVÅ-DIAGRAM

Provföremål	Mätpunkt	Mätriktning	Mätpunkt	Mätriktning	Datum
500 EL/oi Magazine 70	Magazine 70	Y			1981-06-05

Vibrationsriktning	Provning nr	Filtrerad	Ofiltrerad	Filtrerad	Ofiltrerad	Utförd
Y	Res. Search	yes				Claes M

Stränghetsgrad	Bandbredd Hz/Frekvensområde Hz	Bandbredd Hz/Frekvensområde Hz	Anmärkning
12 m/s² 2 oct/min	12 % vel		

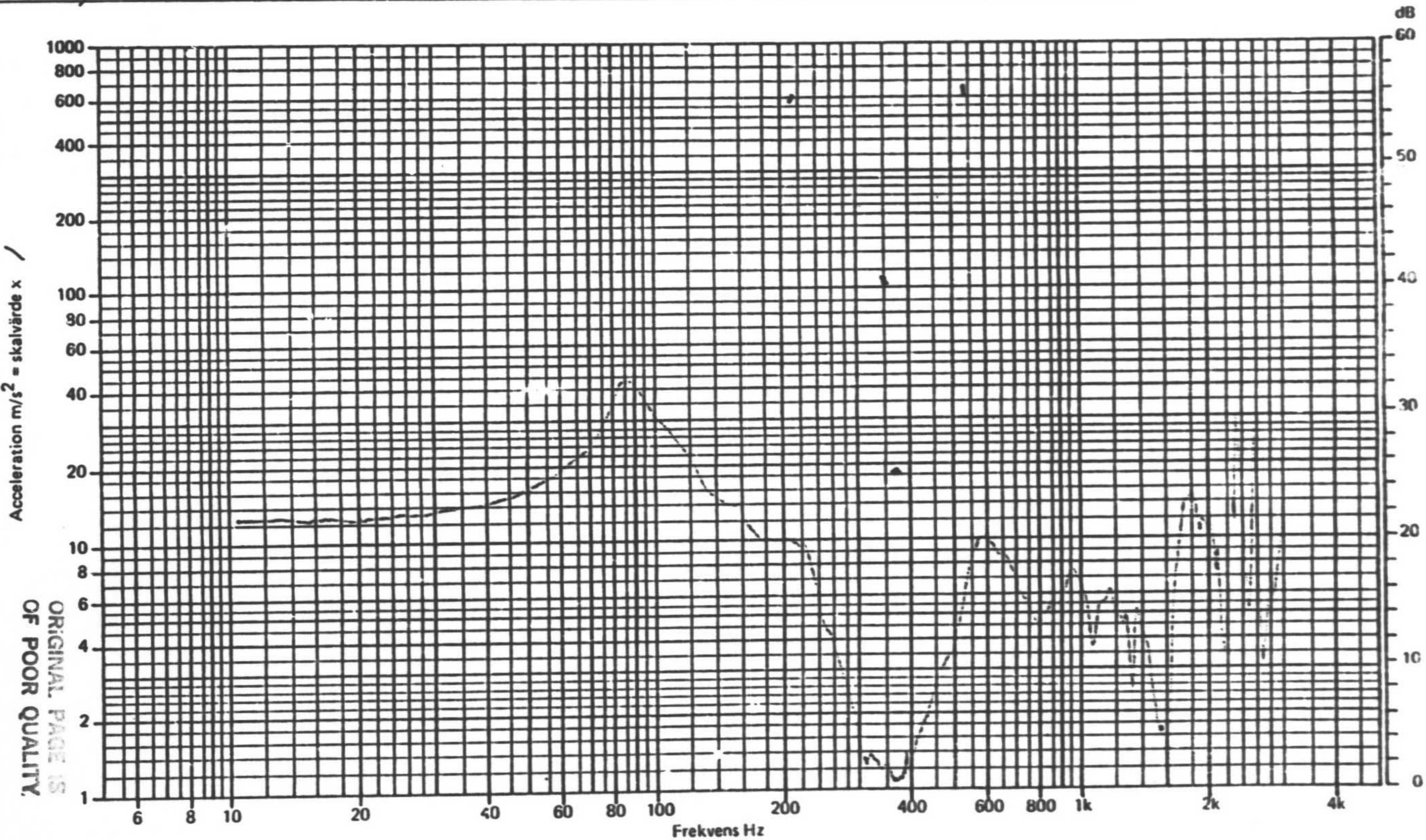

SAAB-SCANIA

ACCELERATIONSNIVÅ-DIAGRAM

Provföremål	Mätpunkt	Mätriktning	Mätpunkt	Mätriktning	Datum
500 EL/M Magazine 70	Magazin 70	Z			1984-06-05
Vibrationsriktning	**Provning nr**	**Filtrerad**	**Ofiltrerad**	**Filtrerad**	**Ofiltrerad**	**Utförd**
Z	Res. Search	yes				Claes P
Stränghetsgrad	**Bandbredd Hz/Frekvensområde Hz**	**Bandbredd Hz/Frekvensområde Hz**	**Anmärkning**
12 m/s² 2 oct/min	12 %		

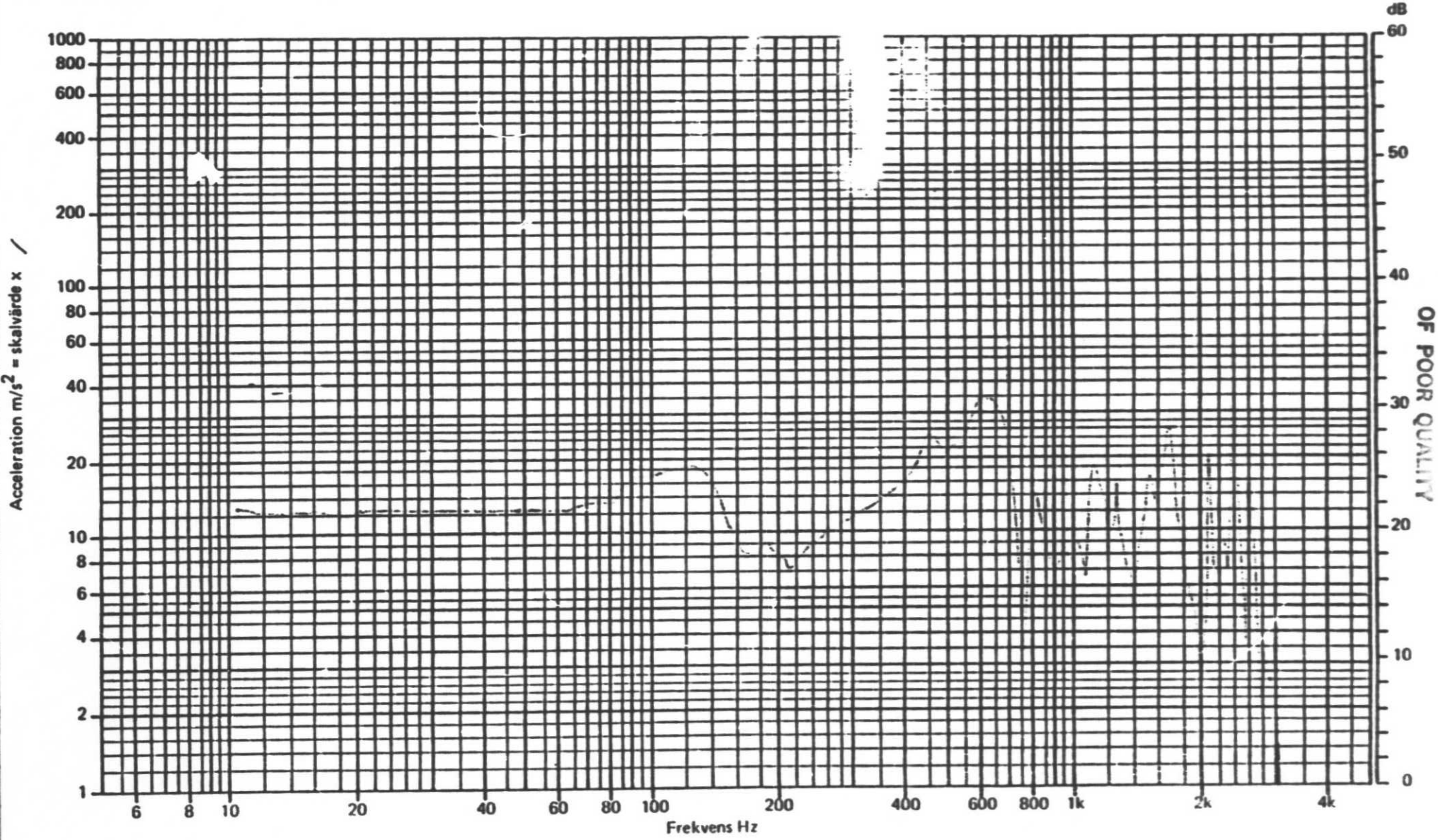

Diagram, shock

First and second test

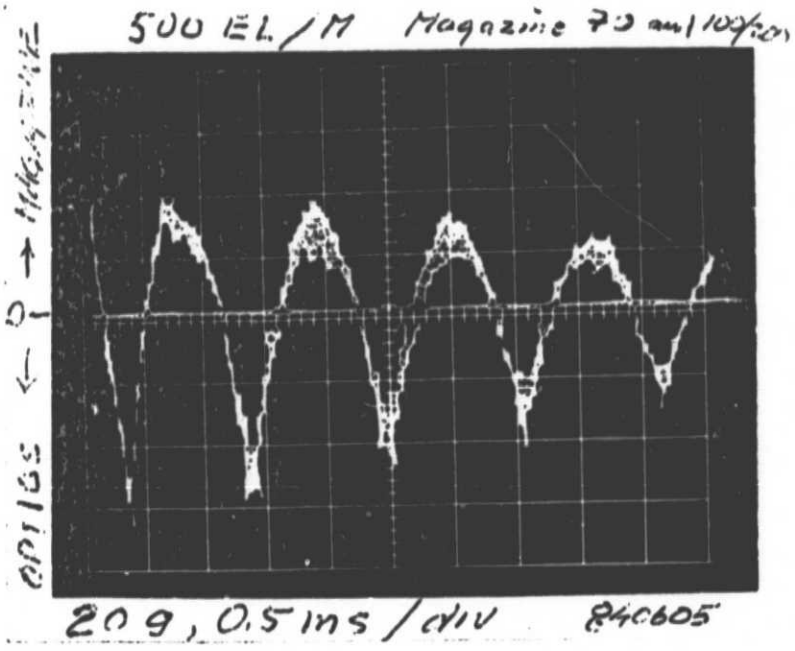

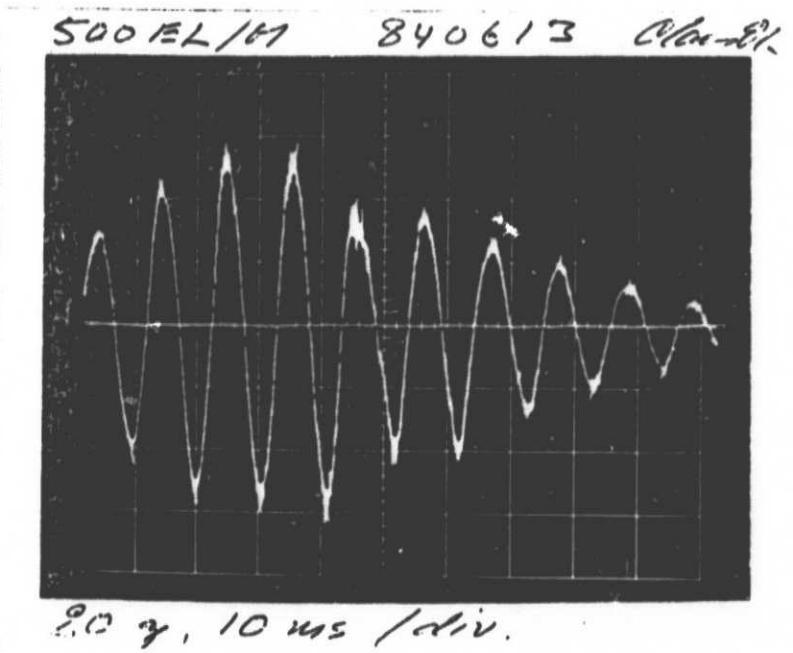

Diagram, shock

Third test

500 GL/M STÖT 1 X- 840627

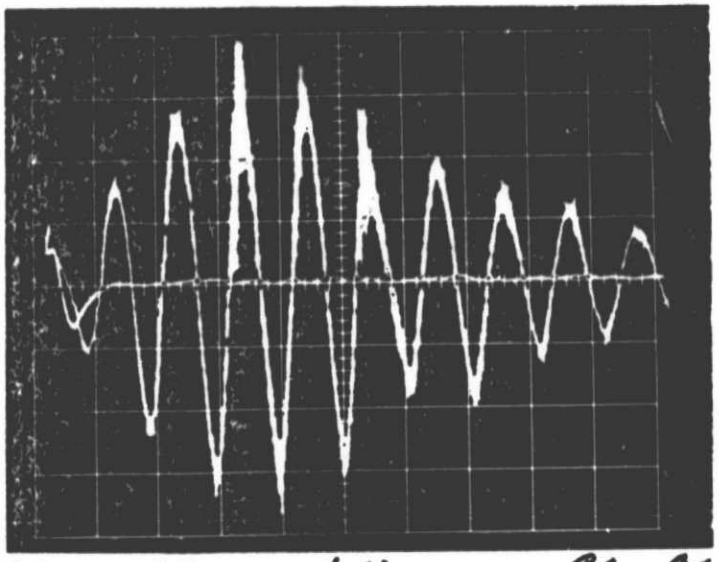

20 g. 10 ms/div Claes M.

500 GL/M STÖT 2 X- 840627

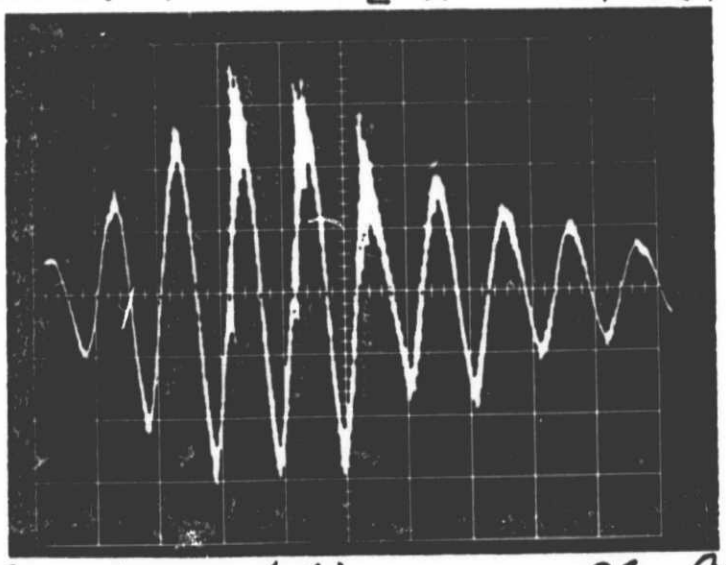

20 g. 10 ms/div Claes M.

SAAB-SCANIA

ACCELERATIONSNIVÅ-DIAGRAM

Provföremål	Mätpunkt	Mätriktning	Mätpunkt	Mätriktning	Datum
500 EL/H Plogspinc 70	Control	x			1991-06-0
Vibrationsriktning / **Provning nr**	**Filtrerad** / **Ofiltrerad**		**Filtrerad** / **Ofiltrerad**		**Utförd**
x / Sin. Endurance	yes				Claes 91
Stränghetsgrad	**Bandbredd Hz/Frekvensområde Hz**		**Bandbredd Hz/Frekvensområde Hz**		**Anmärkning**
2 oct/min	12% rel				

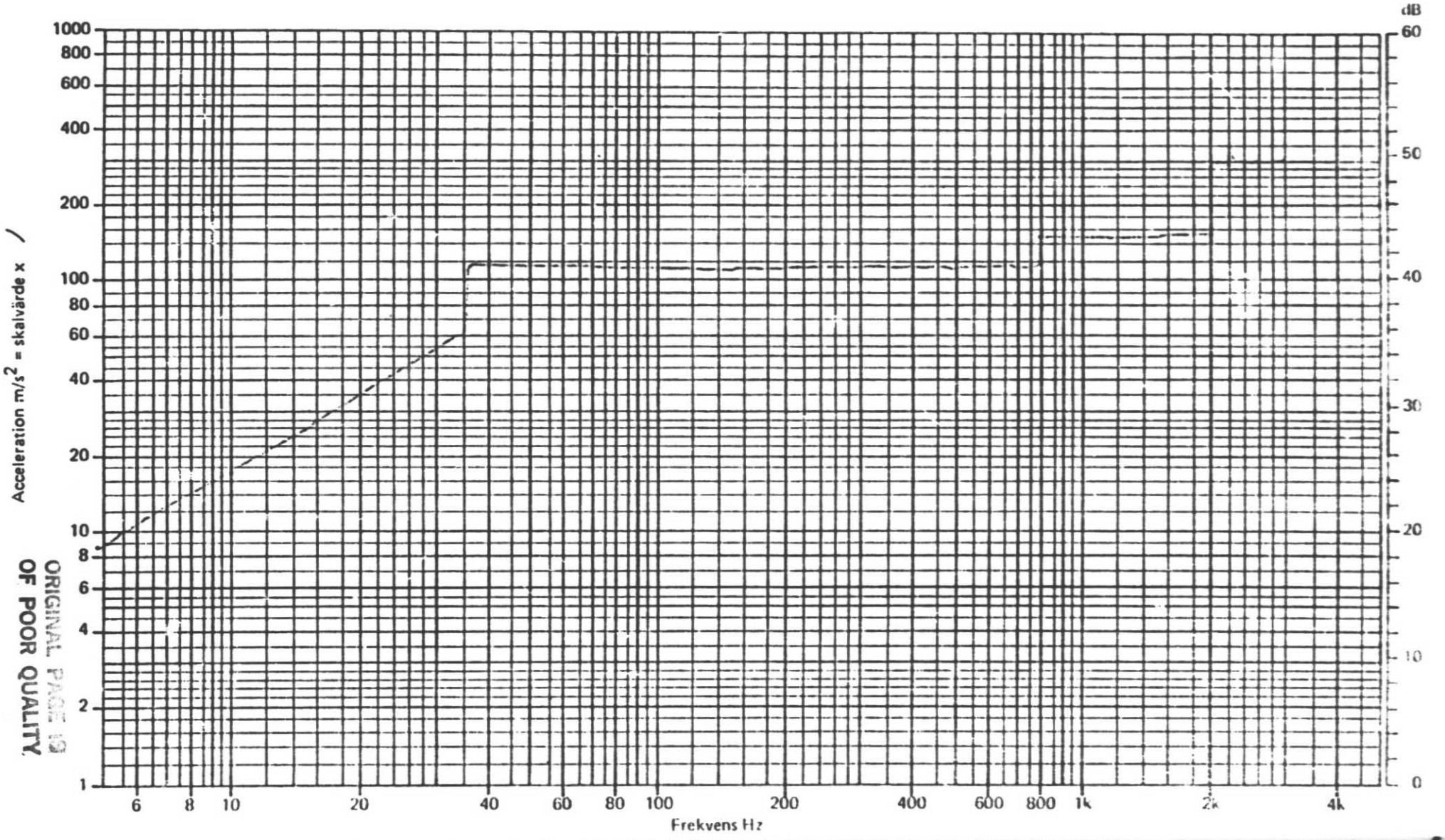

SAAB-SCANIA

ACCELERATIONSNIVÅ-DIAGRAM

Provföremål	Mätpunkt	Mätriktning	Mätpunkt	Mätriktning	Datum
500 EL/E-1 Magazine 70	Control	Z			1981-06-0
Vibrationsriktning / **Provningsnr**	**Filtrerad** / **Ofiltrerad**		**Filtrerad** / **Ofiltrerad**		**Utförd**
Z / Sim. Endurance	Yes				Claes E
Stränghetsgrad	**Bandbredd Hz/Frekvensområde Hz**		**Bandbredd Hz/Frekvensområde Hz**		**Anmärkning**
2 000/min	12 %				

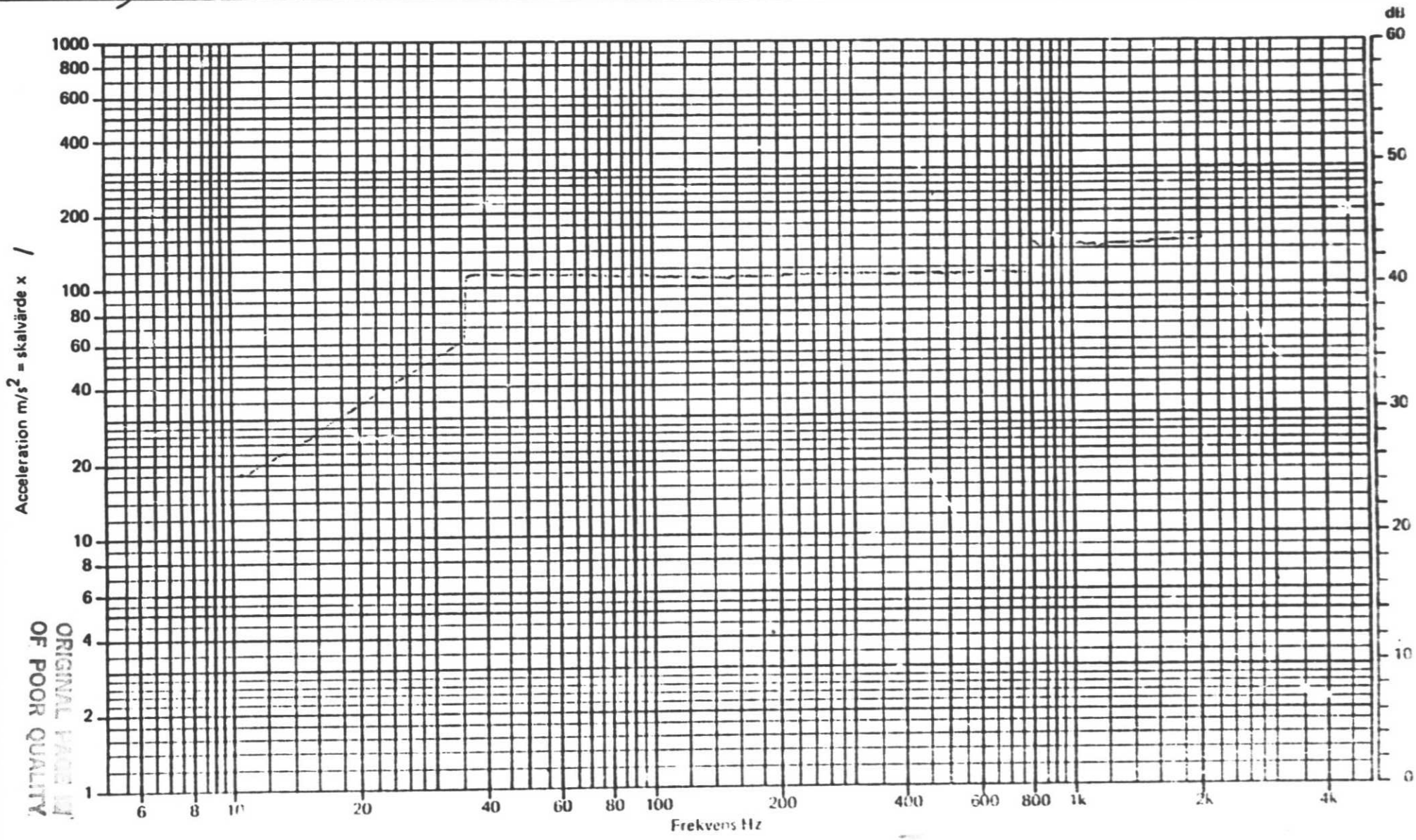

SAAB-SCANIA

ACCELERATIONSNIVÅ-DIAGRAM

Provföremål	Mätpunkt	Mätriktning	Mätpunkt	Mätriktning	Datum
500 EL/41 Magazine 70	Magazine 70				1984-06-0
Vibrationsriktning	**Provning nr**	**Filtrerad**	**Ofiltrerad**	**Filtrerad**	**Ofiltrerad**	**Utförd**
Y	Sin. Endurance	Yes				Olan 91
Stränghetsgrad	**Bandbredd Hz/Frekvensområde Hz**		**Bandbredd Hz/Frekvensområde Hz**		**Anmärkning**
2 octaver/minute	12% rel				

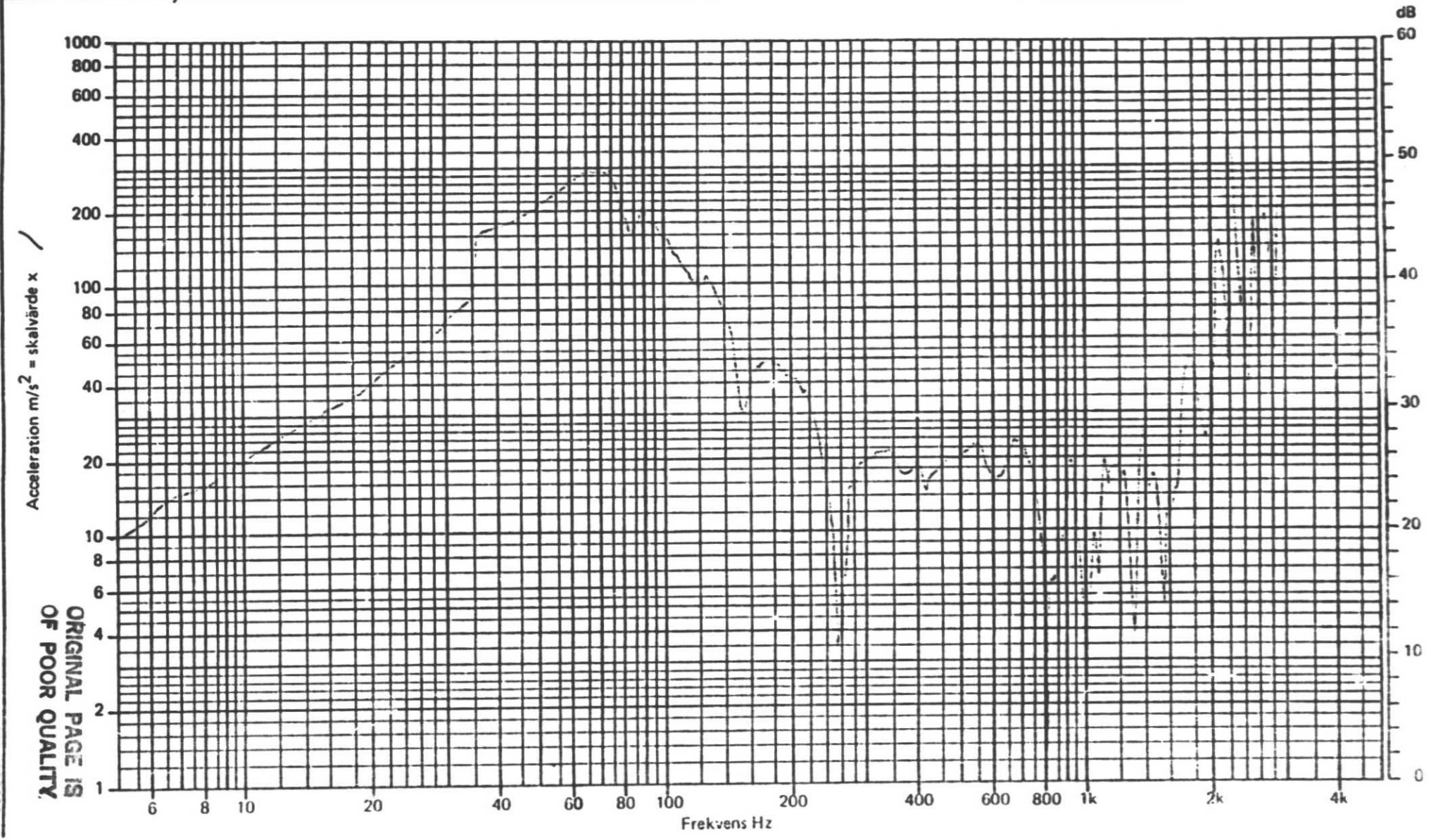

SAAB-SCANIA

ACCELERATIONSNIVÅ-DIAGRAM

Provföremål	Mätpunkt	Mätriktning	Mätpunkt	Mätriktning	Datum
500 EL/H1	Magazine	Y			1984-06-2?
Vibrationsriktning	**Provning nr**	**Filtrerad**	**Ofiltrerad**	**Filtrerad**	**Ofiltrerad**	**Utförd**
Y						Claes 91
Stränghetsgrad	**Bandbredd Hz/Frekvensområde Hz**	**Bandbredd Hz/Frekvensområde Hz**	**Anmärkning**
11.07 IN/SEC 5-35 Hz			

11.3 g 35-800 Hz , 15.0 g 800-2000 Hz , 30.0 g 2000-3000 Hz

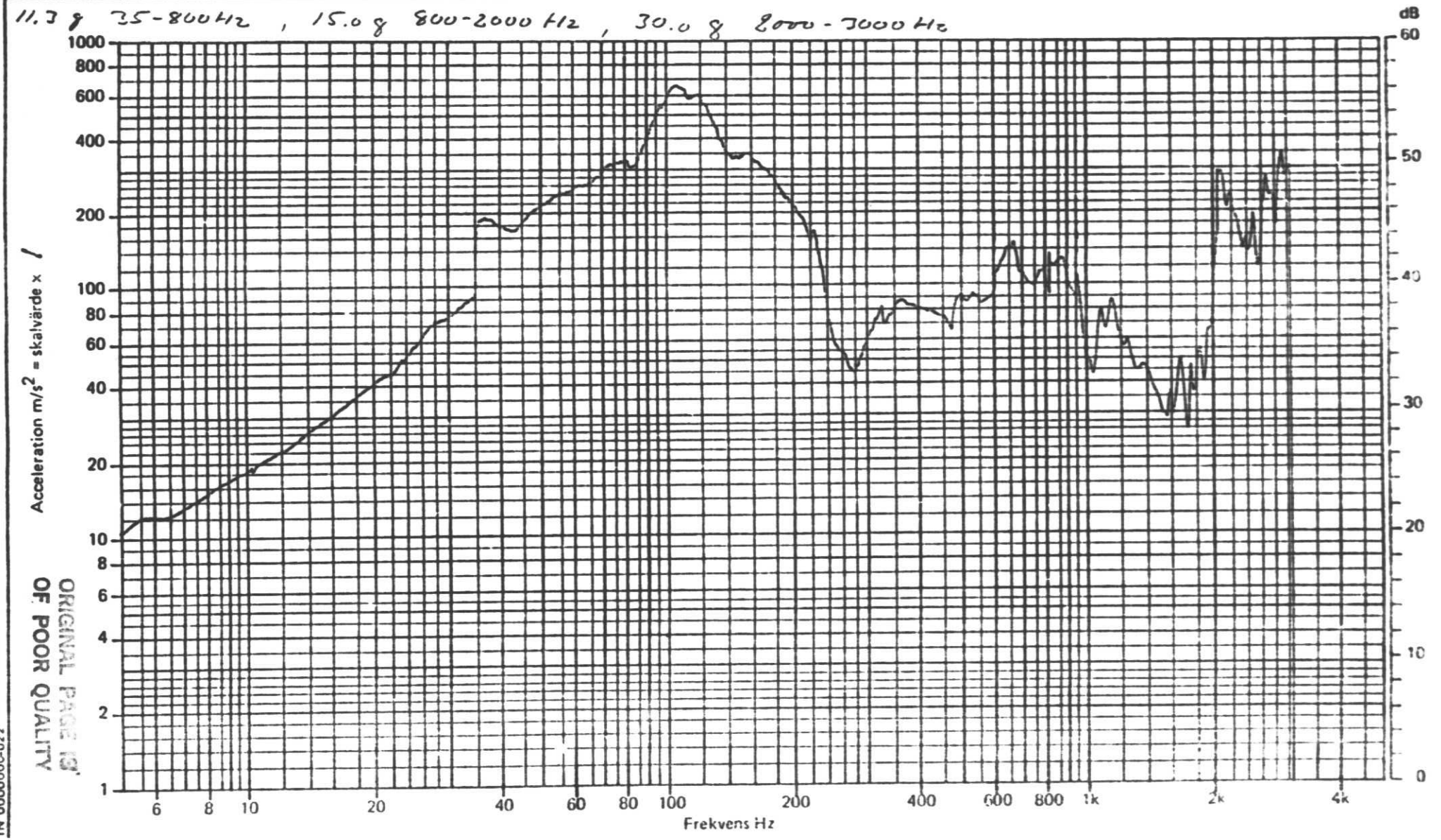

IN 0000000C-022

SAAB SPACE

Date 840605 Clam 97

Document No

Page

500 EL/M

Magazine 100/200, x-direction, 20 seconds

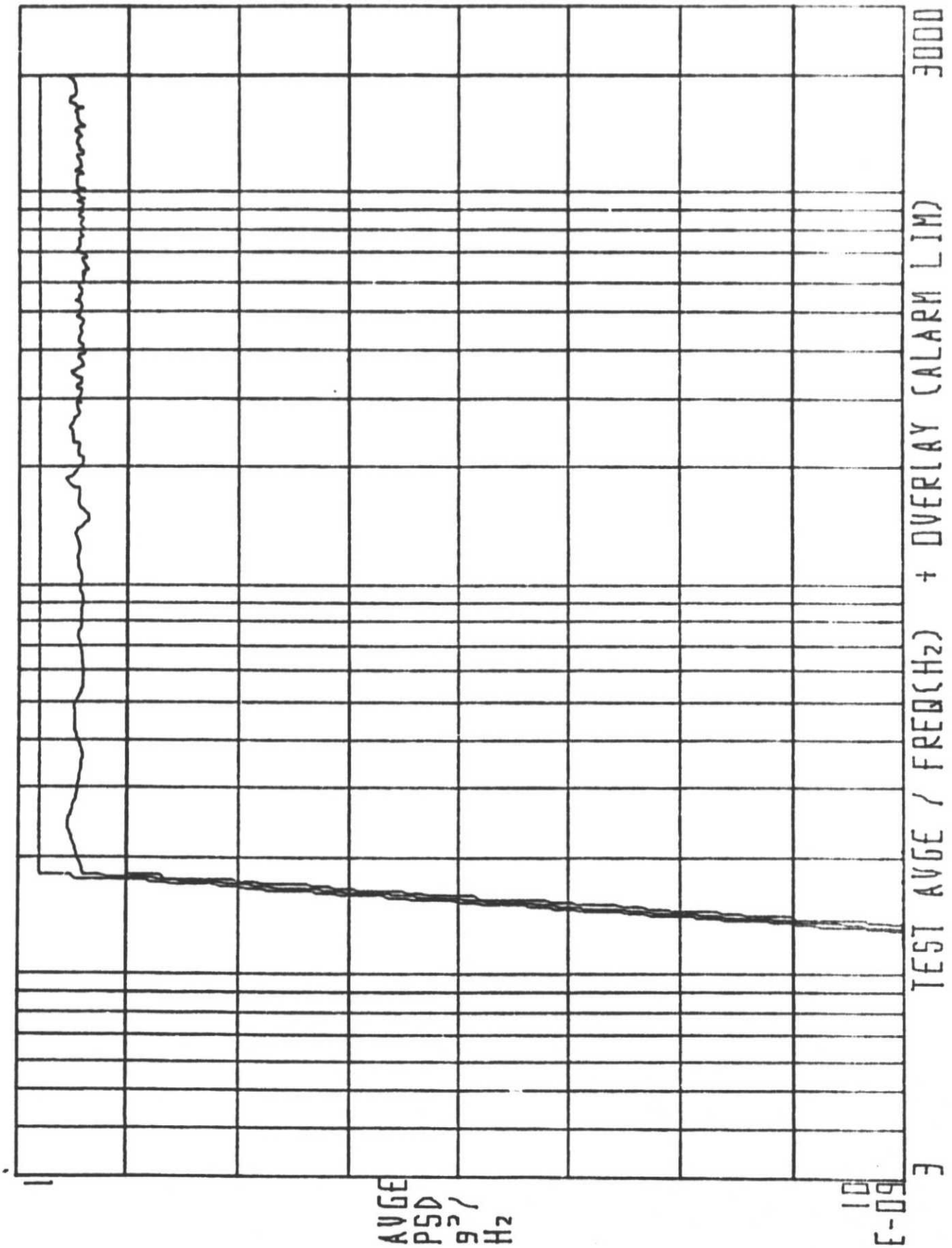

SAAB SPACE

Date 840605 Clas 87

Document No

Page 19

500 EL/M

Magazine 70, x-direction, 20 seconds

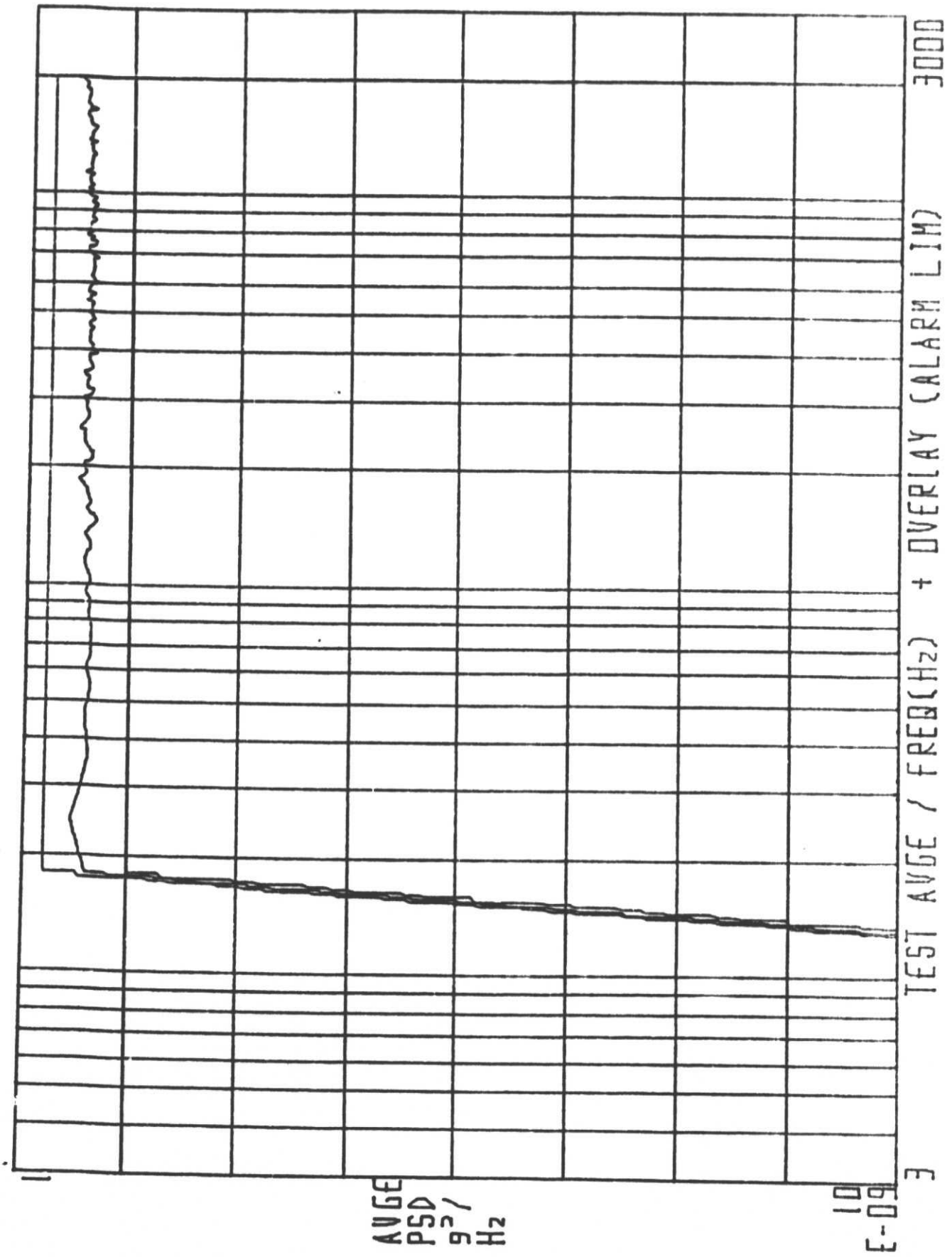

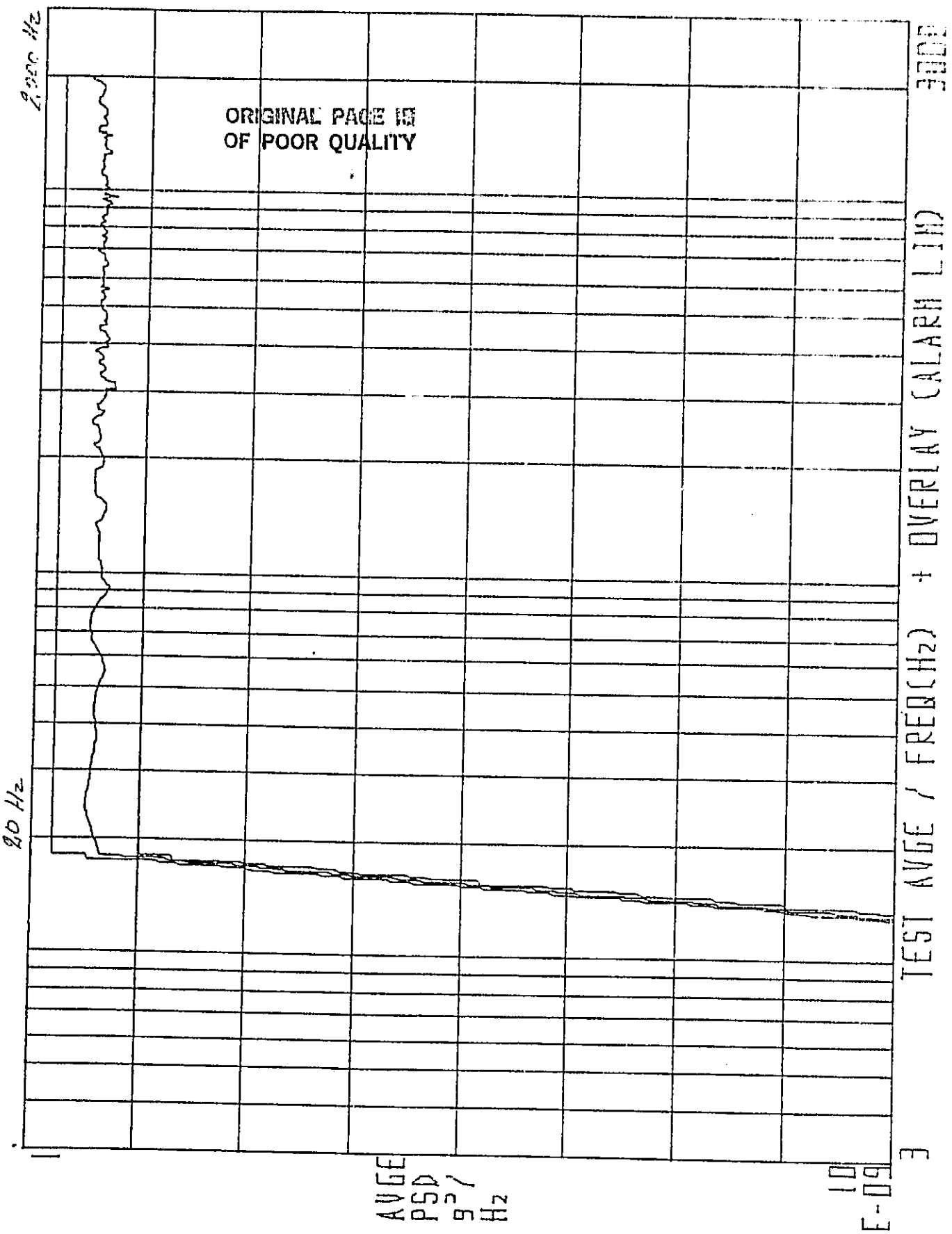
ORIGINAL PAGE IS
OF POOR QUALITY
2000 Hz
20 Hz
TEST AVGE / FREQ(Hz) + OVERLAY CALARM LIMD
AVGE PSD g²/Hz
E-09
E-03

SAAB SPACE

Date 840605 Clan M

Document No

Page 21

500 EL/M

Magazine 70 Y-direction 20 Seconds

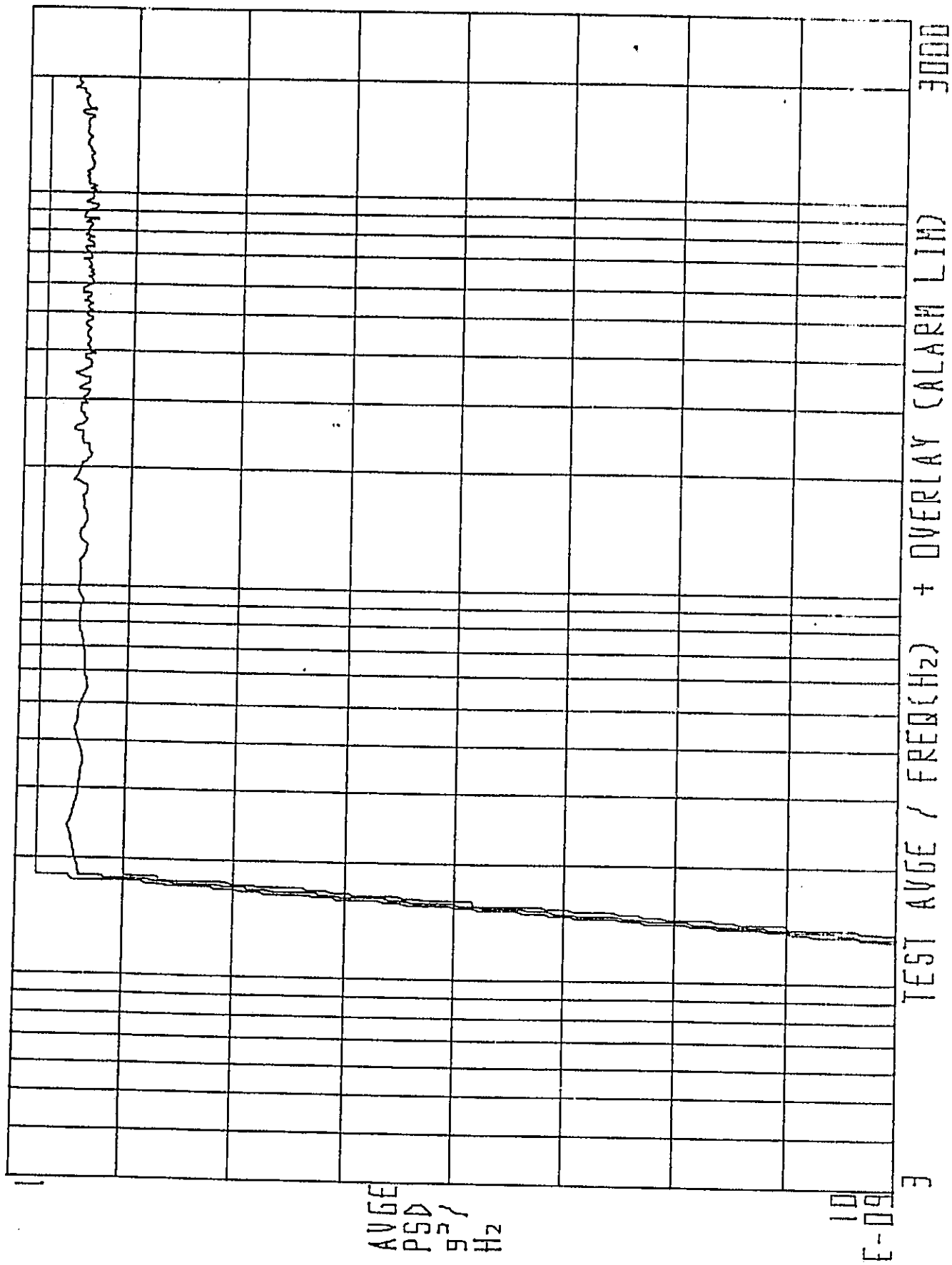

SGD EL/M

Magazine 100/200 Z-direction 20 seconds

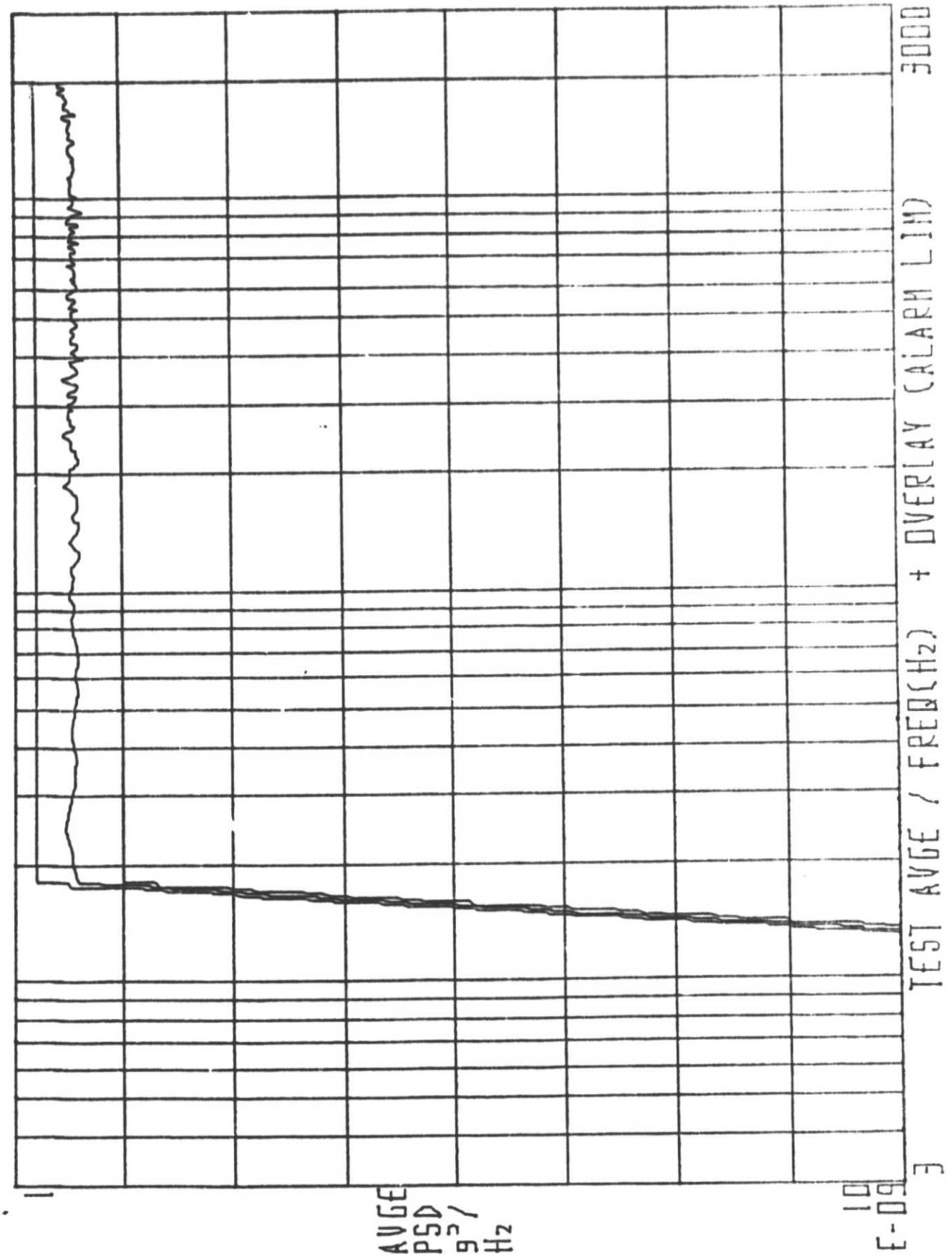

ORIGINAL PAGE IS
OF POOR QUALITY

SAAB SPACE

Date 840605 Clamp A

Document No

Page

500 EL/M

Magazine 70 Z-direction 20 seconds

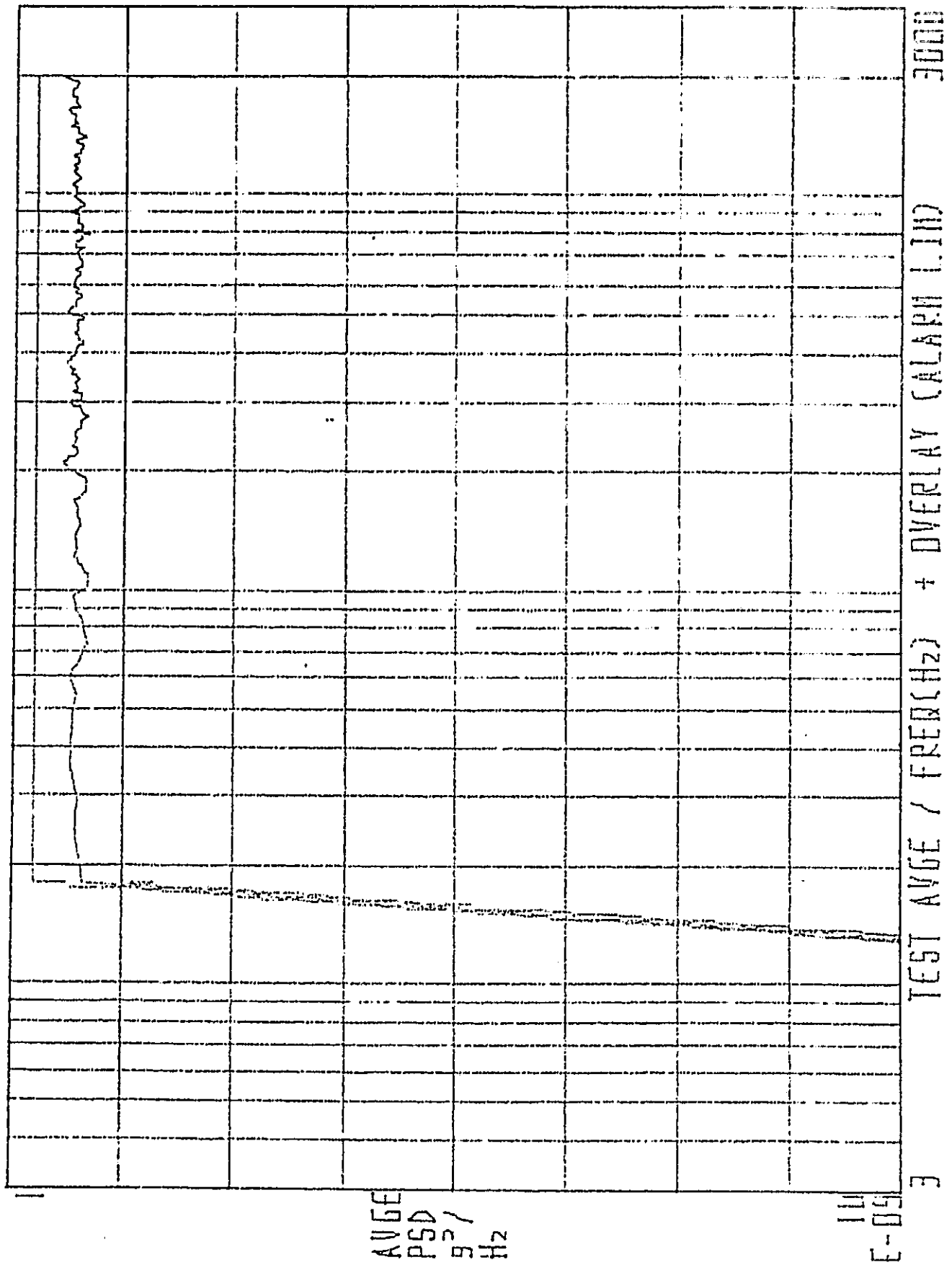

FORM 4 ZATA Å 83.4753

SAAB-SCANIA

ACCELERATIONSNIVÅ-DIAGRAM

Provföremål: 500 ELA-i Magazine 70	Mätpunkt: Magazine 70	Mätriktning: X	Mätpunkt:	Mätriktning:	Datum: 1984-06-05
Vibrationsriktning: X (THRUST)	Provning nr: Res. Search	Filtrerad: yes	Ofiltrerad:	Filtrerad:	Ofiltrerad:	Utförd: Chalmers
Stränghetsgrad: 12 m/s² 2 oct/min	Bandbredd Hz/Frekvensområde Hz: 12 % vid			Bandbredd Hz/Frekvensområde Hz:	Anmärkning:

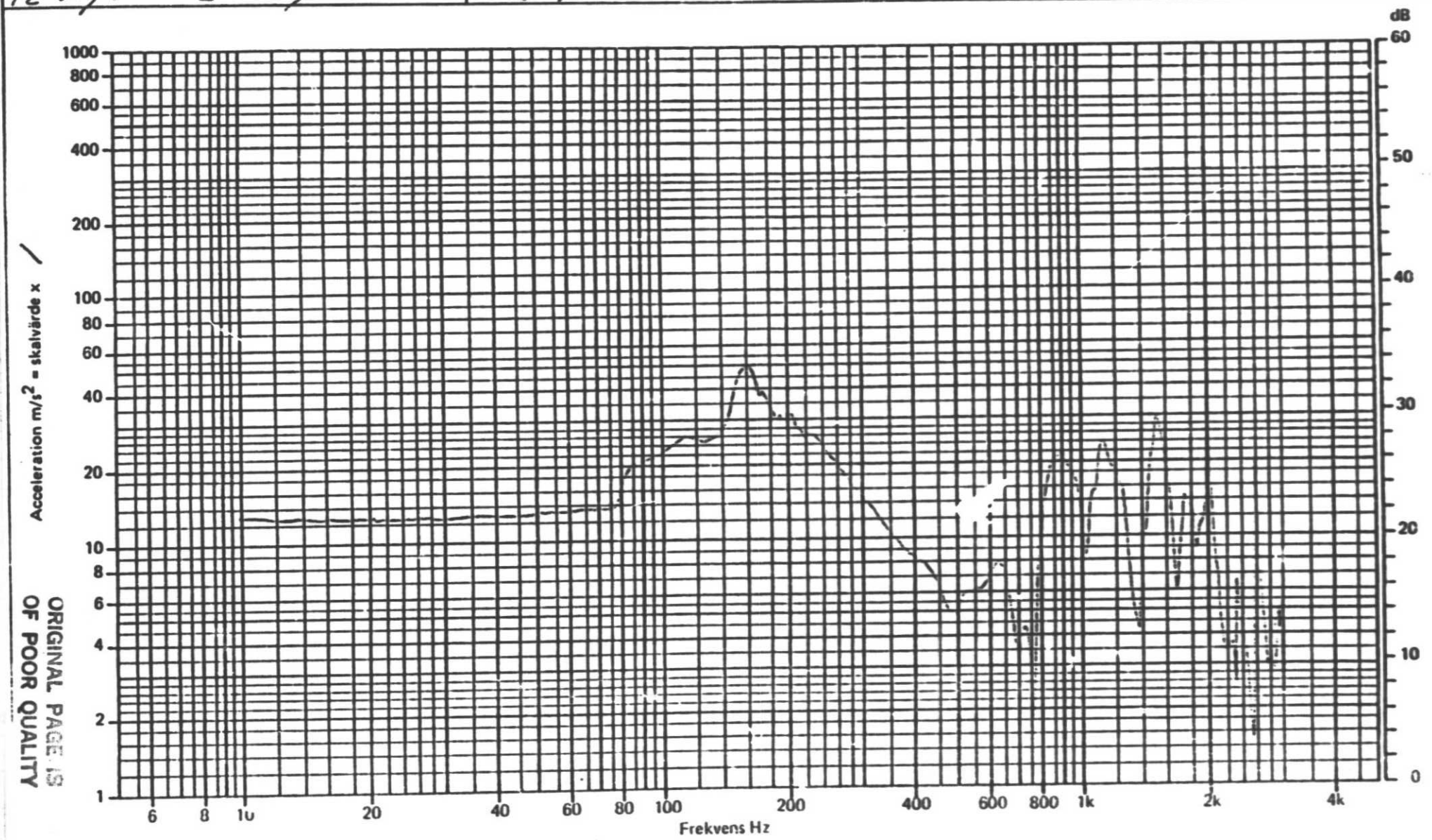

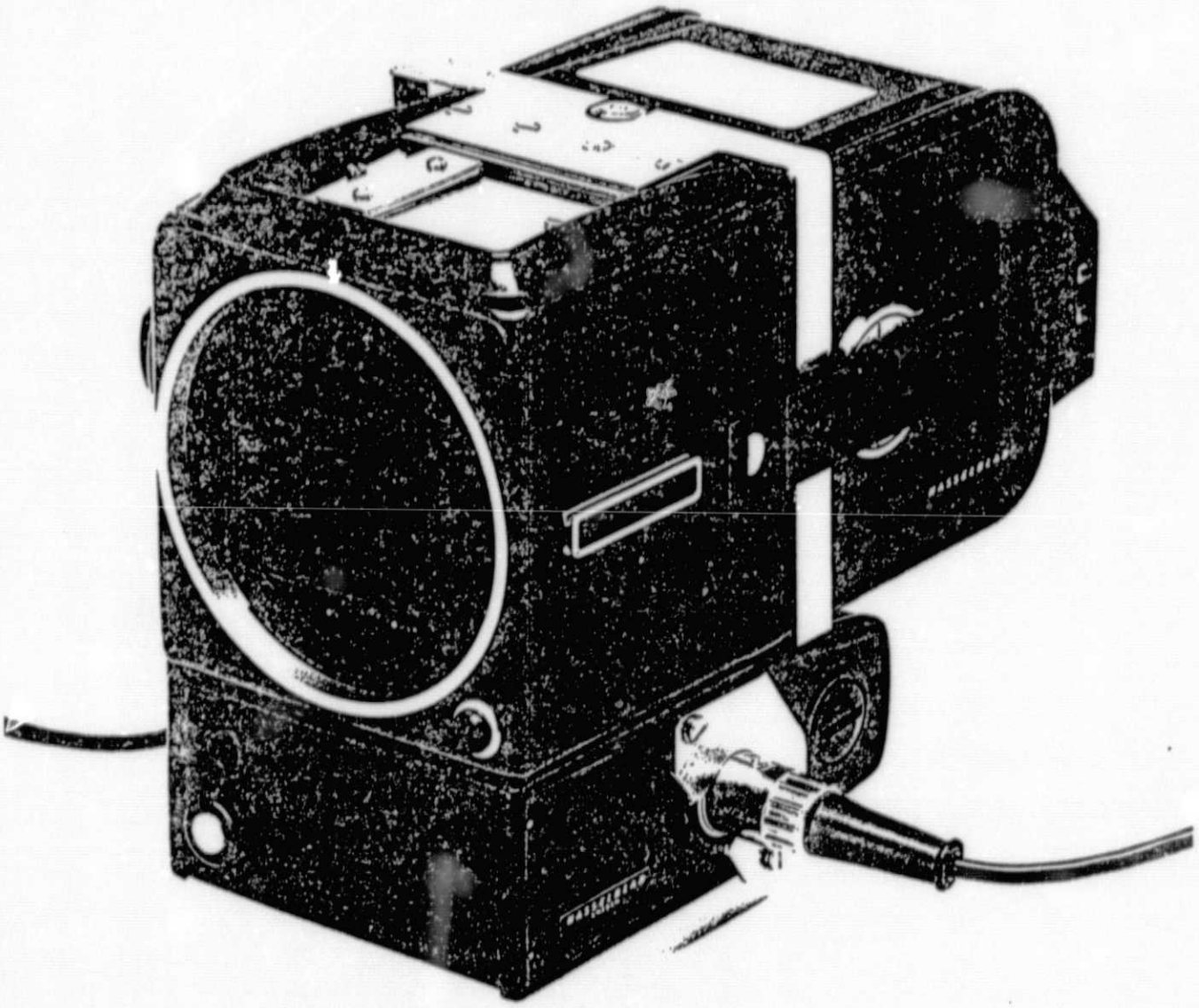

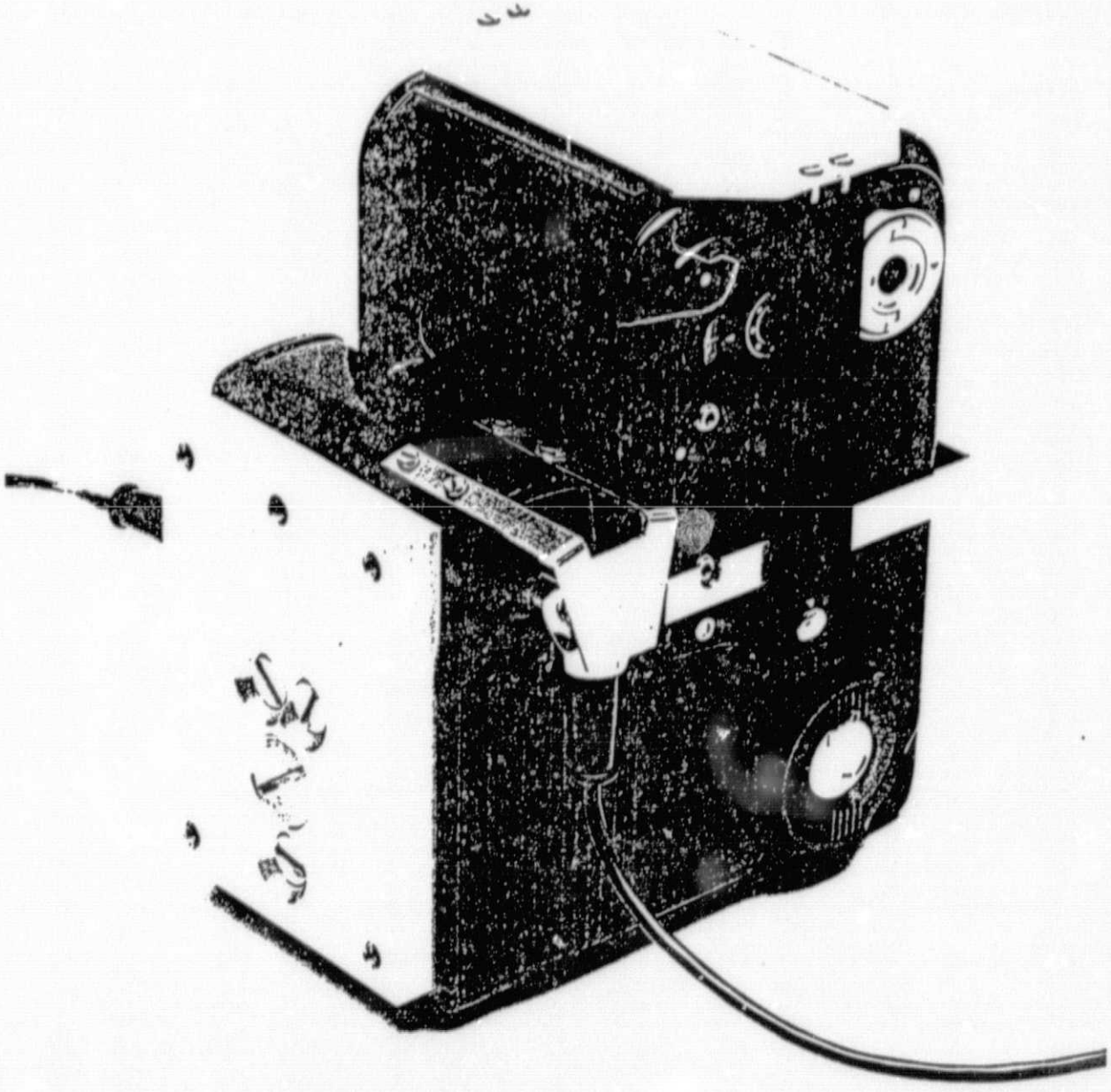

4. Preliminary NIXT Electronic Design

MEMORANDUM

To: Distribution

From: H. Penfield HP

Date: September 5, 1984

Subject: Review of NIX-T Electronic Design

This memorandum together with the referenced drawings represents the current state of the NIX-T Electronic Design. The design utilizes a hardwired logic approach and the microprocessor serves only to facilitate programming of the exposure code sequence in the EEPROM and to output the proper exposure code in response to input from the hardwired logic. An alternate approach is to more fully utilize the microprocessor by implementing most of the logic in software.

Primary scientific data is recorded on film which will be recovered from the rocket at the conclusion of the flight. Housekeeping data is transmitted to the ground over a telemetry link and stored on tape for post flight analysis.

A telemetry command link from the ground to the rocket will provide four discrete commands that are used to generate the "ABORT" and "RESTART" signals.

Electronics System Overview

Drawing No. NIXT-203 shows the block diagram for the NIXT electronics. The command telemetry, data telemetry, telemetry interface, camera battery and electronics battery are shown as dotted blocks because these items are supplied by NASA. With the exception of the batteries, all of the NASA supplied items are located outside

the experiment package and the connections to them would be carried through hermetic connectors. The batteries are located within the experiment package inside a hermetically sealed container to avoid any out-gassing problem.

While the rocket is on the ground, an umbilical connection provides the following lines to the experiment package;

1. Battery Charge, - provides direct current for the purpose of charging both batteries in the experiment package.

2. Light Test, - provide excitation for the test light source which is used prior to launch to check the operation of the light sensor.

3. Camera Test, - contact closure operates camera shutter in an open-and-close fashion on alternate contact closures.

4. RS-232REC. and. RS-232XMT., - provide two-way communication to the microprocessor in the programmable sequencer.

5. Clock Start, - contact closure to generate master reset or to start the experiment clock. Normally the experiment clock will be started 30 to 60 seconds prior to lift-off. At this same time a master reset pulse places the control flip/flops and counters in their inactive state and initializes the programmable sequencer to the first exposure code.

Following lift-off, the sun acquired signal from SPARCS (Solar Pointed Aerobee Rocket Control System) is continuously monitored. When sun acquired goes true (contact closure) the automatic sequence of exposures is enabled. In the event that sun acquired does not go true prior to "N" sec (N might typically be 120 seconds, 30 prior to

launch + 90 post launch), the automatic sequence will be enabled regardless. Once the sequence is enabled, the state of sun acquired is immaterial. Detailed description of the control logic is discussed later when the operation of the cycle control, exposure timer and programmable sequencer are described.

Housekeeping data is transmitted to the ground over a data telemetry link operating at 1 megabits per second. Each word is 10 bits in length, a subframe consists of 32 words and a frame contains 32 subframes. Thus, there is a total of 10,240 bits per frame, the frame time is 10.24 milliseconds and the subframe time is 0.32 milliseconds. Since time is recorded at the start of each subframe, our time accuracy will be 0.32 millseconds. Digital data utilizes all 10 bits of a word. Analog data is converted to digital form in a 9 bit successive approximation analog-to-digital converter and output as the first 9 bits of a word. Odd parity is calculated on these 9 bits and is output as the tenth bit.

The NIX-T housekeeping data will consist of 3 digital words and 18 analog words as summarized below.

Digital Word #1 - Frame No.

Digital word #2 - Exposure Time to 0.2% accuracy.

Count of 500 = 100% of nominal exposure time.

Digital Word #3 - Status

Bit 0 - Shutter, 0 = closed, 1 = open

Bit 1 - Lift-off, 0 = pre lift-off, 1 = post lift-off

Bit 2 - Sun Acquired, 0 = false, 1 = true

Bit 3 - Restart, 0 = not activated, 1 = activated

Bit 4 - Abort, 0 = not activated, 1 = activated

Bit 5 - Not used

Bit 6 thru bit 9 - Exposure Code

Analog Word #1 - Light Sensor Level

Analog Word #2 thru #4 - 3 Axis Accelerometer

Analog Word #5 - Pressure Sensor

Analog Word #6 - Camera Current Monitor

Analog Word #7 thru #12 - Temperature Sensors (6)

Analog Word #13 thru #16 - Circuit Voltage Monitors (4)

Analog Word #17 & #18 - Battery Voltages

Each of the Analog inputs must be limited to the range of 0 to 5 volts.

Electronics System Operation

The normal mode of operation involves a series of preprogrammed exposure times that occur automatically once the sun acquired signal goes true or the "N" second timer runs out. Drawing NO. NIXT-206 shows the control logic flow diagram. In addition to the normal mode of programmed exposure times, the system responds to a "RESTART" command and an "ABORT" command.

The RESTART command terminates an exposure in progress by closing the shutter and advancing the film. However, the exposure code remains unchanged and a new exposure is started with the same exposure time as the exposure that was interrupted.

The ABORT command locks out the automatic programmed exposure sequence and control of the shutter is in an open-close mode controlled by successive ABORT commands. Thus, once the ABORT command has been issued, all subsequent operation of the camera is essentially "manual" via the ABORT command.

The key subsystems in the automatic operation of the camera are:

1. Experiment Clock — Drawing No. NIXT-207
2. Cycle Control — Drawing No. NIXT-205
3. Programmable Sequencer — Drawing No. NIXT-204
4. Exposure Timer — Drawing No. NIXT-208

The referenced drawings show functional diagrams for each of the units.

The experiment clock utilizes a 1 MHz crystal oscillator followed by two cascaded decade dividers to produce a 10 KHz clock signal. A clock start input (momentary contact closure) is routed to the experiment clock circuit through the umbilical connector. This clock start input serves the dual purpose of generating a master reset pulse and opening a clock gate to allow the 10 KHz clock signal to be output to the cycle control and exposure timer subsystems. A single momentary clock start contact closure generates master reset and opens the clock gate. Two momentary clock start contact closures, with the 2nd closure occurring within the time of the delay gate (say, 3 seconds), stops the 10 KHz output and generates master reset. Drawing No. NIXT-207 shows the logic circuitry required for the experiment clock and also shows typical timing waveforms.

The cycle control circuit provides a shutter gate signal that determines the time during which the camera shutter is commanded open. Drawing No. NIXT-205 shows the circuitry required in the cycle control subsystem. The master reset pulse clears all counters and resets all flip/flops. The 10KHz signal from the experiment clock is divided down to 1 Hz by four cascaded decade dividers. This 1 Hz signal provides synchronization for the start of each exposure in the automatic sequence and also drives a divide by N counter chain. When

either sun acquired goes true (contact closure) or the divide by N counter overflows, the sequence enable flip/flop is triggered and the next lo-to-hi transition of the 1 Hz signal triggers the shutter gate flip/flop which in turn triggers the exposure start flip/flop. At the end of the exposure time (as determined in the exposure timer subsystem), exposure stop goes hi and resets the shutter gate flip/flop which then triggers the cycle reset flip/flop thru a NAND gate. Cycle reset occurs on the next 1 Hz pulse following the triggering of the cycle reset flip/flop. The cycle reset and exposure start flip/flops are reset by the cycle reset pulse through an RC delay. Cycle reset is also used to reset the shutter gate and RESTART flip/flops and to generate the increment input required by the programmable sequencer. When a RESTART input triggers the RESTART flip/flop, the increment output is disabled and the cycle reset flip/flop is triggered thus resetting the cycle control for a new exposure but maintaining the current exposure time. When an ABORT input triggers the control select flip/flop, the shutter gate is derived from the state of the test/abort flip/flop. The test/abort flip/flop is a divide by two circuit that switches logic level on successive clock inputs. The clock input is obtained either from the ABORT signal or from a camera test input (contact closure) that is routed to the cycle control subsystem through the umbilical connector. Camera test allows check out of the camera shutter/film advance operation prior to launch.

A sample cycle control timing diagram is shown in drawing No. NIXT-210. Note that the 1 Hz signal synchronizes the exposure start and cycle reset and that a 1 to 2 second period is provided for film advance between exposures.

The exposure timer subsystem, shown in drawing No NIXT-208, utilizes a series of decade dividers and a divide by three circuit to derive an exposure clock signal whose period is 0.001 of the desired exposure time. The 10 KHz signal from the experiment clock is fed thru an AND gate to four cascaded decade counters that provide outputs of 1 KHz, 100 Hz, 10 Hz, and 1 Hz. The control signal for the AND gate is the exposure start signal generated in the cycle control circuit. When the exposure start signal goes hi, the 10 KHz, 1 KHz, 100 Hz, 10 Hz, and 1 Hz signals will be present on the 0 through 4 input lines of a 1 of 8 data select circuit. The selection is controlled by the three hi bits of the exposure code. The exposure code is a four bit input that comes from the programmable sequencer. The lowest bit of the exposure code is used to select either the direct output of the data select circuit or the output divided by three.

Nine exposures times have been selected for use in the NIX-T system. The following table lists these exposure times along with the corresponding exposure clock rate and exposure code.

Exposure Time	Exposure Clock Rate	Exposure Code
0.1 seconds	10 KHz	0000
0.3	3.333 KHz	0001
1.0	1 KHz	0010
3.0	333.3 Hz	0011
10.0	100 Hz	0100
30.0	33.33 Hz	0101
100.0	10 Hz	0110
300.0	3.333 Hz	0111
1000.0	1 Hz	1000

The exposure clock signal is divided by 1000 in a chain of three cascaded decade counters to provide the exposure stop signal required by the cycle control subsystem.

The programmable sequencer utilizes a microprocessor with an EEPROM as part of its memory to provide the capability of editing the stored exposure code sequence via an RS-232 link thru the umbilical connector. The microprocessor also responds to the master reset and the increment signal generated by the cycle control subsystem. Master reset initializes the microprocessor and places the first exposure code on the 4 bit parallel output to the exposure timer subsystem. Increment selects the next exposure code and places it on the 4 bit parallel output.

A line driver and receiver circuit is required to interface the RS-232 lines to the umbilical connector and approximately 900 feet of cable from the launch pad to the block house.

A shutter open sensor, utilizing an IR source and detector will be used to determine when the camera shutter is actually open. The

output from the sensor will be used to advance the frame counter, serve as a gate for the exposure clock input to the exposure counter and activate bit zero in the status register.

The exposure counter functional diagram is shown in drawing No. NIXT-209. Cascaded four bit binary counters are utilized to derive a 10 bit output that represents actual shutter open time to a resolution of 0.2 percent. In other words, a count of 500 represents a shutter open time that is equal to the exposure time specified by the exposure code.

The command decode subsystem accepts four contact closure inputs from the command telemetry and generates the ABORT and RESTART signals. A specific combination or sequence of the four commands will be required to generate these signals.

The shutter drive circuit accepts the shutter gate signal from the cycle control subsystem, provides isolation (thru an opto-isolator), and provides a low impedance "contact closure" to the camera shutter contacts.

The camera current monitor circuit senses the total current drawn by the camera and presents this (thru an opto-isolator) to one of the analog inputs to the data telemetry. The camera current monitor circuit also includes a DC-to-DC converter to reduce the 24 volt battery voltage to the 6 volt level required by the camera.

The power distribution subsystem utilizes DC-to-DC converters to transpose the battery voltage to the voltage levels of +5 volts and ± 15 volts required by the electronics. Also included in the power distribution is the filtering and decoupling required to maintain "clean" voltage supply to all circuits.

A hi volt power supply is shown on the electronics system block to cover the case where an avalanche type photodiode is used as the light sensor.

In addition to the light sensor, the system includes a pressure sensor, a 3 axis accelerometer and several temperature sensors.

Future Design Effort

Utilizing the functional diagrams it is now possible to generate a detailed design with specific components selected to pe_form each function. Based on the functional design it is estimated that the system will require approximately 60 integrated chip packages and should lend itself well to a layout utilizing 3 circuit boards.

The GSE and/or special test equipment requirements for the electronics will have to simulate the following interfaces.

1. Umbilical
2. SPARCS
3. Command Telemetry
4. Data Telemetry

The degree of sophistication in the GSE required during testing of the system is probably a matter of economics. For instance, digital telemetry data could be checked using a simple array of LEDs and analog telemetry data could be checked with a digital voltmeter. Contact closures, as required for the command telemetry and SPARCS, could be simulated by switches.

The umbilical lines will terminate in the GSE equipment that will be located in the block house at White Sands. This equipment will include a computer terminal (such as a VT-100), a line driver and receiver, a battery charge supply, a variable power source (for the Light Test Source), and momentary contact switches for camera test and clock start.

HP/pk

Distribution:
B. Dias
J. Gerdes
L. Golub
F. Licata
G. Nystrom

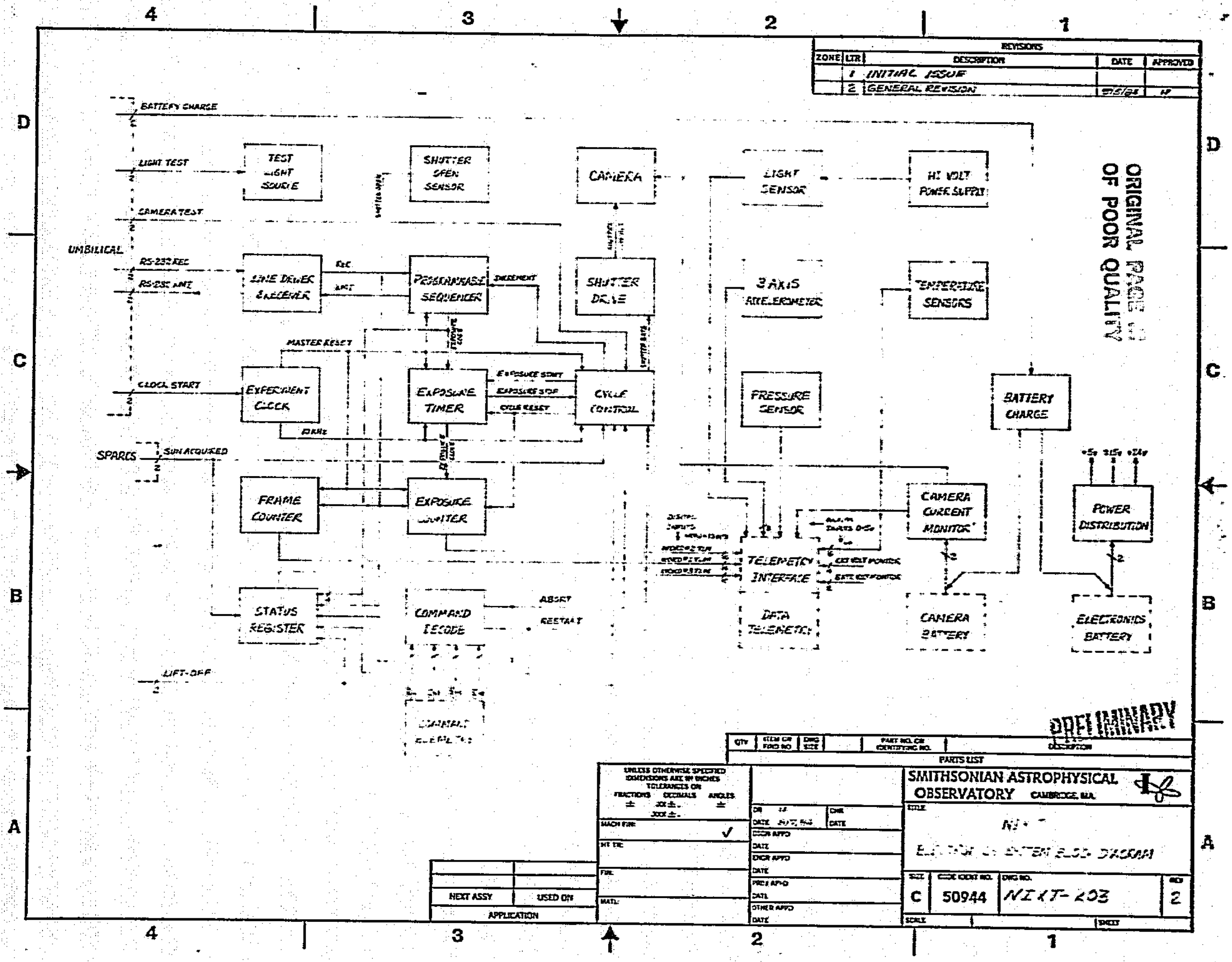
ORIGINAL PAGE IS
OF POOR QUALITY
REVISIONS
ZONE
LTR
DESCRIPTION
DATE
APPROVED
1 INITIAL ISSUE
2 GENERAL REVISION
BATTERY CHARGE
LIGHT TEST
CAMERA TEST
UMBILICAL
RS-232 REC
RS-232 XMT
CLOCK START
SPARES
SUN ACQUIRED
LIFT-OFF
TEST LIGHT SOURCE
SHUTTER OPEN SENSOR
CAMERA
LIGHT SENSOR
HI VOLT POWER SUPPLY
LINE DRIVER RECEIVER
REC
XMT
PROGRAMMABLE SEQUENCER
INCREMENT
SHUTTER DRIVE
3 AXIS ACCELEROMETER
TEMPERATURE SENSORS
MASTER RESET
EXPERIMENT CLOCK
EXPOSURE TIMER
EXPOSURE START
EXPOSURE STOP
CYCLE RESET
CYCLE CONTROL
PRESSURE SENSOR
BATTERY CHARGE
FRAME COUNTER
EXPOSURE LIMITER
CAMERA CURRENT MONITOR
POWER DISTRIBUTION
+5v ±15v +24v
DIGITAL INPUTS
TELEMETRY INTERFACE
DATA TELEMETRY
CAMERA BATTERY
ELECTRONICS BATTERY
STATUS REGISTER
COMMAND DECODE
ABORT
RESTART
PRELIMINARY
QTY
ITEM OR FIND NO
DWG SIZE
PART NO. OR IDENTIFYING NO.
DESCRIPTION
PARTS LIST
UNLESS OTHERWISE SPECIFIED DIMENSIONS ARE IN INCHES
TOLERANCES ON
FRACTIONS
DECIMALS
ANGLES
MACH FIN
HT TR
FIN
MATL
NEXT ASSY
USED ON
APPLICATION
DR
DATE
CHK
DATE
DSGN APPD
DATE
ENGR APPD
DATE
PROJ APPD
DATE
OTHER APPD
DATE
SMITHSONIAN ASTROPHYSICAL OBSERVATORY CAMBRIDGE, MA.
TITLE
SIZE
C
CODE IDENT NO.
50944
DWG NO.
NIXT-203
REV
2
SCALE
SHEET

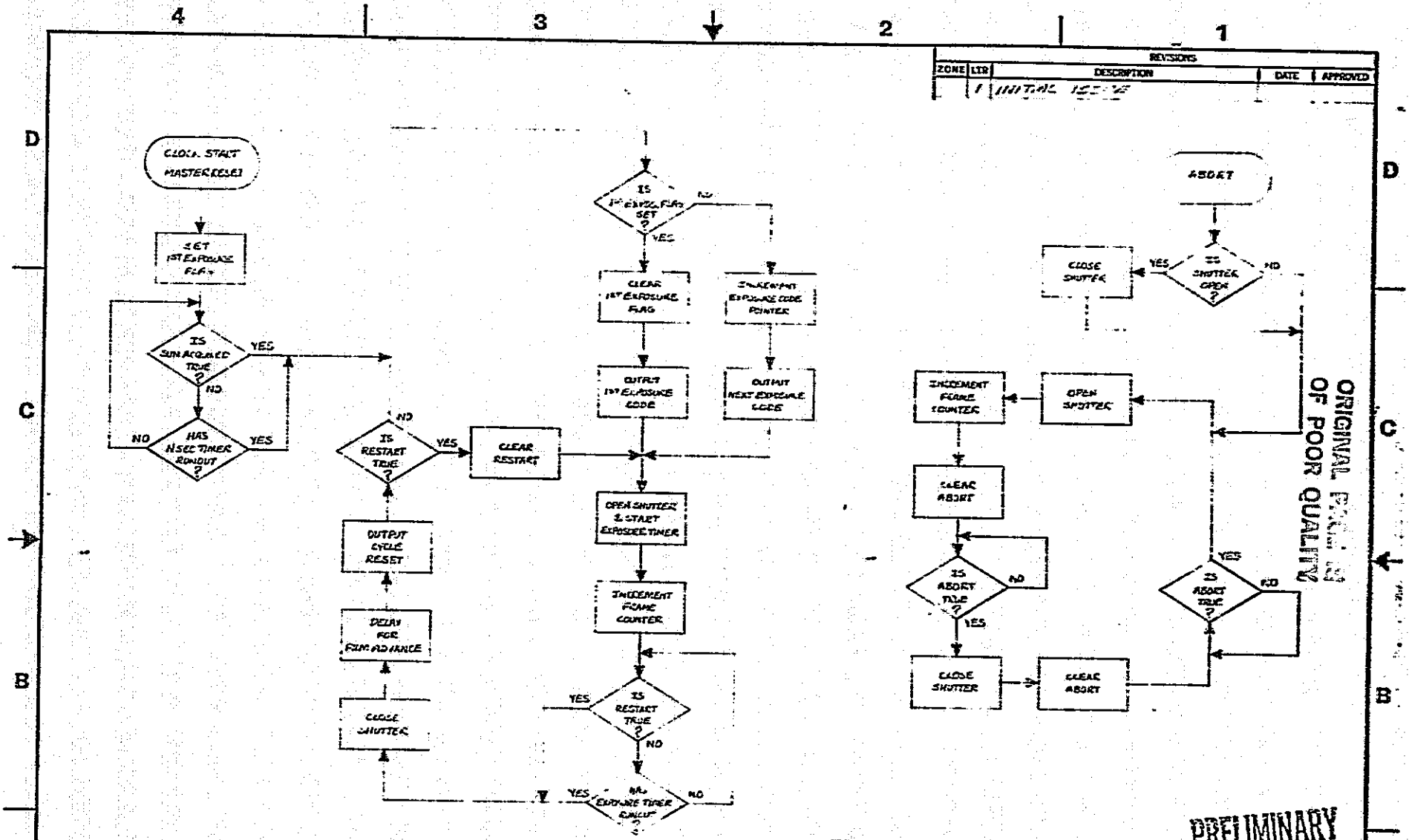

ORIGINAL PAGE IS OF POOR QUALITY

PRELIMINARY

REVISIONS				
ZONE	LTR	DESCRIPTION	DATE	APPROVED
	1	INITIAL RELEASE		

QTY	ITEM OR FIND NO.	DWG SIZE	PART NO. OR CONTRACT NO.	DESCRIPTION

PARTS LIST

UNLESS OTHERWISE SPECIFIED DIMENSIONS ARE IN INCHES
TOLERANCES ON
FRACTIONS ± DECIMALS ± ANGLES ±
.XX ±.
.XXX ±.

MACH FIN ✓
HT TR
FIN
MATL

NEXT ASSY | USED ON
APPLICATION

DR | CHK
DATE 5/13/82 | DATE
CONT APPD | DATE
ENGR APPD | DATE
PROJ APPD | DATE
OTHER APPD | DATE

SMITHSONIAN ASTROPHYSICAL OBSERVATORY CAMBRIDGE, MA.

TITLE
NIXT
CONTROL LOGIC FLOW DIAGRAM

SIZE	CODE IDENT NO.	DWG NO.	REV
C	50944	NIXT-206	1

SCALE | SHEET

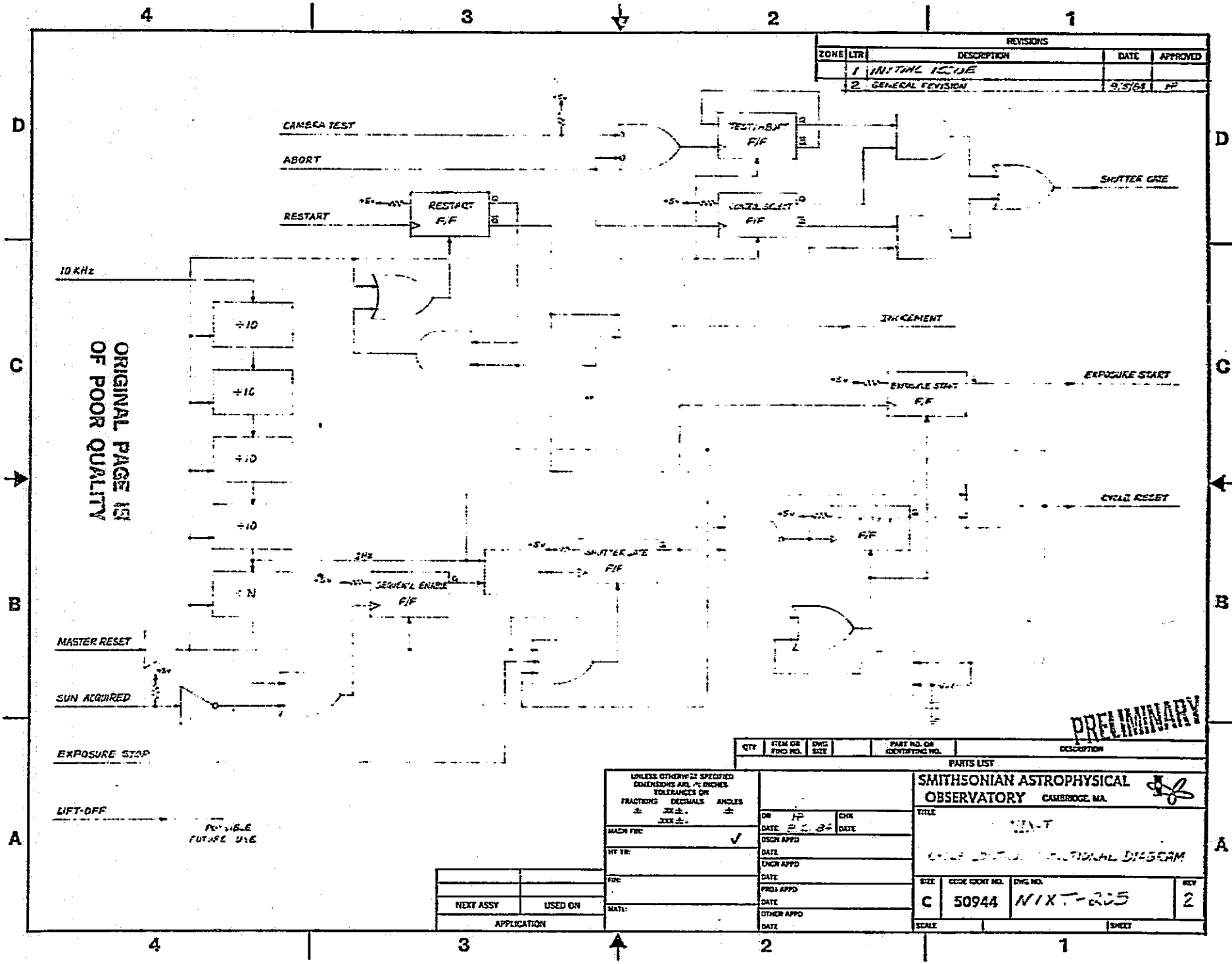
CAMERA TEST
ABORT
RESTART
RESTACT F/F
TEST ABORT F/F
SHUTTER GATE
10 KHz
÷10
÷16
÷10
÷10
÷N
INCREMENT
EXPOSURE START
CYCLE RESET
SEQUENCE ENABLE F/F
MASTER RESET
SUN ACQUIRED
EXPOSURE STOP
LIFT-OFF
POSSIBLE FUTURE USE
PRELIMINARY
ORIGINAL PAGE IS OF POOR QUALITY
REVISIONS
ZONE LTR DESCRIPTION DATE APPROVED
1 INITIAL ISSUE
2 GENERAL REVISION 9.5.84 HP
PARTS LIST
QTY ITEM OR FIND NO. DWG SIZE PART NO. OR IDENTIFYING NO. DESCRIPTION
UNLESS OTHERWISE SPECIFIED DIMENSIONS ARE IN INCHES TOLERANCES ON FRACTIONS DECIMALS ANGLES ± .XX ± .XXX ±
MACH FIN:
HT TR:
FIN:
MATL:
NEXT ASSY USED ON
APPLICATION
DR HP DATE 8.2.84 CHK DATE
DSGN APPD DATE
ENGR APPD DATE
PROJ APPD DATE
OTHER APPD DATE
SMITHSONIAN ASTROPHYSICAL OBSERVATORY CAMBRIDGE, MA.
TITLE
NIXT
CYCLE CONTROL FUNCTIONAL DIAGRAM
SIZE C
CODE IDENT NO. 50944
DWG NO. NIXT-225
REV 2
SCALE
SHEET

REVISIONS				
ZONE	LTR	DESCRIPTION	DATE	APPROVED
	1	INITIAL RELEASE		

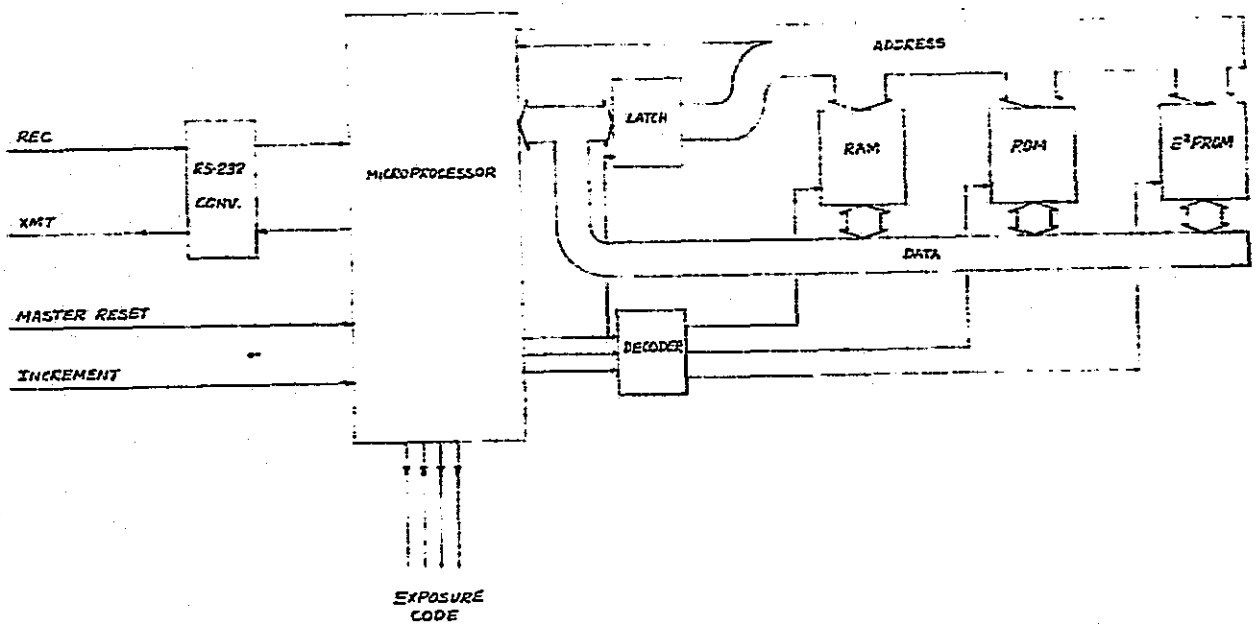

ORIGINAL PAGE IS
OF POOR QUALITY

PRELIMINARY

QTY	ITEM OR FIND NO.	DWG SIZE	PART NO. OR IDENTIFYING NO.	DESCRIPTION

PARTS LIST

UNLESS OTHERWISE SPECIFIED DIMENSIONS ARE IN INCHES
TOLERANCES ON
FRACTIONS ± DECIMALS .XX ± .XXX ± ANGLES ±

MACH FIN: ✓
HT TR:
FIN:
MATL:

NEXT ASSY	USED ON
APPLICATION	

DR IP DATE 8/22/84 CHK DATE
DSGN APPD DATE
ENGR APPD DATE
PROJ APPD DATE
OTHER APPD DATE

: Rockwell – R65F11

SMITHSONIAN ASTROPHYSICAL OBSERVATORY CAMBRIDGE, MA.

TITLE
NIX-T
PROGRAMMABLE SEQUENCER FUNCTIONAL DIAGRAM

SIZE	CODE IDENT NO.	DWG NO.	REV
C	50944	NIXT-204	1

SCALE SHEET

REVISIONS				
ZONE	LTR	DESCRIPTION	DATE	APPROVED
	1	INITIAL ISSUE		

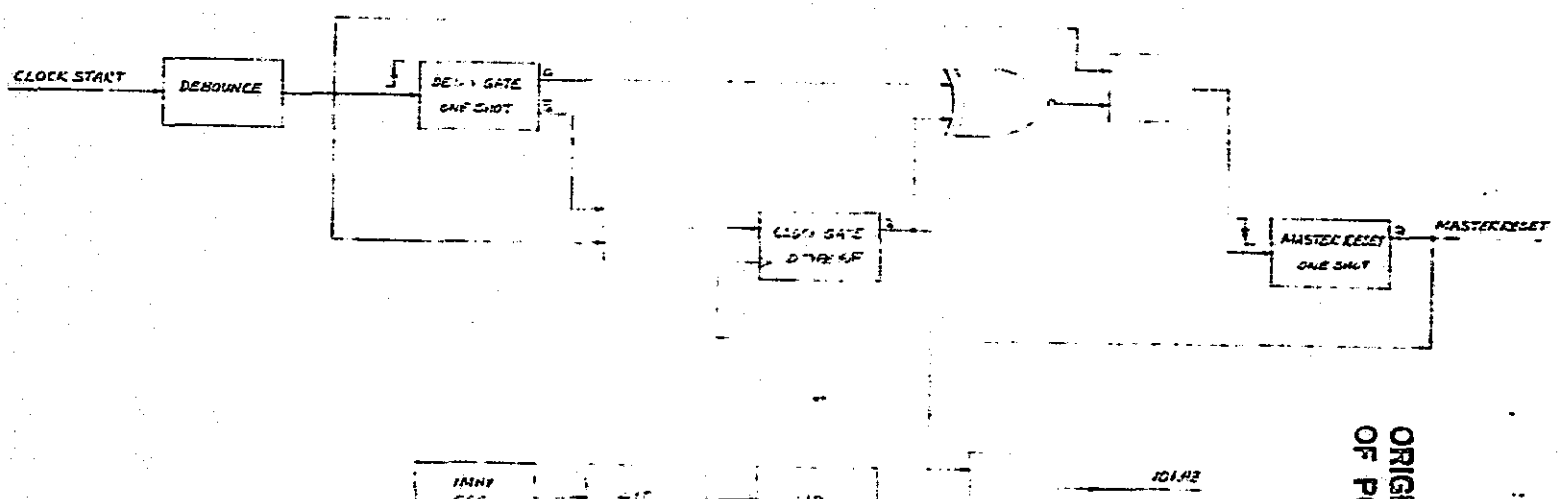

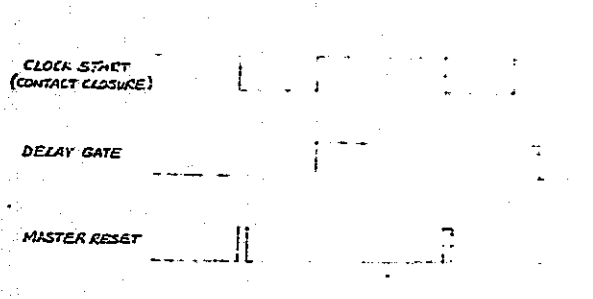

ORIGINAL PAGE IS
OF POOR QUALITY

PRELIMINARY

SINGLE MOMENTARY CLOCK START CONTACT CLOSURE GENERATES MASTER RESET AND OPENS CLOCK GATE TO ALLOW 10 kHz OUTPUT.

TWO MOMENTARY CLOCK START CONTACT CLOSURES, WITH THE 2ND CLOSURE OCCURRING WITHIN THE TIME OF THE DELAY GATE, STOPS THE 10 kHz OUTPUT AND GENERATES MASTER RESET.

QTY	ITEM OR FIND NO.	DWG SIZE	PART NO. OR IDENTIFYING NO.	DESCRIPTION

PARTS LIST

UNLESS OTHERWISE SPECIFIED DIMENSIONS ARE IN INCHES
TOLERANCES ON FRACTIONS ± DECIMALS ± ANGLES ±
.XX ± .
.XXX ± .

MACH FIN: ✓
HT TR:
FIN:
MATL:

DR	HP	CHK
DATE	8/1/84	DATE

DSGN APPD DATE
CNCR APPD DATE
PROJ APPD DATE
OTHER APPD DATE

NEXT ASSY	USED ON
APPLICATION	

SMITHSONIAN ASTROPHYSICAL OBSERVATORY CAMBRIDGE, MA.

TITLE
NIX-T
EXPERIMENT CLOCK FUNCTIONAL DIAGRAM

SIZE	COGC IDENT NO.	DWG NO.	REV
C	50944	NIXT-207	1

SCALE SHEET

REVISIONS				
ZONE	LTR	DESCRIPTION	DATE	APPROVED
	1	INITIAL ISSUE		

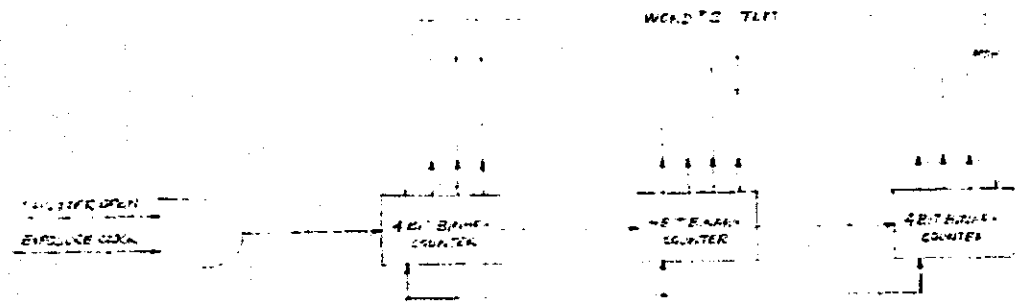

ORIGINAL PAGE IS OF POOR QUALITY

PRELIMINARY

QTY	ITEM OR FIND NO.	DWG SIZE		PART NO. OR IDENTIFYING NO.	DESCRIPTION

PARTS LIST

UNLESS OTHERWISE SPECIFIED DIMENSIONS ARE IN INCHES
TOLERANCES ON
FRACTIONS ± DECIMALS .XX ± .XXX ± ANGLES ±

MACH FIN: ✓
HT TR:
FIN:
MATL:

DR	HF	CHK
DATE	8/15/94	DATE
DSGN APPD		DATE
ENGR APPD		DATE
PROJ APPD		DATE
OTHER APPD		DATE

NEXT ASSY	USED ON
APPLICATION	

SMITHSONIAN ASTROPHYSICAL OBSERVATORY CAMBRIDGE, MA.

TITLE: NIX-T

EXPLICIT COUNTER FUNCTIONAL DIAGRAM

SIZE	CODE IDENT NO.	DWG NO.	REV
C	50944	NIXT-209	1

SCALE | SHEET

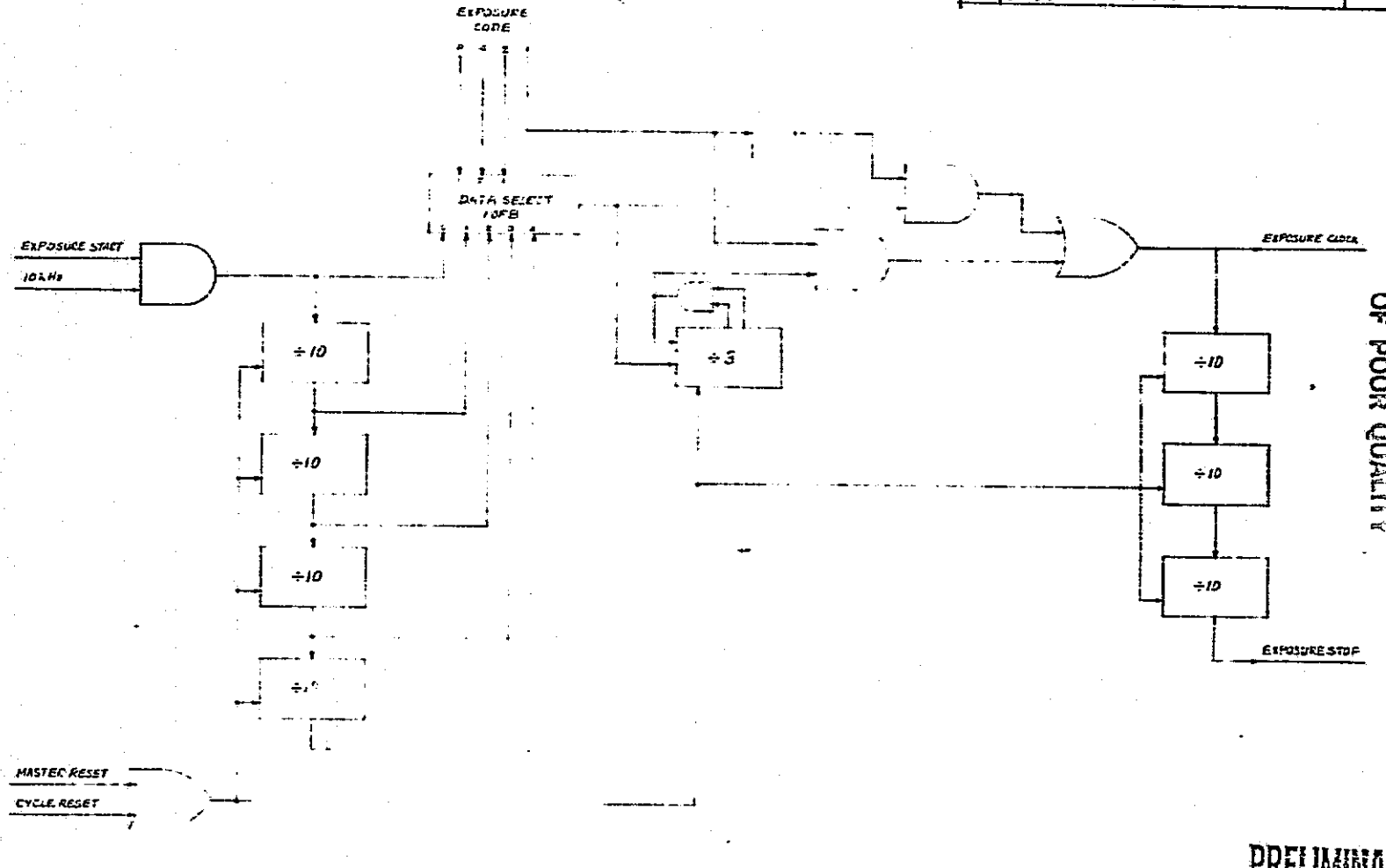

REVISIONS				
ZONE	LTR	DESCRIPTION	DATE	APPROVED
	1	INITIAL ISSUE		

PRELIMINARY

QTY	FROM OR FIND NO.	DWG SIZE	PART NO. OR IDENTIFYING NO.	DESCRIPTION

PARTS LIST

NEXT ASSY	USED ON
APPLICATION	

UNLESS OTHERWISE SPECIFIED DIMENSIONS ARE IN INCHES
TOLERANCES ON
FRACTIONS ± DECIMALS ± ANGLES ±
.XX ± .
.XXX ± .

MACH FIN: ✓
HT TR:
FIN:
MATL:

DR DATE 5/13/94
CHK DATE
DSGN APPD DATE
ENGR APPD DATE
PROJ APPD DATE
OTHER APPD DATE

SMITHSONIAN ASTROPHYSICAL OBSERVATORY CAMBRIDGE, MA.

TITLE
NIX-T
EXPOSURE TIMER FUNCTIONAL DIAGRAM

SIZE	CODE IDENT NO.	DWG NO.	REV
C	50944	NIXT-208	1

SCALE SHEET

REVISIONS				
ZONE	LTR	DESCRIPTION	DATE	APPROVED

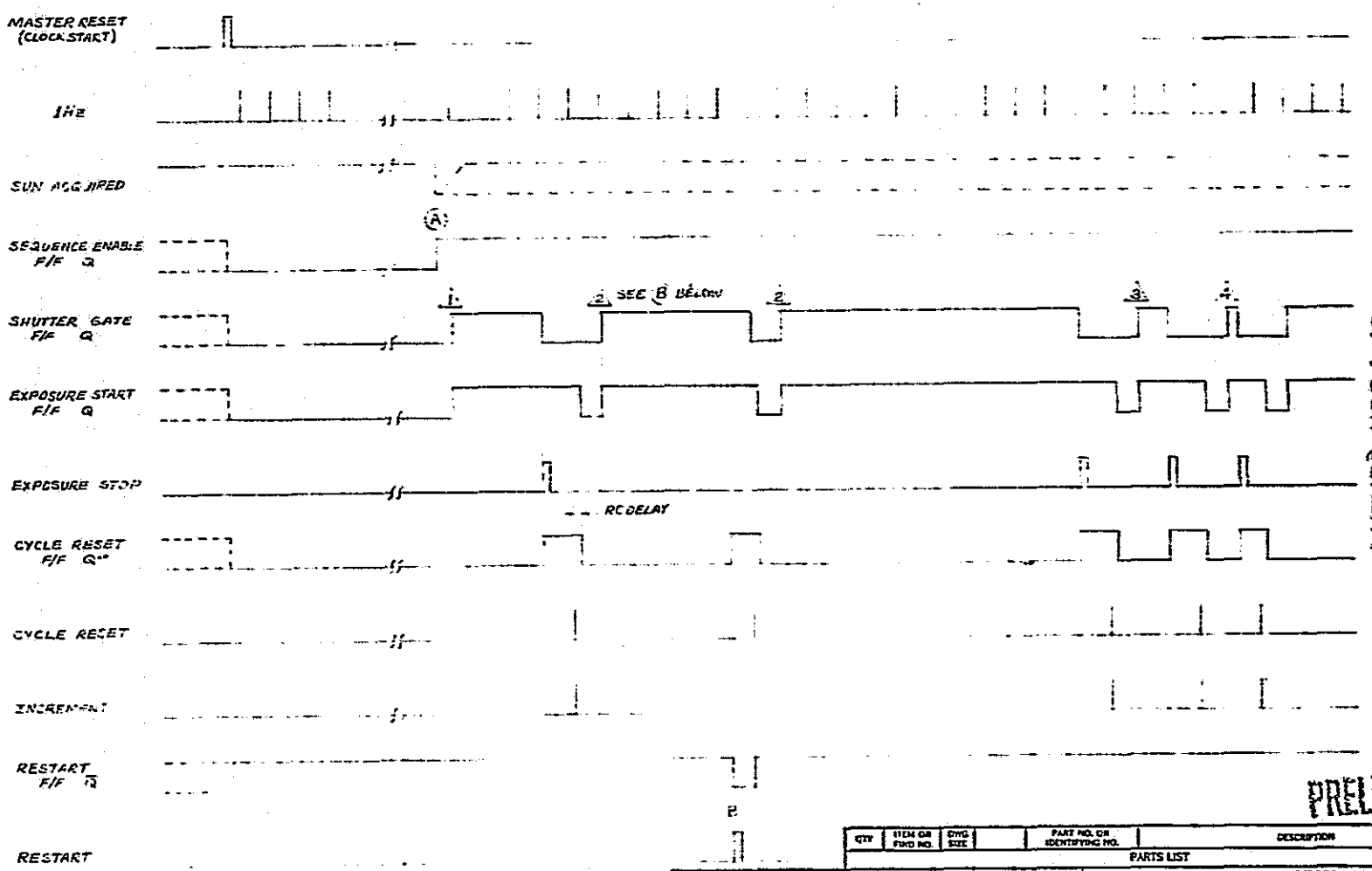

ORIGINAL PAGE IS OF POOR QUALITY

PRELIMINARY

CODE SEQUENCE FOR SIMPLE TIMING DIAGRAM

SEQUENCE NO.	EXPOSURE TIME	CODE
1	3 sec.	0011
2	10 sec	0100
3	1 sec.	0010
4	0.3 sec.	0001

(A) SUN ACQUIRED GOES TRUE (CONTACT CLOSURE) OR N SEC. COUNTER OVERFLOWS TO SET SEQUENCE ENABLE F/F.

(B) RESTART TRIGGERS RESTART F/F, DISABLES INCREMENT AND TRIGGERING CYCLE RESET TO END EXPOSURE.

NEXT ASSY	USED ON
APPLICATION	

QTY	ITEM OR FIND NO.	DWG SIZE	PART NO. OR IDENTIFYING NO.	DESCRIPTION

PARTS LIST

UNLESS OTHERWISE SPECIFIED DIMENSIONS ARE IN INCHES
TOLERANCES ON
FRACTIONS ± | DECIMALS .xx ± | .xxx ± | ANGLES ±

MACH FIN: ✓
HT TR:
FIN:
MATL:

DR HP DATE 6/22/84 CHK DATE
DSGN APPD DATE
ENGR APPD DATE
PROJ APPD DATE
OTHER APPD DATE

SMITHSONIAN ASTROPHYSICAL OBSERVATORY CAMBRIDGE, MA.

TITLE
NIX-T
CYCLE CONTROL TIMING DIAGRAM

SIZE	CODE IDENT NO.	DWG NO.	REV
C	50944	NIXT-210	/

SCALE SHEET

5. PIC AT Wallops Flight Facility

National Aeronautics and
Space Administration

Goddard Space Flight Center
Greenbelt, Maryland
20771

NASA

Reply to Attn of 1040

July 20, 1984

TO: Distribution

FROM: 1040/Sounding Rocket and Balloon Projects Office

SUBJECT: Project Initiation Conference (PIC) on 27.099US - Golub/SAO

The subject meeting was held in the 3rd floor conference room in building E108 at the Wallops Flight Facility on July 18, 1984. Those attending were:

NAME	ORGANIZATION
R. Windsor	GSFC/1040
W. Gurkin	WFF/1041
W. Wallace	WFF/1022.4
R. Burns	WFF/1022.4
B. Ballance	WFF/1041.2
F. Boykin	WFF/1022.3
J. Smolinski	WFF/1040
R. Pless	WFF/1040
J. Gerdes	SAO
H. Penfield	SAO
G. Nystrom	SAO
L. Golub	SAO
T. Laughlin	Lockheed
H. Zimmer	Lockheed

Experiment

The experimenter prepared and distributed a handout outlining his techniques and requirements. Dr. Golub plans to build and fly a new concept in X-ray imaging that is called a "Normal Incidence X-Ray Telescope (NIXT). This telescope will be used to obtain very high resolution X-ray spectra from the sun. The data will be recorded on film using a specially ruggedized Hasselblad for a film transport and shutter assembly. A tentative exposure sequence is 75 seconds, 2 seconds, 20 seconds, 1 second. Still to be determined is the altitude this sequence should start. The P.I. has requested that the skins be anodized and polished to protect the film from heating prior to recovery. In discussing the resolution it was determined that a rig section would be required since he is looking for 1/4 arc second stability. There will be a Calroc type vacuum door in the forward experiment. The vacuum requirement will be in the order of $1x10^{-6}$.

Future

The scientific instruments will consist of:

1. Multi-MIXT: Three coaligned mirrors, each tuned to a selected spectral line.

2. MIXT/Spectrograph with transmission grating (1000 lp/mm at entrance aperture)
Resolution of $\sim$ 1.5 Å/mm $\equiv$ .01 Å resolution

3. X-Ray Polarimeter: Add $\sim$ 45° reflection (Brewster angle) to obtain >90% polarized images.

A breakdown of components and weights is contained in Attachment 1 and a milestone chart for the telescope is contained in Attachment 2.

The P.I. has asked for use of the Goddard solar constant facility for calibration 6 months prior to launch.

Experimenter Action

1. Provide comprehensive and minimum success criteria, i.e., number of exposures time above altitude, etc.

2. Provide alternatives for moving experiment weight aft.

3. Inhibit light source prior to launch.

4. Provide mechanical drawings by November 15, 1984.

Mechanical

R. Burns has agreed to provide anodized experiment sections with pressure bulkheads and an aft extension if required.

Performance

There will be no problems from a performance standpoint with the possible exception of ballast to keep altitude to $\geq$200 miles.

Action

Provide mass properties of launch and recoverable payload using existing lengths and weights. Zimmer/LMSC

Instrumentation

The instrumentation system that will be used for this flight will be from 27.053US. Battery power for the rigs will be provided by instrumentation. The PCM will be reformatted and submitted to SAO for review.

The B/H feed-thru connectors may be hermetically sealed as opposed to the glass type. The P.I.'s GSE will access his equipment through the ITS, and his umbilical lines will be through the instrumentation umbilical. A command system will be flown.

Action

Coordinate required commands with P.I.

Vehicle

This will be a 4 fin Nike Black Brant a possibly use the new aluminum igniter housing.

SPARCS

The P.I. will require some still to be determined solar activity and the only other launch constraints will be the ETA angles. Pointing requirements to achieve the resolution are such that a rig will be required to maintain low roll drift rates. Other requirements such as pointing accuracy and limit cycle are well within the SPARCS capabilities.

Schedule

PIC	Complete
Design Review	November 15, 1984
Skins to SAO	April 15, 1985
Telescope to GSFC for calibration	August 15, 1985
Field Ops	January 22, 1986
PIR	January 23, 1986
FRR	February 12, 1986
Launch	February 15, 1986

Contacts

Science, PI	L. Golub, 617-495-7177
Mech	G. Nystrom, 617-495-7190
Elec	H. Penfield, 617-495-7195
Mission Chief	R. Windsor, 301-344-5871
Mechanical	R. Burns, X548
Performance	W. Gurkin, X566
Vehicle	B. Ballance, X422
Instrumentation	T. Laughlin, 408-742-1941
SPARCS/WSMR Support	H. Zimmer, 505-679-9442
Scheduling	J. Smolinski, X366

Wallops numbers may be reached commercially by dialing 804-824-3411 and giving the operator the extension number. On FTS, dial 928-5 plus three digit extension. White Sands may be reached on FTS by dialing 899-9442 or 9449.

R M Windsor

Richard M. Windsor

Attachments: 2

Distribution: Attendees
D. Bohlin/HQ/EZ
J. Holtz/HQ/EZ
L. Early/1040

NIXT PRELIMINARY EXPERIMENT WEIGHT ESTIMATE

EXPERIMENT		
Telescope Section:	Pounds	
Primary Mirror Assembly	41.3	
Secondary Mirror Assembly	31.5	
Camera Assembly	15.1	
	87.9	
Electronics:		
Electronics	14.0	
Batteries	24.0	
Cables, Connectors, etc.	6.0	
	44.0	
Total Experiment Weight		131.9
VEHICLE		
Rocket Skin Sections	116.4	
Thermal Shields	17.4	
Vacuum Door	6.5	
Aft Bulkhead	8.5	
Trim Weights	5.0	
		153.8
TOTAL WEIGHT EXPERIMENT SECTION		285.7 Pounds

NIX-T PROGRAM
MILESTONE CHART

MILSTONES	CALENDAR DATES
Fabricate Primary Mirror	5 September 1984
Receive Telescope G/E Tube	15 September 1984
Receive Secondary Parts	1 October 1984
Telescope Tube Assembly	1 November 1984
Electronics Comp.	10 November 1984
Secondary System Tested	15 November 1984
Fabricate Secondary Optic	30 November 1984
Electronics Comp.	20 January 1985
Telescope Optics Complete	1 March 1985
Multi-Layer Coatings Complete	1 April 1985
X-Ray Telescope Complete	1 May 1985
Brookhaven X-Ray Tests Complete	15 June 1985
Begin Final Assembly	15 July 1985
Begin Test Program	5 September 1985
Test Program Complete	15 January 1986
Ship to WSMR	15 February 1986
FLT	7 March 1986

AGENDA

SAO NIXT PRESENTATION

	PRESENTOR
1. SCIENCE OBJECTIVES	L. GOLUB
2. EXPERIMENT DESIGN OVERVIEW	G. NYSTROM
3. MECHANICAL DESIGN ASPECTS	G. NYSTROM
4. ELECTRICAL DESIGN ASPECTS	H. PENFIELD
5. PROJECT MILESTONES	G. NYSTROM
6. WSMR ASPECTS	G. NYSTROM
7. PROGRAMMATICS	J. GERDES
8. OPEN DISCUSSION	L. GOLUB

(i) Solar simulation GSFC - prefilters in vacuo

(ii) SPARCS performance, espec. role stability

NIXT

MASS MOMENT OF INERTIA
AND PRODUCTS OF INERTIA
ABOUT EXPERIMENT C.G

AXIS	X	Y	Z
X	2.1	0	0
Y	0	[illegible]	0
Z	0	0	[illegible]

SI Units $Kg - M^2$

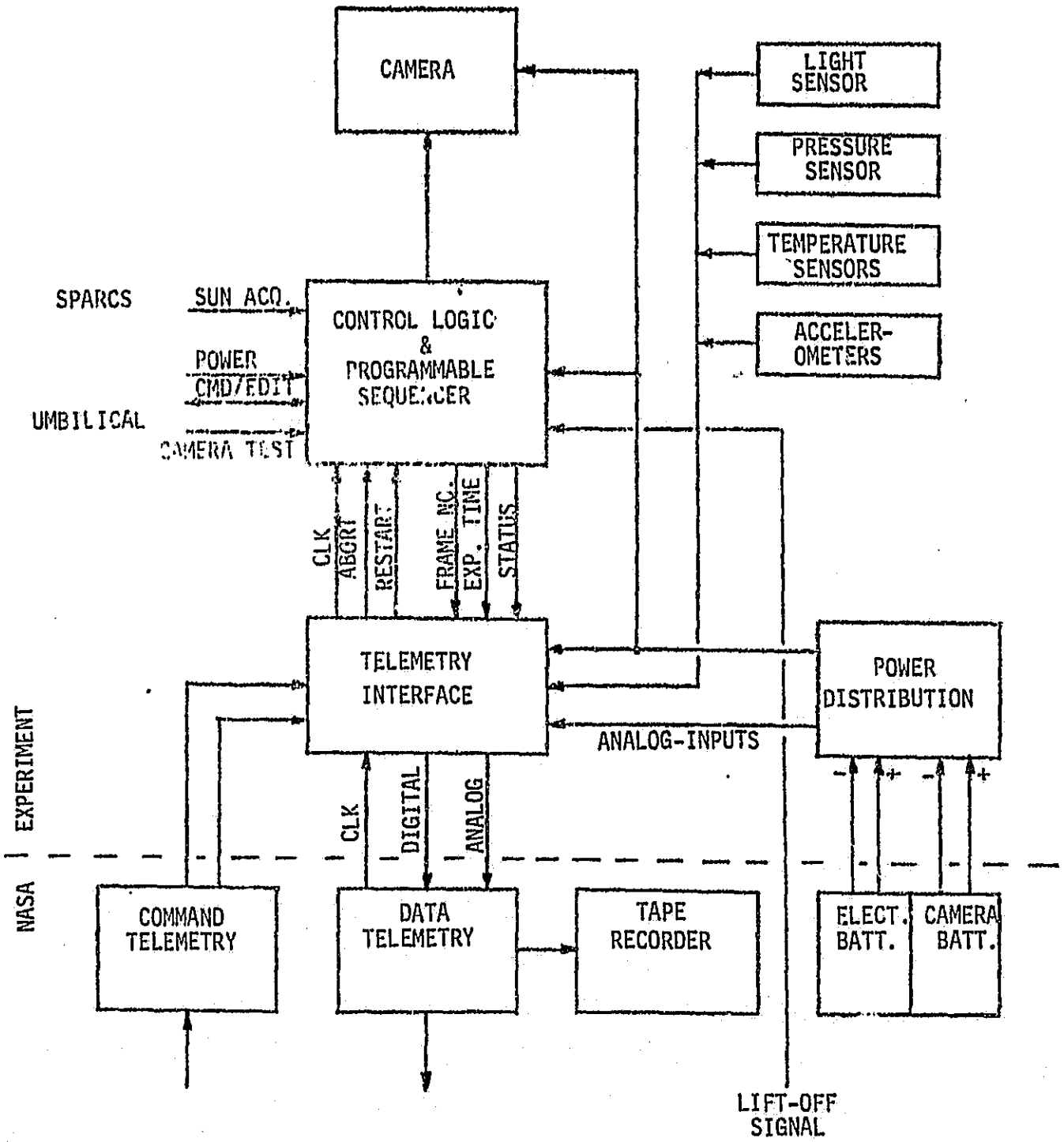

NEA-1 ELECTRONICS BLOCK DIAGRAM

NIXT- INTERFACE REQUIREMENTS

SPARCS

SUN ACQUIRED SIGNAL

UMBILICAL

TWELVE (12) LINES

BATTERY PACK

CAMERA BATTERY	4AH
ELECTRONICS BATTERY	4AH

LIFT-OFF SIGNAL

NIX-T TELEMETRY REQUIREMENTS

DIGITAL DATA

FRAME NO., FN
EXPOSURE TIME, ET
STATUS, ST

ANALOG DATA

LIGHT LEVEL, LL
PRESSURE, PR
BATTERY VOLTAGE, BV
FILM ADVANCE MOTOR CURRENT, MC
TEMPERATURES (8), T1-T8
ACCELERATIONS (8), A1-A8
CIRCUIT VOLTAGES (8), V1-V8

COMMANDS

RESTART
SEQUENCE ABORT

NIX-T TELEMETRY FRAME MAP

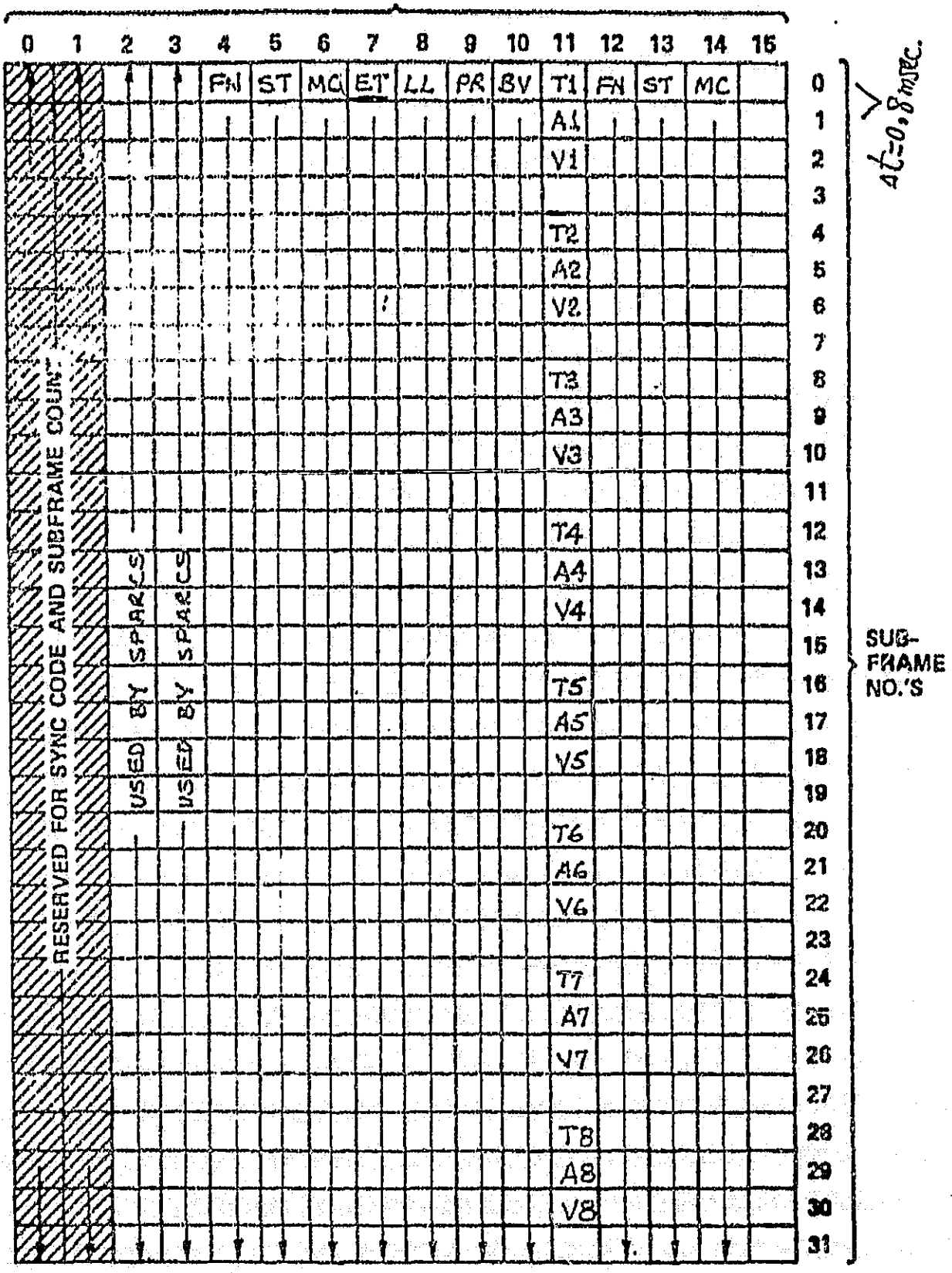

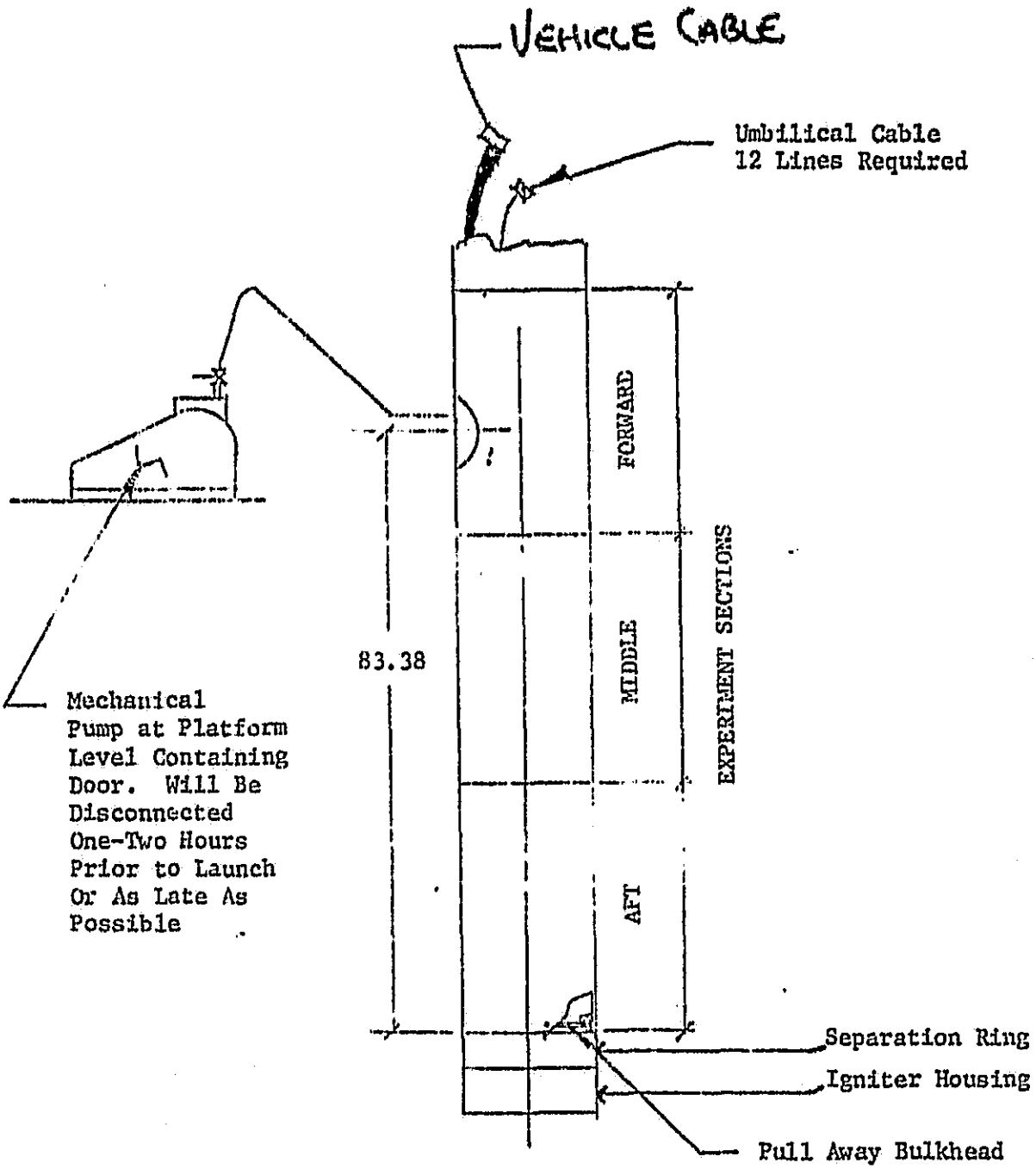

NIX-T EXPERIMENT

TOWER REQUIREMENTS

NIXT PROGRAM MILESTONE CHART

MILESTONES	CALDENDAR DATES	FY YEAR
Fabricate Primary Mirror	5 Sept 84	84
Receive Telescope G/E Tube	15 Sept 84	
Receive Secondary Parts	1 Oct 84	
Telescope Tube Assembly	1 Nov 84	
Electronics Comp.	10 Nov 84	
Secondary System Tested	15 Nov 84	
Fabricate Secondary Optic	30 Nov 84	
Telescope Optics Complete	1 Mar 85	85
Multilayer Coatings Complete	1 Apr 85	
X-ray Telescope Complete	1 May 85	
Brookhaven X-ray Tests Complete	15 June 85	
Begin Final Assembly	15 July 85	
Begiin Test Program	5 Sept 85	
Test Program Complete	15 Jan 86	
Ship to WSMR	15 Feb 86	86
FLT	7 Mar 86	

Appendix: "Solar Coronal Studies Using Normal-Incidence X-ray Optics"

Invited presentation at COSPAR meeting,
Graz (1984).

SOLAR CORONAL STUDIES USING NORMAL-INCIDENCE X-RAY OPTICS

Leon Golub

Smithsonian Astrophysical Observatory, Cambridge 02138 MA U.S.A.

ABSTRACT

We describe the progress which has been made in constructing a new type of X-ray telescope, which operates at normal incidence in the soft X-ray region by the use of multilayer coatings. The principles involved in state-of-the-art multilayer technology and some recent high-resolution imaging results are discussed. A rocket payload incorporating a multilayer X-ray mirror is presently being constructed. It is of Ritchey-Chretien design and the expected spatial resolution is 1/4 arcsec. The scientific program for solar coronal studies and future instrumental developments are also discussed.

INTRODUCTION

During the twenty years in which X-ray imaging has been used in astronomy, every major advance in imaging techniques has resulted in significant new scientific achievements. The continued development of grazing-incidence techniques has led to the great success of the Skylab missions in the Solar case and of the Einstein Observatory in the case of non-solar X-ray astronomy. Optical figuring and polishing techniques have progressed to the point that sub-arcsecond imaging is now possible with a large grazing-incidence broadband system such as the AXAF.

Complementary to the progress in grazing incidence imaging has been the development of multilayer coatings which provide usable normal incidence reflectivity at soft X-ray wavelengths. As we will describe below, it is now possible to deposit large numbers of layers without accumulating signif ant total thickness errors in the stack (Spiller /1/, Barbee /2/). This breakthrough means that one can now fabricate normal incidence mirrors for use at X-ray wavelengths, down to the limit imposed by a drop in performance caused by the effects of interlayer boundary roughness at $\sim$ 30 Å. The ability to reflect X-rays at normal incidence provides an immediate improvement in image quality compared with grazing incidence mirrors (Henry et al.) /3/ and the technique is also capable of providing simultaneous moderate resolution spectroscopy because the multilayers can be designed to provide quite narrow bandpasses. The grazing incidence and multilayer techniques provide complementary lines of development since the high spatial resolution and spectroscopic capabilities of normal incidence optics are offset by the enhanced short wavelength response and broad bandpass of grazing incidence optics. At the present time the fabrication of multilayer coatings for normal incidence X-ray optics is in a state similar to that of grazing-incidence techniques in the early 1960's: it has now been demonstrated that normal incidence imaging at X-ray wavelengths is feasible and that high spatial resolution combined with moderate reflectivity can be achieved. However, the technique has not yet been used for observations in space and it has not yet been developed to the level of quality in imaging which will be achieved in the near future.

Figure 1 provides a visual demonstration of the resolution which has up to now been achieved: the row of dots in the picture is a series of exposures through the plane of best focus, where each of the images is of a 0.7 mm X-ray spot at a distance of 1000 feet (angular size $\sim$ 1/2 arcsec). The mirror was a 3" spherical multilayer coated optic, coated to reflect at the Boron K_α wavelength of 67.6 Å and the X-ray source was a Boron target. Vibration at the MSFC test facility (see §2) kept the measurement limits to the arcsecond level. The production of a high resolution X-ray image on film using normal-incidence optics is a breakthrough and constitutes a major success for the program.

We have thus been able to show that a multilayer coating tuned to a specific well-defined wavelength can be produced and very high quality X-ray imaging obtained. However, while the experimental technique of producing multilayer coatings at a specific desired X-ray wavelength is now understood, such mirrors have not yet been used for any astronomical studies.

In this paper we discuss the present status of the program in which we are involved, whose goal is to develop a large aperture telescope for very high-resolution studies of the Solar corona. The Solar corona is the ideal target for an initial application of normal incidence techniques: it is characterized by high X-ray photon fluxes in a number of suitable emission lines, and is already known to be structured down to the arcsecond level. Furthermore, there are cogent scientific arguments for suspecting substantially greater structuring at yet

smaller spatial scales, so that there exists a pressing need for a breakthrough in our ability to resolve spatial detail in the corona. We therefore expect to begin answering the numerous theoretical questions which have been raised by results from Skylab regarding plasma processes occurring on spatial scales which have heretofore not been resolved.

From this viewpoint, high spatial resolution observations of the solar corona form a scientifically important complement to ongoing diagnostic studies of laboratory plasmas, in which the stability properties of hot magnetically confined plasmas are studied under parameter regimes rarely if ever encountered in the laboratory. For this reason alone, subarcsecond spatial resolution solar observations are recognized as carrying great scientific impact, and the importance of understanding local transport processes in the solar corona from the astronomical perspective simply adds yet another compelling reason for carrying out this research.

MULTILAYER PERFORMANCE AT X-RAY WAVELENGTHS

Multilayer coatings are widely used in the optical region to fabricate mirrors with enhanced reflectivity. These coatings are analogous to a quarter-wave stack, in which the high reflectivity is made possible by producing a standing wave in the material. In order to avoid the rapid absorption of X-rays, a modified quarter-wave stack is produced in which the most absorbing layers are centered on the nodes of the standing wave. The best performance of a multilayer coating in the soft X-ray region is obtained by alternating layers of high and low absorption indices (Spiller /4/) and placing the high absorber at the nodes of the standing wave.

The reflectivity at normal incidence for a single surface is $R \simeq (\delta^2+k^2)/4$, where the complex refractive index is $n(\lambda) = 1-(\delta+ik)$. For wavelengths in the soft X-ray region of the spectrum $\delta \sim k << 1$ and $R \approx \delta^2/2 \approx (n_e r_e \lambda^2/4\pi)^2$, where n_e is the effective electron density and r_e is the classical electron radius. Thus, for soft X-rays $R \sim 10^{-5}$ so that practical normal incidence devices cannot be fabricated for work at these wavelengths.

However, it is theoretically possible to achieve high reflectivities from multilayer coatings. Recent advances in multilayer fabrication techniques (Haelbich et al. /5/, and references therein) indicate that these coatings will allow the achievement of normal incidence reflectivities greater than 10% for wavelengths as short as 44 Å. As described below our work has shown not only that high reflectivities can be achieved but also that exceptionally good image quality can be maintained in a multilayer coated mirror.

The number of layers needed at any X-ray wavelength to achieve a reflectivity R~30% increases as $N \propto 1/\lambda^2$; about 60 layers are required for λ=100 Å. In practice, it is extremely important to control film thickness in the deposition process such that the accumulated thickness error is a small fraction of the wavelength. This type of nearly perfect thickness control has been achieved via an in situ soft X-ray monitoring system (Spiller et al./1/). With this system an error in a deposited layer can be corrected in the next layer so that the number of layers in the stack need not be limited by errors in the individual layer thicknesses. Coatings have been fabricated with more than 200 layers and an accumulated total thickness error below 5 Å.

The imaging performance of a normal incidence spherical mirror at the B Kα wavelength of 67.6 Å has been tested by Henry et al. /3/. The tests were performed at the MSFC 1000-foot long X-ray test and calibration facility. The mirror (manufactured by the Zygo Corp.) was 7.6 cm in diameter with a focal length of 5.24 m. The Zerodur blank was figured to λ/100 rms and superpolished. A multilayer coating consisting of 124 alternating layers of C and a Re-W alloy was deposited directly on the Zerodur substrate. The reflectivity of the coating was monitored during the deposition, using N Kα (31.6 Å) at an angle of incidence of 62°. Because of geometrical constraints, the first round of tests was performed at an angle of 1.°5 off-axis; the detector used was the backup High Resolution Imager (Einstein brassboard), a two-dimensional photon counting imaging detector.

The results of the test are shown in Table 1, in which we compare the performance of the normal incidence mirror at 1.°5 off axis to that of the Einstein Observatory grazing incidence mirror performance on axis; the latter mirror is chosen as an example of the current state of the art in grazing incidence design. The data show that the normal incidence mirror compares quite favorably with the Einstein mirror. The test results also indicate a total reflectivity of 5-10%, the major uncertainty being due to uncertainty in the detector's quantum efficiency as used in this test. We note also that the figure of 1" for the FWHM of the mirror represents an upper limit to the true response, since this was the resolution limit of the test setup.

TABLE 1. Normal Incidence Mirror Performance

	Normal Incidence (1.°5 off-axis)	Einstein (on axis)
FWHM (arcsec)	< 1.0	3.4
50%	5.0*	8.4
70%	8.5*	15.2

* Normalized to detector field of 512 arcsec

A TELESCOPE FOR SOLAR STUDIES

We are in the process of building a normal incidence X-ray telescope (NIXT) fo very high spatial resolution studies of the Solar corona. The telescope is a Ritchey-Chretien design, consisting of a pair of mirrors with hyperbolic figure arranged in a Cassegrain configuration. After figuring and polishing of the optics are complete, they will be coated with a multilayer designed to provide usable normal incidence reflectivity at a soft X-ray wavelength chosen to coincide with a strong coronal emission line formed in the $1.5\text{-}3 \times 10^6$ K temperature range.

An optical schematic of the telescope, which is presently being fabricated, is provided in Figure 2. For reasons of thermal stability as well as finer optical surface quality, it is intended that the mirror substrate material be Zerodur. Extensive testing over the past several years has demonstrated that Zerodur flats can be polished to better than 5 Å surface roughness. The desired figure tolerance for the flight instrument is $\lambda/10$ peak to valley or $\lambda/40$ rms.

The proposed telescope will consist of a 25 cm diameter primary and a 5.9 cm secondary. The radii of curvature are approximately 394 cm and 126 cm, respectively, and the EFL of the system is 750 cm. Because of the extremely high spatial resolution which we are seeking to obtain ($\sim$ 4 times better than the λ5000 diffraction limit), the main support structures for the instrument will be a large Invar ring holding the primary mirror and a graphite-epoxy monocoque optical bench for positioning of the secondary. Because of the limited duration of a rocket flight, an athermalized telescope cell is not felt to be necessary, and therefore the Invar metering structure will suffice.

The design, fabrication, test and assembly of the telescope optics are following conventional optical shop procedures for aspheric surfaces. Null lenses will be required for final figuring of primary and secondary mirrors, in conjunction with fringe measurements on a Zygo 12" laser interferometer. It should be noted that because the telescope is to be used at a wavelength of about 50 Å, the demands on optical figure are severe. Using the telescope at wavelengths one hundred times shorter than visible demands strict attention be paid to precise figure control throughout the manufacturing process. Also, since the thickness of each interference coating layer pair is of order $\lambda/2$, the surface finish of the optics must be state-of-the art.

The detector for this instrument will be film, since there are no electronic detectors available which have the required spatial resolution, even with our 7.5m focal length. The film which was used for the X-ray instruments on Skylab was SO-212. This film, or its parent emulsion Panatomic-X Aereographic (3412), would be acceptable for our purposes. However, we anticipate the need for a higher resolving power since the resolution of the NIXT may be an order of magnitude better than that of the S-054 or S-056 instruments. We are testing a new Kodak product, Technical Pan Film (2415), which has higher resolving power than 3412 and may also have higher sensitivity; combined with the factor of 3 greater plate scale of the NIXT it will be possible to achieve 1/4 arcsec resolution in the flight instrument.

SCIENTIFIC PROGRAM

Having assessed the initial test results for our existing normal incidence mirror, it is evident that true sub-arcsecond spatial resolution is now a realistic possibility in observations of the Solar corona. We are thus in a position to consider a qualitatively new kind of observing program. In this section we propose and briefly sketch some of the most obvious new observations, both Solar and non-Solar, which can now be envisaged.

At the present time we anticipate three major Solar areas in which normal incidence X-ray optics will have immediate impact:

1. Fine structure of coronal loops. The progress which has been made in studying the structure of the Solar corona has served to define a set of questions regarding local energy release and mass and energy transport which can be addressed by higher resolution observations. These questions may all be grouped under the general heading of heating, structure and stability of hot plasma-filled loops observed to be confined by magnetic fields (Fig. 3). This general problem of plasma heating and confinement is, of course, presently being vigorously studied in terrestrial laboratories by those interested in controlled nuclear fusion and many of the same theoretical and instrumental techniques are being used in both fields.

The situation in the solar coronal case is that at present theory has too much freedom to construct possible models. Present observations are insufficient to constrain theoretical parameters: we do not at this time know the radial temperature and density structure within a coronal loop, the rate of magnetic field expansion at the base of a loop, the magnitude of coherent plasma flows within the loop, the importance of rapid, transient heating for loops (Sheeley and Golub /6/), and so forth. A major aim of our overall program is to resolve these issues by means of extremely high spatial and temporal resolution X-ray imaging. In so doing, this research will contribute not only to our understanding of the solar corona, but also of confined hot plasmas in general.

2. Flare reconnection regions. The area of coronal research which has received the most attention over the years and which still seems far from solution is the Solar flare.

Proposed explanations, other than agreeing that rapid release of magnetic energy is involved, still offer a discouragingly large range of possible mechanisms (see Sturrock /7/ for a summary). The Skylab and SMM observations have provided some help by showing that there are two general classes of flares, those with large and diffuse loop systems associated with eruptive prominences and compact active region flares with small or unresolved loops, higher plasma pressures and more rapid evolution (Pallavicini, Serio and Vaiana /8/). Furthermore, SMM observations have shown that the likely site for particle acceleration is coronal, and that electrons and ions are accelerated on essentially the same time scale, contrary to theoretical expectations.

The basic unresolved problem is the mechanism of flare energy release. There is general agreement that the problem to be solved involves the storage of energy in coronal magnetic fields and the rapid release of this stored energy in a flare event, presumably via magnetic reconnection. "Reconnection" involves the dissipation of magnetic flux at a finite resistivity boundary layer and the associated conversion of magnetic energy into heat and accelerated particles. These reconnection boundary layers are both at the heart of the flare problem and pure theoretical constructs: they have never been observed. Because predicted sizes for the associated current layers begin about one order of magnitude below the best spatial resolution achieved to date, the absence of observational confirmation has not at all constrained flare models. At a resolution of 0.1 arcsec the possibility exists, particularly in the larger scale flares, that we may begin to resolve the reconnection region and hence begin to constrain available theories for the flare energy release. Furthermore, high resolution soft X-ray images will provide a direct confrontation of recent hydrodynamic flare models with the data.

3. Emerging magnetic flux. A third area of study is the investigation of small-scale emerging (bipolar) magnetic flux. We now know that most of the magnetic flux emerging from the Solar interior is in small spatial scale "shredded" or intermittent form, and that magnetic flux emergence is associated with vigorous X-ray emission at the emergence site. X-ray observations thus provide a very good diagnostic for magnetic flux emergence on the Sun (Golub /9/). Large active regions, although of crucial importance in determining the large-scale form of the corona and the level of activity, represent only a small fraction of the total magnetic flux which emerges. The only exception seems to be at times of Solar maximum, when the active regions may dominate the emergence process. The overall balance between large and small emerging regions is a function of phase in the Solar cycle and is such that the total amount of flux emerging is nearly constant (Golub /9/); the solar cycle can thus be visualized as an oscillation in the wavenumber distribution of emerging flux (Fig. 4). This observational constraint on solar magnetic dynamo theory remains to be tested on smaller spatial scales: because of the apparent importance of magnetic flux emergence on small spatial scales, it is of great interest to know whether flux emergence on as yet unresolved scale sizes vitiates the present observational picture. Our observations can thus provide a direct answer to these questions.

An intimately related problem is whether there are any smaller scale emerging fields at all. That is, we have not answered the question, at what scale size, if any, does the emergence process stop. It is certain that at some small spatial scale length magnetic diffusion will dominate, so that the size spectrum of emerging flux will cut off. In addition, the spectrum of flux emergence determined by Golub et al. /9/ is such that the integrated contribution of small bits of flux increases in importance down to the smallest scale size observed ($\sim 10^{19}$ Mx). Hence the shape of the distribution must turn over at some small scale size and this spatial scale is accessible to our observations, then we will be able to test directly theories for magnetic flux emergence and diffusion on small spatial scales.

FUTURE APPLICATIONS

Although the principal aim of our initial application of normal incidence optics at soft X-ray wavelengths is high-resolution imaging, we emphasize that one of the most important ultimate contributions of normal incidence technology is in the field of high-resolution X-ray spectroscopy. This prospect is a natural consequence both of the relatively narrow passband inherent in such optics, as well as of the inherent optical configuration which, as we shall show, is far better suited than grazing incidence optics for feeding spectrographs of extremely high wavelength resolution.

Spectroscopic applications of multilayer technology range from the most simple case, in which several mirrors are flown at the same time, each tuned to a particular spectral feature to more sophisticated instruments, e.g., one in which a normal incidence telescope is used as a feed for an echelle type spectrometer. In this section we describe spectroscopic instrumental developments which we foresee at this time as being the most promising and productive avenues to pursue for the immediate future.

Multiple-Mirror NIM

The notion that spectrographs of fairly high wavelength resolution are essential to perform plasma diagnostics based on, for example, line ratios is common wisdom and under most circumstances entirely warranted. However, an important exception to this rule exists, which normal incidence optics can take advantage of. The spectrum of a coronal (i.e., X-ray emitting) plasma in the temperature range of 1-20 million degrees contains many narrow

wavelength intervals in which: (a) the number of spectral line features per unit wavelength interval is low, and (b) the emission is virtually *completely dominated* by a small number of specific transitions whose intensities are characterized by different dependences on plasma temperature. Broadband soft X-ray spectroscopy has taken advantage of this fact for some time, but has been limited by the relatively wide passband of typical transmission filter arrangements ($\Delta\lambda/\lambda$ of approximately 0.1).

It is possible to choose wavelength intervals in the spectra of plasma at coronal temperatures such that the mirror bandpass transmission at any fixed temperature is dominated by a single (resonance) line. By appropriate "tuning" of the bandpass, the contribution of continuum emission and other lines can be made to constitute a very small fraction of the total bandpass flux. Thus, by taking advantage of sparsely populated wavelength intervals in the spectra of coronal plasma and then matching the bandpass of the normal incidence optics to the wavelength extent of these spectrum intervals, we can obtain a level of spectral isolation of soft X-ray lines more commonly associated with high-resolution spectrographs such as transmission or reflection gratings, but with far greater effective area. If one now employs several normal incidence mirrors, each "tuned" to a different wavelength interval in which the emission is dominated by a single line, it is then possible to measure line ratios with a minimum of contaminating emission. The emissivity vs. coronal temperature for three candidate bandpasses is shown in Figure 5.

Extremely High-Resolution Spectroscopy

It goes without saying that most of the techniques developed for high-resolution spectroscopy with grazing incidence optics can be readily applied in the normal incidence case. For example, objective gratings (with $\lambda/\Delta\lambda \sim 100$-$1000$) can be readily adapted to our optical geometry, with the considerable advantage that grating fabrication is simplified by less stringent optical constraints. For example, the requirement for coma-corrected transmission gratings in the grazing incidence case no longer applied. Of considerably greater interest in the long term, however, is the possibility of conducting spectroscopy with wavelength resolution of the order of $\lambda/\Delta\lambda \sim 10{,}000$ or more, e.g., with resolution which begins to be comparable to that enjoyed by optical astronomers. At this resolution it becomes possible, for example, to measure line doppler shifts for X-ray emitting plasma moving at the modest velocities expected in stellar atmospheres and to determine detailed line profiles.

For our present purposes, the essential element of, e.g., an echelle spectrometer design is the requirement for two distinct nested grazing incidence telescopes: the first being the imaging telescope, which focuses the source onto the entrance slit of the spectrograph proper, the second being the collimator, which is necessary to produce the parallel beam fed to the echelle gratings. Such telescope/spectrographs thus require at least four grazing incidence reflections before the beam arrives at the echelle gratings. The key point of our normal incidence telescope design is that only two reflections are necessary: by placing the spectrograph entrance slit at the focus of the normal incidence primary mirror, a second normal incidence mirror behind the slit can be used as a collimator, analogous to conventional echelle spectrographs. The major advantage of this design over the corresponding grazing incidence case is the substantially simpler optical train, while the elimination of two grazing incidence reflections largely compensates for the lower reflection efficiency of the normal incidence mirrors. For extended objects, the normal incidence design also allows one to maintain high spatial resolution along the slit, as is achieved in the HRTS instrument of NRL.

This work was supported in part by NASA under grant NAGW-397. Travel to the COSPAR meeting was supported by the Smithsonian Secretary's Fluid Research Fund.

REFERENCES

1. E. Spiller in "Low Energy X-ray Diagnostics", eds. Attwood and Henke, AIP (1981).
   E. Spiller, A. Segmüller, J. Rife, and R.-P Haelbich, Appl. Phys. Lett., 37, 1048 (1980).
2. T.W. Barbee in "Low Energy X-ray Diagnostics", op. cit. (1981).
3. J.P. Henry, E. Spiller and M. Weisskopf, Appl. Phys. Lett., 40, 27 (1982).
4. E. Spiller, Appl. Opt., 16, 89 (1976).
5. R.-P. Haelbich, A. Segmüller and E. Spiller, Appl. Phys. Lett., 34, 184 (1979).
6. N.R. Sheeley, Jr. and L. Golub, Sol. Phys., 63, 119 (1979).
7. P.A. Sturrock ed. "Solar Flares", Colorado U. Press (Boulder) (1980).
8. R. Pallavicini, S. Serio and G.S. Vaiana, Ap.J., 216, 108 (1977).
9. L. Golub Phil. Trans R. Soc. London A, 297, 595 (1980).
   L. Golub, A.S. Krieger, J.W. Harvey, and G.S. Vaiana, Sol. Phys., 53, 111 (1977).

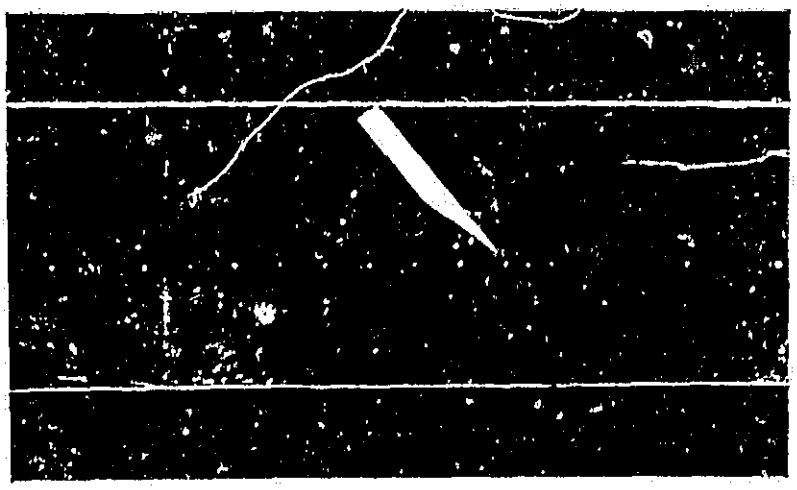

Fig. 1. A series of x-ray images through the plane of best focus, taken with the prototype normal incidence x-ray telescope (NIXT). Images are of a Boron target, spot size 0.7 mm, at a distance of 300 m; emission is at the B K_α line, 67.6 Å radiation. Arrow points to best-focus spot.

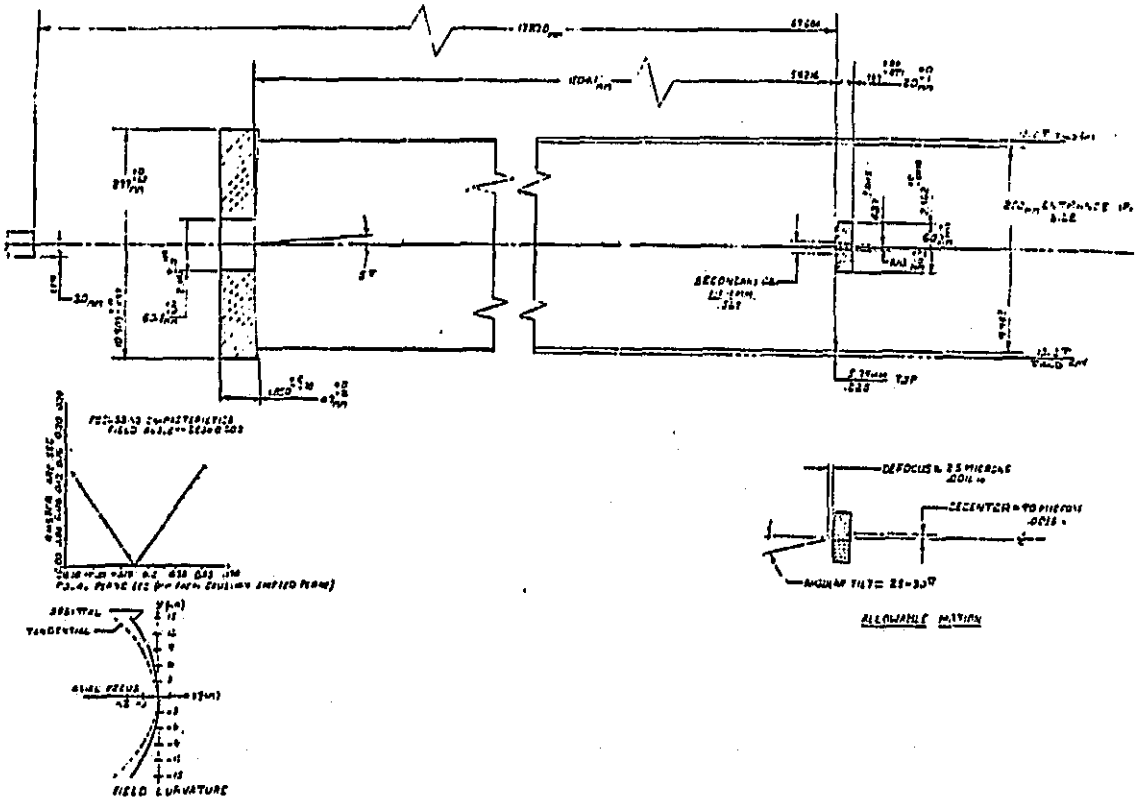

Fig. 2. Optical schematic of the NIXT rocket instrument, a Ritchey-Chretien x-ray telescope with 10" primary and expected spatial resolution of 1/4 arcsec.

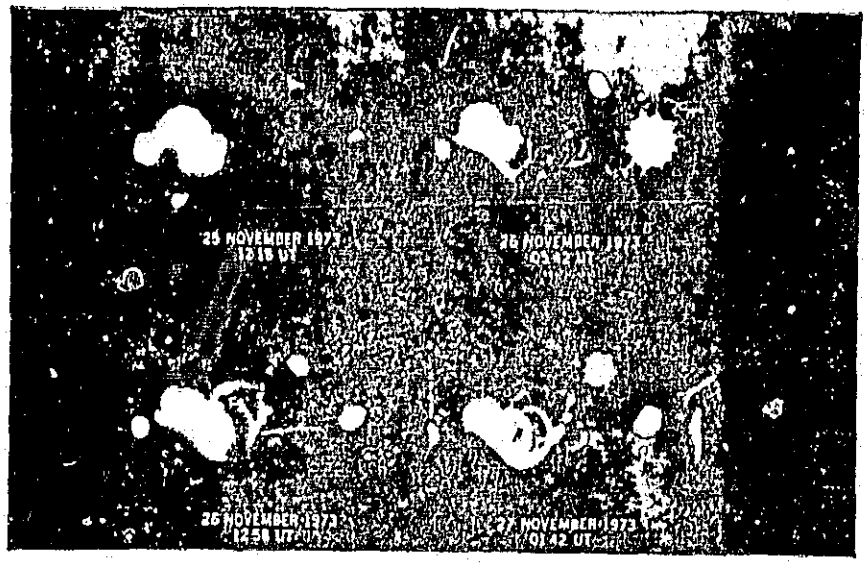

Fig. 3. Fine structure of coronal loops as seen by the S-054 xray telescope on Skylab.

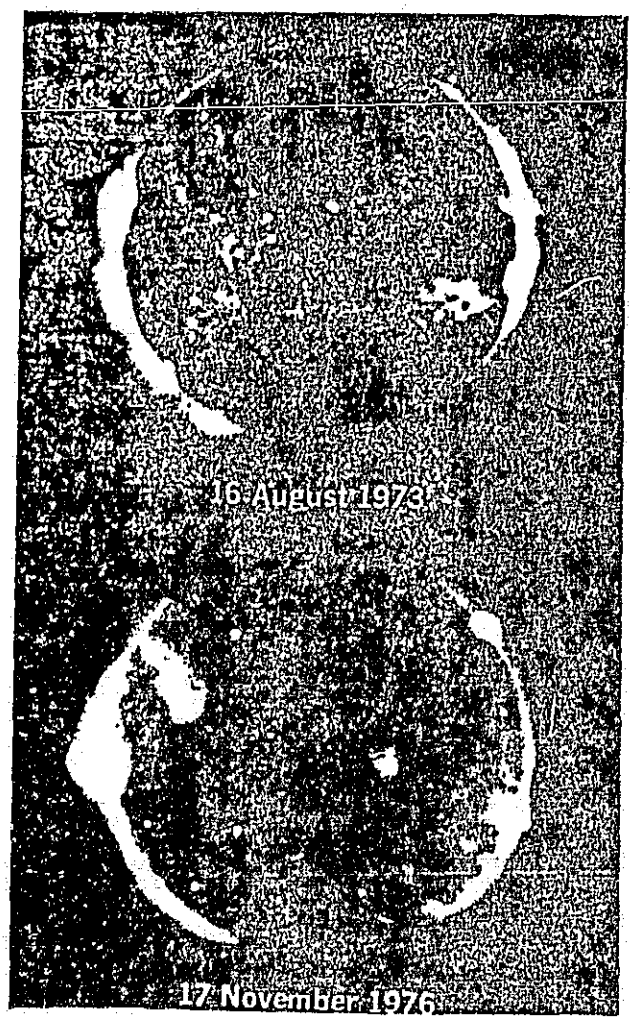

Fig. 4. Solar cycle variation in emergence rate of small-scale magnetic fields, as determined from the number of x-ray bright points and from simultaneous magnetograms.

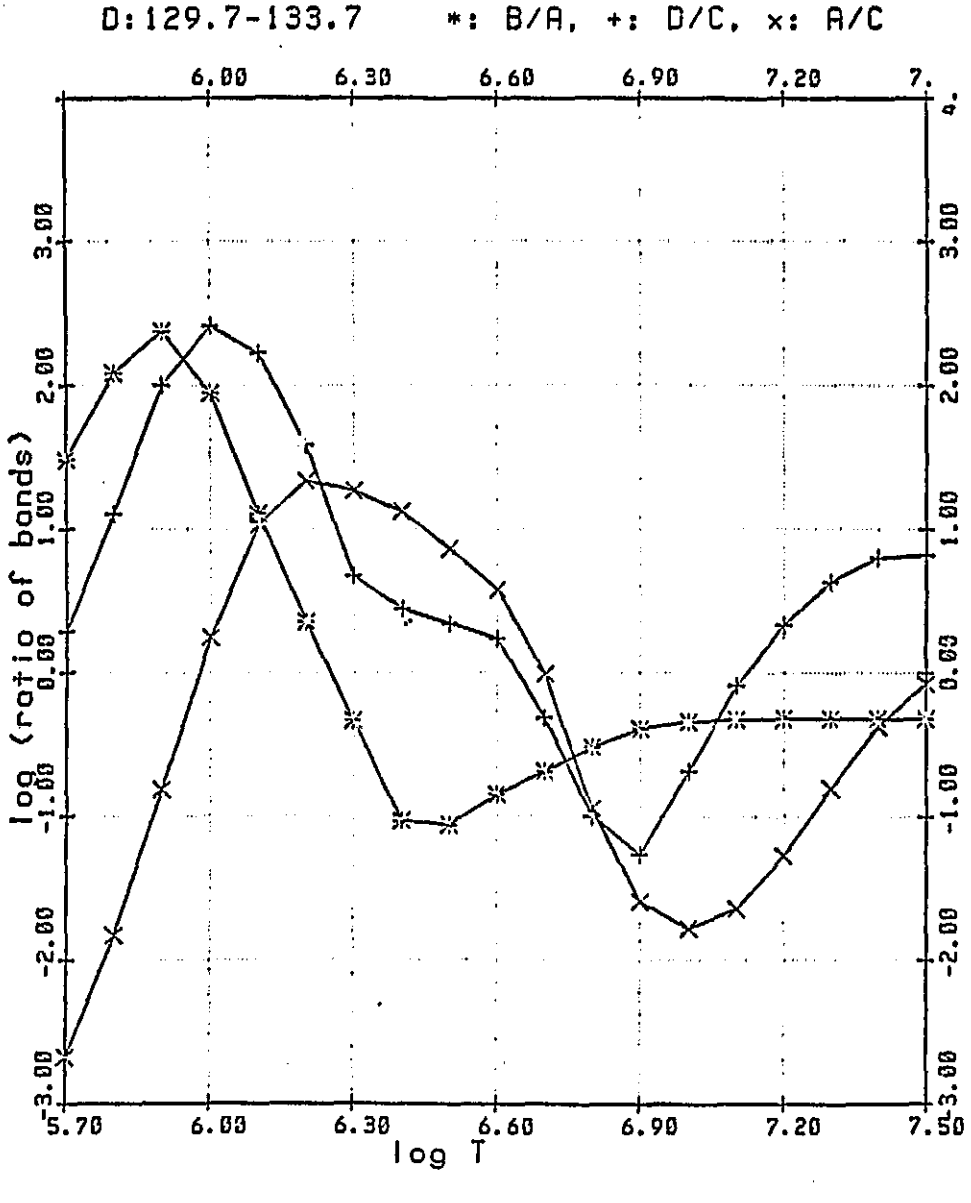

Fig. 5. Flux ratios through pairs of multilayer coated mirrors tuned to the indicated wavelength intervals. Note that at nearly all temperatures encountered in the Solar corona there are suitable pairs with good temperature discrimination.

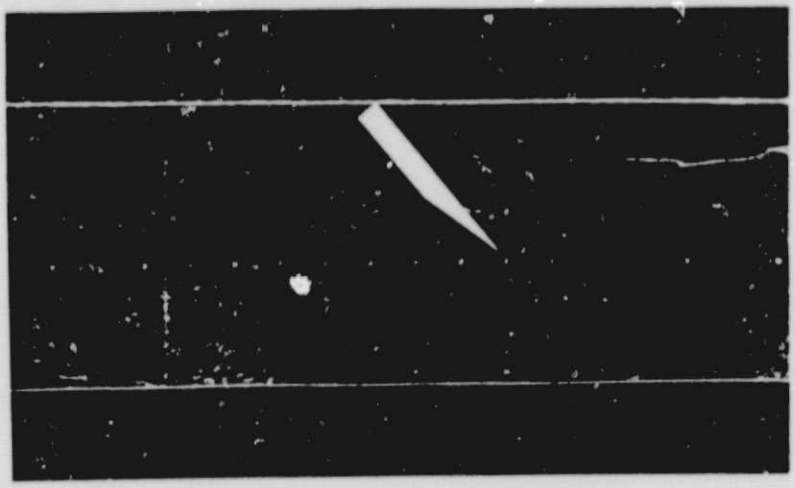

Fig. 1. A series of x-ray images through the plane of best focus, taken with the prototype normal incidence x-ray telescope (NIXT). Images are of a Boron target, spot size 0.7 mm, at a distance of 300 m; emission is at the B K_α line, 67.6 Å radiation. Arrow points to best-focus spot.

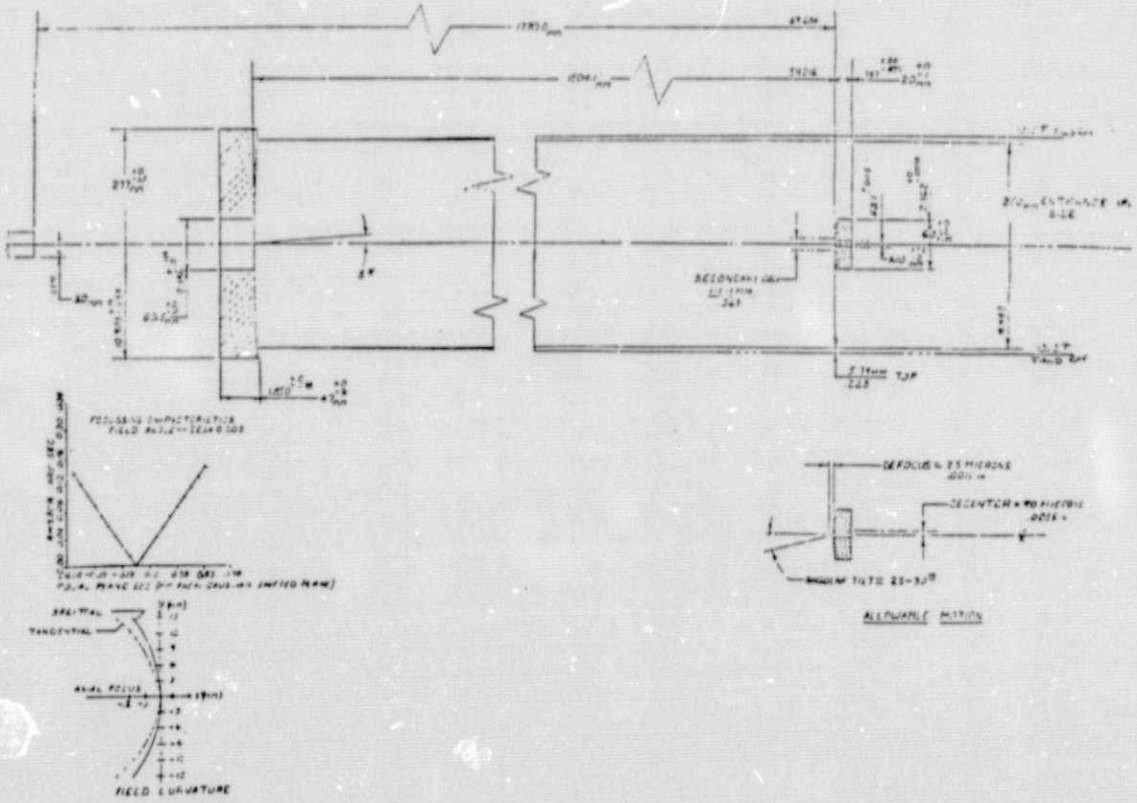

Fig. 2. Optical schematic of the NIXT rocket instrument, a Ritchey-Chretien x-ray telescope with 10" primary and expected spatial resolution of 1/4 arcsec.

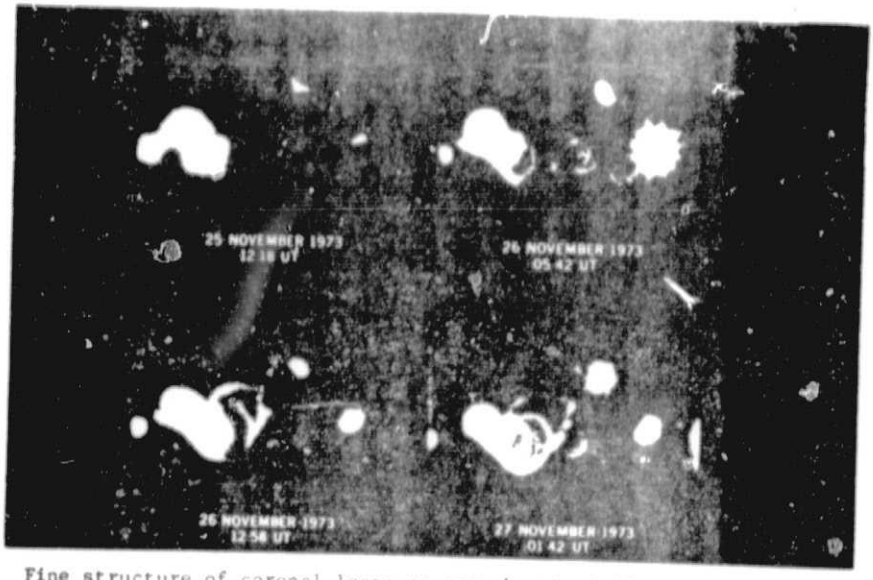

Fig. 3. Fine structure of coronal loops as seen by the S-054 xray telescope on Skylab.

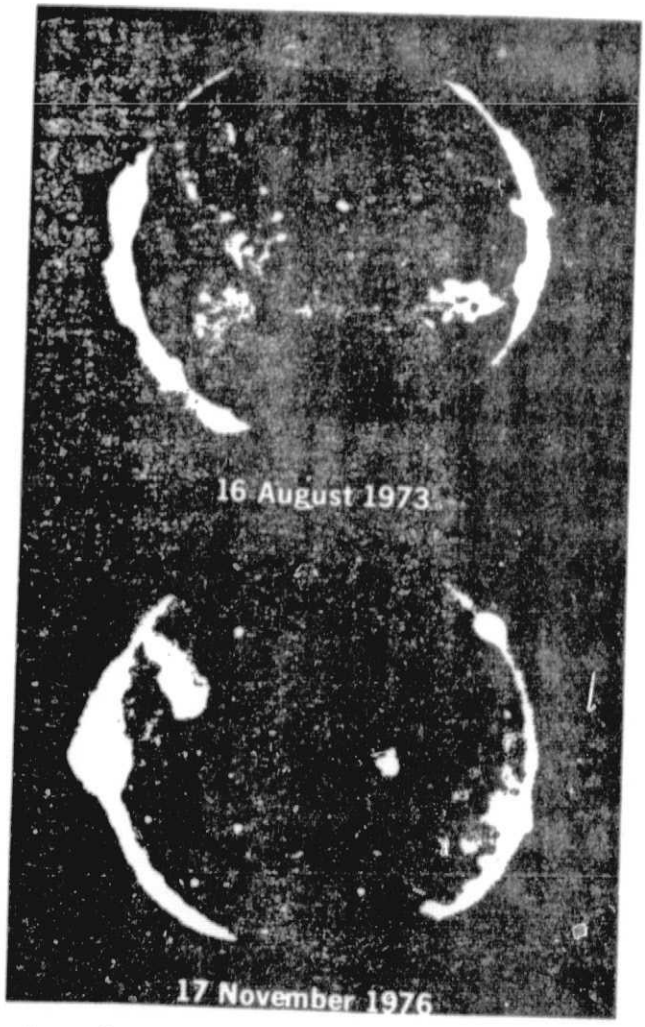

Fig. 4. Solar cycle variation in emergence rate of small-scale magnetic fields, as determined from the number of x-ray bright points and from simultaneous magnetograms.

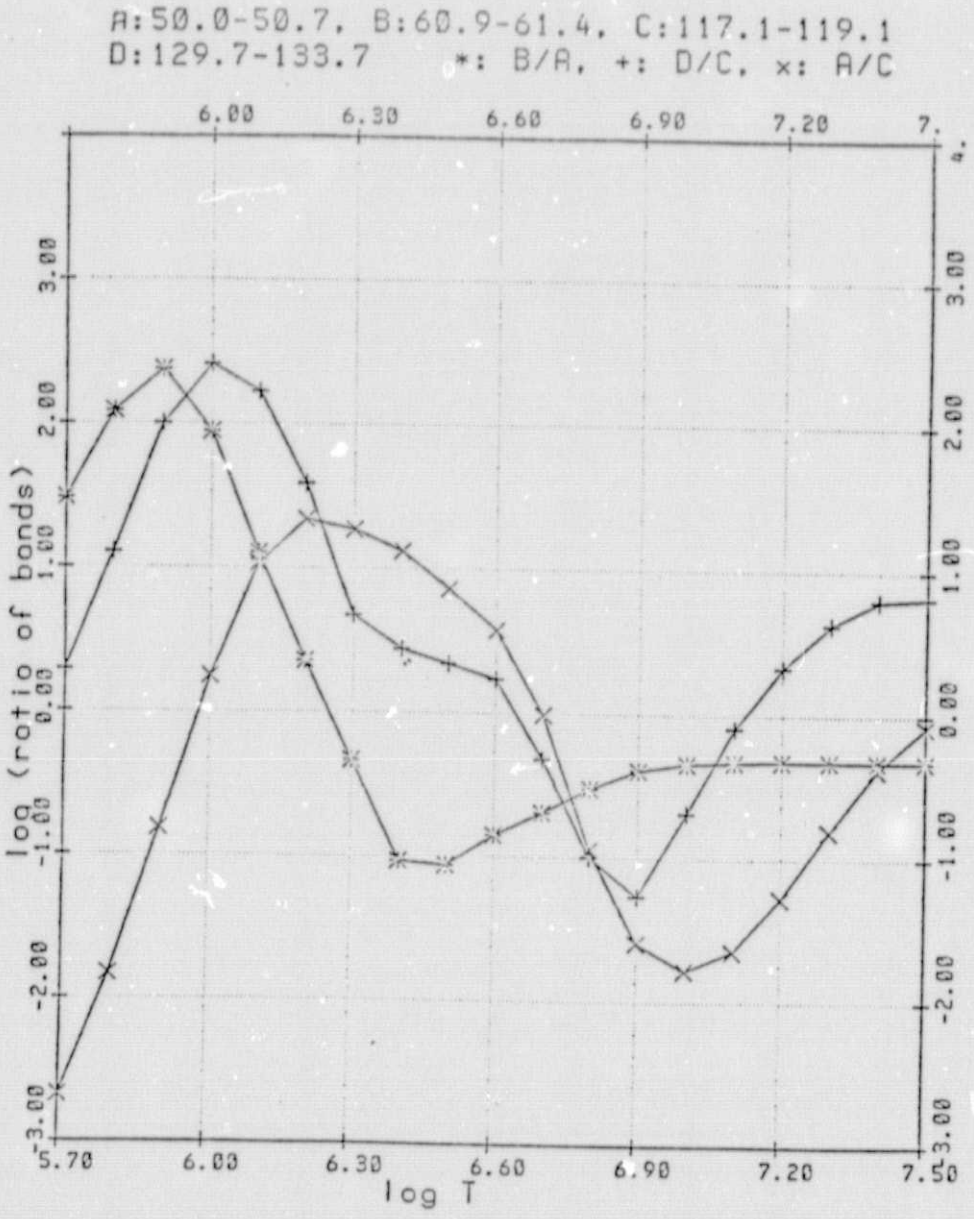

Fig. 5. Flux ratios through pairs of multilayer coated mirrors tuned to the indicated wavelength intervals. Note that at nearly all temperatures encountered in the Solar corona there are suitable pairs with good temperature discrimination.